Journal of Research of the National Bureau of Standards Vol. 46, No. 2, February 1951 Research Paper 2178

Temperature Variation of Mass Spectra of Hydrocarbons[1]

Robert M. Reese, Vernon H. Dibeler, and Fred L. Mohler

The temperature variations of the mass spectra of a variety of hydrocarbons have been measured by using a Consolidated mass spectrometer. Measurements have been made in the temperature range of 100° to 300° C on a number of selected mass peaks in the spectra of 21 compounds. The sensitivity (current per unit pressure) of the maximum peak and the ratio of other peaks to the maximum peak have been measured as a function of temperature of the ion source. The percentage change of sensitivity or of pattern per degree C at 250° C has been defined as the temperature coefficient. This changes very little with temperature. The temperature coefficients of sensitivity for A and N_2 are -0.23 and -0.18. Sensitivity coefficients of the maximum peaks of the hydrocarbons range from -0.2 to 0; and pattern coefficients of most of the peaks have small negative or positive values, but the molecule ions have larger negative coefficients up to -1.5 percent per degree. There is an inverse correlation between the size of the molecule ion peak relative to the sum of all the peaks and the temperature coefficients. Spontaneous dissociation of molecule ions because of thermal energy can account for this correlation between peak height and temperature coefficient. Published appearance potential data for a few of these molecules give a basis for computing the stability of the ions and show that thermal dissociation is to be expected at 200° to 300° C.

I. Introduction

In 1944, Hipple [1][2] reported a marked temperature effect on the relative abundance of various ions in mass spectra of hydrocarbons. In a subsequent note, Fox and Hipple [2] briefly described the effects of temperature on normal and isobutane and 2,2,3-trimethylpentane and pointed out that such effects were useful as a means of measuring the temperature of the ion source. More recently, Stevenson [3] has reported the temperature effects on a number of simple molecules and has discussed the theoretical reasons for the existence of such effects. Berry [4] has examined the effect of temperature on the mass spectra of nine saturated and seven unsaturated hydrocarbons. These experiments show that for monatomic gases and simple, stable molecules there is a relatively small decrease in ion current per unit of pressure with increasing temperature, arising from the decrease in gas density and from a decrease in the efficiency of collecting ions of higher initial kinetic energies. In the hydrocarbons, the molecule ions and some fragment ions show a temperature effect of a much larger magnitude. The decrease in the molecule ion is greater than for any of the fragment ions, and Stevenson [3] finds that an inverse correlation exists between the temperature effect and the fraction of total ionization contributed by the molecule ion.

This temperature effect is a phenomenon of importance in understanding the mechanism of ionization of polyatomic molecules, and it is of a magnitude sufficient to cause large errors in mass spectrometric analysis if the ionization chamber is not held at a constant temperature. For these reasons, it has seemed worth while to extend the research on temperature effects to a wide variety of hydrocarbons.

[1] A preliminary report of this work was made at the New York meeting of the American Physical Society, February 1950.

[2] Figures in brackets indicate the literature references at the end of this paper.

II. Experimental Details

A Consolidated model 21-102 mass spectrometer, equipped with a thermostatted ionization chamber and automatic control of the electron emission was used to measure the effect of temperature on mass spectra. The leads of the thermocouple that normally operates the thermostatic control were connected to a potentiometer in order to measure the temperature of the ion source. With the filament off and the source at room temperature, a sample was introduced and the filament was raised to full emission as rapidly as possible. The relative abundance of a selected group of ions was repeatedly recorded at constant magnetic field as the temperature increased to about 200° C due to the heat of the filament. At this point the external heat lamp was turned on, and data were recorded to over 300° C. As each mass peak was recorded, the temperature was read. Berry [4] has stated that the gas is in thermal equilibrium with its surroundings before ionization takes place. The gas temperature is assumed to be some function of the temperature measured by the thermocouple. Total elapsed time was also recorded, and periodic readings of the sample pressure in the gas reservoir were made with an indicating micromanometer [5].

A typical temperature-time curve for the ion source is shown in figure 1. For this ion source a maximum temperature of 250° C was reached in about 1 hour. Radiation from the external heat lamp raised the temperature an additional 75°. If the heat lamp was turned on at 200° C, a temperature of 300° C was reached in about 40 min, and during this time the selected ion peaks were successively recorded as rapidly as possible. One or more mass peaks in each of two to six carbon groups were recorded. In general, only the principal mass peaks in addition to the molecule ion were recorded.

916783—1——51

UNIVERSITY OF MICHIGAN LIBRARIES

The hydrocarbons used were NBS standard samples with a few exceptions. Complete mass spectra of all of the compounds have been published [6] along with information on the source and purity of the compounds. Nitrogen containing approximately 65 atom percent of N^{15} was obtained from Eastman Kodak Co., and argon was obtained from Air Reduction Corp.

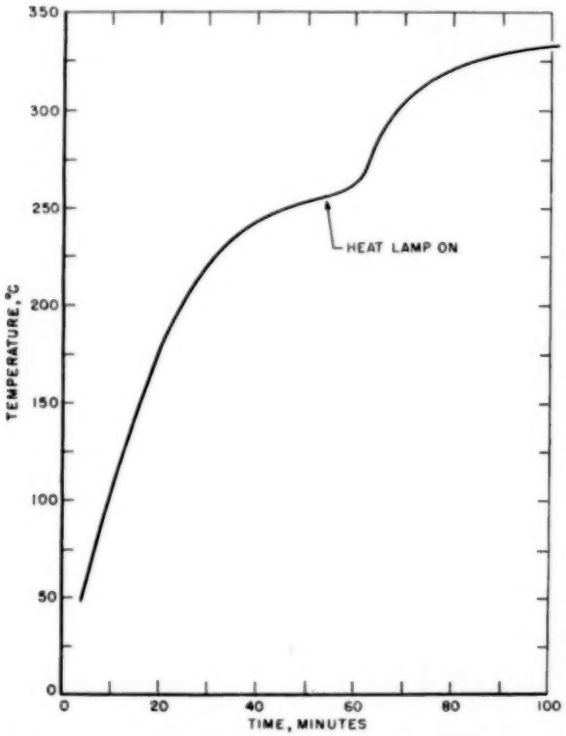

FIGURE 1. *Temperature rise of the ionization chamber as a function of time.*

As a test of the method of measurement, we have repeated the measurements of Stevenson [3] on argon and nitrogen and the measurements of Berry [4] on *n*-butane and two of the octanes. There is satisfactory agreement, and our method of measuring the temperature effect on spectra without waiting for temperature equilibrium seems to be entirely valid. This is important as it permits studying spectra of many compounds without prohibitive interruption of other research and testing programs.

III. Experimental Results

Figure 2 is a plot of the data obtained for 12 peaks of *n*-octane at different temperatures. Ordinates give the sensitivity of the base peak of mass 43 and the pattern ratio for all other ions.[3] When the pattern ratios and sensitivities are plotted on a logarithmic scale against the measured temperature the resulting semilogarithmic plots are nearly

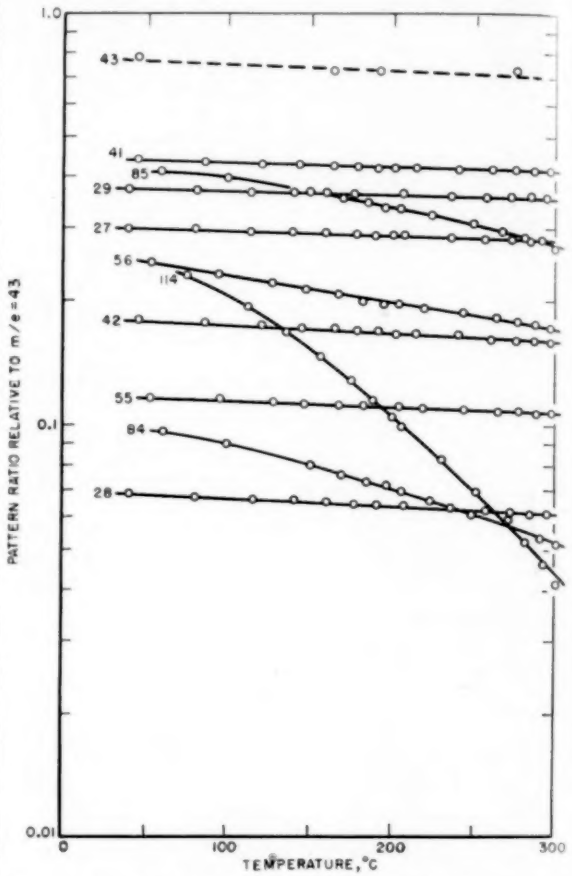

FIGURE 2. *Plot of the effect of temperature on the pattern ratios of selected peaks of n-octane.*

The ordinate for the 43 peak is in terms of sensitivity (divisions per micron) with a scale 100 times that indicated.

straight lines [4] and the slope of these curves at 250° C in units of percentage change per degree centigrade has been taken as the temperature coefficient for the sensitivity and for the pattern ratio. The temperature coefficient for the sensitivity of any ion other than the base peak is equal to the temperature coefficient of the base peak plus the temperature coefficient of the pattern ratio. A temperature of 250° C has been selected as appropriate to the range of normal operating temperatures for the Consolidated mass spectrometer. However, most of the curves are nearly linear, and, in general, the pattern ratios and sensitivities change very slowly with temperature. Berry has used a similar method of evaluating temperature coefficients but has computed values at 160° C.

[3] The following definitions are used: The sensitivity is the ion current per unit pressure in the gas reservoir, the base peak is the maximum peak in the spectrum, and the pattern ratio is the intensity of any other peak relative to the base peak.

TABLE 1. *Temperature coefficients of pattern coefficients and of sensitivity for paraffin hydrocarbons* [a]

m/e	n-Butane	n-Hexane	2-me-Pentane	3-me-Pentane	2,2-me$_2$ Butane	2,3-me$_2$ Butane	n-Octane	2,4-me$_2$ Hexane	2,5-me$_2$ Hexane	me$_4$ Butane	n-Decane
27			+0.02	+0.06	+0.08	+0.07	−0.04	−0.05	−0.03	+0.04	−0.04
28			−.03	+.01	+.07	+.07	−.06	−.02	−.04		−.05
29			+.01	+.07	+.11	+.03	−.02	0	−.02	+.07	−.05
41			+.01	+.03	+.07	+.02	−.02	−0.01	−.03	+.05	−.04
42			−.06	+.02	+.02	−.06	−.06	−.08	−.04	+.05	−.10
43	*−0.15*	+0.03	*−.06*	0	+.09	*−.01*	*−.03*	*−.01*	*−.03*	+.12	*−.01*
53						+.02					
55					+.05	+.02	−.04		−.05	+.01	−.06
56				−0.13	−.26		−.15	−.18	−.13	−.27	−.11
57		−.11		*−.09*	*−.16*		−.04	−.06	−.09	*−.19*	−.03
58	**−.35**										
70			−.25	−.15	−.34	0			−.21		−.16
71			−.13	−.06	−.05	−0.14			−.13		−.06
84							−.31	−.36			
85					−.35	0	−.22	−.21			
86		**−.51**	**−.85**	**−.78**	**−.94**	**−.69**					
99										−.24	
110									−.85		
112									−.59		
113									−.77		
114							**−.90**	**−1.3**	**−1.1**	**−1.3**	
142											**−1.1**

[a] Temperature coefficients are in units of percentage change per degree C. Numbers in italics are temperature coefficients of the sensitivity of the base peak. All other numbers are temperature coefficients of the pattern ratio. Temperature coefficients of the pattern ratios of molecule ions are given in boldface type. Sensitivity coefficients for peaks other than the base peak are given by the sum of the number in italics and the number given.

TABLE 2. *Temperature coefficients for mass spectra of miscellaneous hydrocarbons and other gases* [a]

m/e	1-Hexene	1-Octene	1-Decene	Propyne	4-me-1-Pentyne	1-Octyne	Cyclo-Hexane	Benzene	N^{14}N^{15}	A [b]
26								+0.09		
27	+0.01	−0.04	0		+0.09	0	0	+.07		
28	0	−.04	−0.02		+.08	0	+0.03			
29	−0.01	−.03	0		+.02	+0.02	+.01		*−0.18*	
39				0	+.04			+.07		
40				*−0.14*	+.03					*−0.23*
41	*−.05*	*−.03*	*−0.01*		+.05	+.01	+.01			
42	−.07	−.02	+.01		−.01	−.02	+.01			
43	−.03	*0*	+.04		+.07	*−.10*	+.01			
50								+.07		
51								+.03		
52								+.11		
53										
54					+.02					
55	−.06	−0.03					−.02			
56	−.09	−.10					*−.06*			
57		−.12								
67					*−.11*		−.03			
68							−.10			
69	−.21	−.10	+.05				*−.06*			
70	−.20	−.21	−.09							
76								0		
77								+.01		
78								*−.17*		
79						−.05				
80						−.23				
81	--				−.05	−.19				
82					**−.97**	−.25				
83		−.21	−.18				−.09			
84	**−.41**	−.23	−.26				**−.22**			
95						−.24				
96						−.26				
112		**−.83**								
140			−1.2							

[a] See footnote to table 1.
[b] A^{++}, $m/e=20$, has a temperature coefficient of +0.04 for the pattern ratio and of −0.19 for the sensitivity.

As shown in figure 2, most of the ions give a small negative slope, whereas the molecule ion ($m/e=114$) has a large slope of −0.9 percent per degree. There is a fivefold change in the relative intensity of this peak in the temperature range of 100° to 300° C.

Tables 1 and 2 give temperature coefficients for all of the mass peaks measured in the hydrocarbons, nitrogen and argon. These values have been read from plots like that shown in figure 2 for *n*-octane. Values of the temperature coefficient of the sensi-

UNIVERSITY OF MICHIGAN LIBRARIES

tivity are given for the base peak and are printed in italics. Other values pertain to the temperature coefficient of the pattern ratio. Coefficients of the pattern ratio for molecule ions are printed in boldfaced type, excepting four compounds the molecule ions of which are also the most abundant ions. For these compounds, values of the sensitivity coefficients are given and are printed in italics.

A change in the pattern corresponding to a temperature coefficient of 0.01 percent per degree is measureable and probably significant for the larger peaks. The uncertainty in the measurement of the temperature coefficient of sensitivity is several times as large as this. Some of the molecule ion peaks are very small, and their temperature coefficients are subject to an uncertainty of at least 10 percent of the value given. In 1-octyne the molecule ion peak at $m/e=110$ is almost entirely accounted for by the C^{13} isotope of the 109 peak, $C_8H_{13}^+$. Consequently, the molecule ion is immeasurably small.

The nitrogen measurements were made on a mixture of N^{14} and N^{15} in which the $N^{14}N^{15}$ molecule was the most abundant. The temperature coefficient is probably not significantly different from that of ordinary nitrogen. The experiment was made to investigate a possible temperature effect on the patterns of isotopic nitrogen molecules, but the results were negative.

In tables 1 and 2, compounds have been divided into paraffins and other hydrocarbons for convenience in tabulation only. We see no significant difference in temperature coefficients between saturated and unsaturated compounds. In all hydrocarbons, as in *n*-octane, the molecule ion has the largest temperature coefficient, and in most cases it has by far the largest value with a range of values from -1.3 to -0.14. Temperature coefficients for the sensitivity of the base peak have small values ranging from 0 to -0.2. Pattern ratios sometimes have small positive temperature coefficients of $+0.1$ or less

The peak at $m/e=110$ in 2,5-dimethylhexane is the result of a metastable transition arising from a molecule ion of mass 114, which loses two hydrogen atoms after traversing the ion accelerating field to give an ion with an apparent mass of approximately 110 rather than 112. One would expect a higher energy level for the excited state corresponding to the metastable dissociation. As the temperature coefficient of the 110 peak is definitely less than that of the 114 peak, it would appear reasonable that increased temperature results in increased probability of excitation to the metastable state.

Table 3 summarizes the temperature coefficients of pattern ratio and of sensitivity for all of the molecule ions in tables 1 and 2. For most of the molecules the two coefficients are nearly equal, as the temperature coefficient of sensitivity of the base peak is relatively small. Stevenson [3] has pointed out that there is an inverse correlation between the temperature effect and the fraction of total ionization contributed by the molecule ion. The last column in table 3 gives this fraction for the various molecules. The fraction is computed from published spectra [6].

TABLE 3. *Temperature coefficients for pattern and sensitivity of molecule ions in Percentage per degree at 250° C*

Number	Compound	Pattern coefficient	Sensitivity coefficient	i_m*/sum of ions*
1	n-Butane	−0.35	−0.50	0.040
2	n-Hexane	−.51	−.62	.025
3	2-Me pentane	−.85	−.91	.009
4	3-Me pentane	−.78	−.87	.007
5	2,2-Me_2 butane	−.94	−1.1	.0000
6	2,3-Me_2 butane	−.69	−0.70	.011
7	n-Octane	−.90	−.93	.017
8	2,4-Me_2 hexane	−1.3	−1.3	.004
9	2,5-Me_2 hexane	−1.1	−1.2	.009
10	2,2,3,3-Me_4 butane	−1.3	−1.5	.0001
11	n-Decane	−1.1	−1.1	.013
12	1-Hexene	−0.40	−0.45	.044
13	1-Octene	−.83	−.83	.014
14	1-Decene	−1.2	−1.2	.008
15	Propyne		−0.14	.41
16	4-Me-1-Pentyne	−0.97	−1.1	.005
17	Cyclohexane	−.22	−0.28	.16
18	Benzene		−.17	.43
19	Argon		−.23	1.
20	Nitrogen		−.18	0.94

* Ratio of molecule ion peak to sum of mass peaks at 250° C.

Figure 3 is a plot of the data in the last two columns of table 3 showing the correlation between the temperature coefficient of sensitivity and the reciprocal of the ratio in the last column of table 3. Ordinates give the logarithm of the ratio, and abscissae give the temperature coefficient. The compounds are identified by referring to the index numbers in table 3. Except for two of the points there is a good correlation between the two quantities plotted. The two compounds that give points far above the curve, 2,2-dimethylbutane and 2,2,3,3-tetramethylbutane, have very small molecule ion peaks; and although the measurements are quite inaccurate, the evidence is fairly convincing that the curve cannot be extrapolated to very small values of the ratio of molecule ion to total ionization.

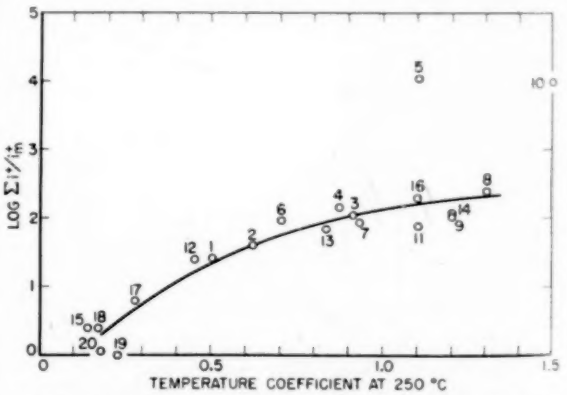

FIGURE 3. *Correlation of the temperature coefficient of the molecule ion with the fraction of total ionization contributed by the molecule ion.*

IV. Discussion of Results

These measurements are in satisfactory agreement with published results on temperature effects. Stevenson's measurements [3] indicate values of −0.21 for the temperature coefficient of sensitivity of argon and −0.18 for nitrogen. (These values are based on data read from published curves). Our values were −0.23 and −0.18, respectively. Berry's [4] values for the molecule ion of *n*-butane (at 160° C) were −0.3 for the coefficient of the pattern ratio and −0.6 for the coefficient of the sensitivity. Our values (table 3) were −0.35 and −0.50, respectively. His values for 2,4-dimethylhexane are −1.0 and −1.4, as compared with values of −1.3 for both coefficients in table 3. Berry's values for temperature coefficients of other mass peaks in this spectrum and in 2,2,3,3-tetramethylbutane differ in detail however from data in table 1.

The sensitivity for monatomic gases and stable molecules will decrease with increasing temperature because of the decrease in gas density, and because the collecting efficiency of the mass spectrometer decreases with increasing kinetic energy of the ions. Stevenson [3] has shown that the temperature effects for the rare gases, N_2 and CO_2 conform to theory. The gas density effect will give a temperature coefficient of −0.10 percent per degree, and the collecting efficiency will decrease by an amount that depends on the instrumental operating conditions. In the Consolidated mass spectrometer the ion accelerating voltage and the voltage drawing ions from the ion source vary inversely as the mass of the ions, so there will be a larger temperature coefficient for larger values of m/e. The small differences in temperature coefficients of sensitivity for A^+ and A^{++} and for A^+ as compared with N_2^+ are accounted for by this mass effect.

The temperature coefficients for molecule ions of most of the hydrocarbons listed in table 3 are much larger than the approximate value of −0.2 percent per degree arising from the changing gas density and collecting efficiency. The experiments suggest that higher temperatures result in an increased probability of excitation to states corresponding to ionization with dissociation rather than to states corresponding to ionization alone. This accounts for the inverse correlation of the temperature coefficients and the relative size of the molecule ion. Furthermore, for stable molecules in which the energy of the excited state corresponding to dissociation is considerably higher than that of the state corresponding to ionization, the temperature coefficient of the molecule ion would be expected to be small, and a large fraction of the total ionization would be contributed by the molecule ion. For benzene and propyne the temperature coefficients are actually slightly less than for monatomic gases (the small difference may not be significant), and the molecule ions are evidently quite stable.

For other molecules, a decrease in the molecule ion peak with increasing temperature must result in an increase in some of the fragment ions, and it is to be expected that the total ionization will have a small negative temperature coefficient comparable to that of a monatomic gas. The data in tables 2 and 3 support this conclusion, for although the spectra are incomplete most of the large peaks are included. Thus, in *n*-octane if each temperature coefficient of sensitivity is multiplied by the peak height and the sum of these products is divided by the sum of the peaks, the resulting weighted mean temperature coefficient of sensitivity is approximately −0.1 percent per degree. This indicates that the probability of ionization of a molecule is not affected by temperature, but the dissociation of the ions into fragments is temperature sensitive.

The stability of a molecule ion may be measured by the appearance potential of the molecule ion as compared with that of the fragment ions. These potentials are known for a few of the molecules listed in table 3, and data are given in table 4. The third column gives the appearance potential of the molecule ion, the fourth column is the lowest appearance potential at which a fragment ion appears. The fifth column is the difference of these two potentials, and it measures the stability of the molecule ion in electron volts. The last column is the temperature coefficient of sensitivity from table 3. The molecule ion must have an excess of energy equal to or greater than the value in column 5 to dissociate spontaneously and give a fragment ion. The appearance potentials of propyne have not been measured, but the isomer propadiene (allene) has a nearly identical mass spectrum, and it must have nearly the same appearance potential. As appearance potentials are subject to uncertainties of several tenths of a volt, the small differences listed for these compounds are quite uncertain. (The two sets of values for *n*-hexane indicate uncertainties of the same magnitude as the differences.)

TABLE 4. *Stability of molecule ions and temperature coefficient of sensitivity*

Compound	Reference	Appearance potentials			Temperature coefficient
		Molecule ion	Fragment ion	Difference	
		Volts	*Volts*	*Volts*	
Nitrogen	[7]	15.7	24.3	8.6	−0.18
Benzene	[8]	9.8	15.5	5.7	−.17
Propyne					−.14
Propadiene	[9]	9.9	12.5	2.6	
Cyclohexane	[8]	11.0	11.7	.7	−.28
n-Butane	[10]	10.34	10.94	.6	−.50
n-Hexane	[11]	10.2	10.2	0	−.62
	[13]	10.1	10.9	.8	
2-me Pentane	[13]	10.0	9.5	−.5	−.91
3-me Pentane	[13]	9.8	10.5	.7	−.87
2,3-me$_2$ Butane	[13]	10.1	10.9	.8	−.76

The data indicate that benzene and propyne are quite stable compared to the other hydrocarbons listed, and one would not expect to find appreciable thermal dissociation at 300° C. This is consistent with the experimental values of the temperature coefficient. Molecule ions of most of the compounds listed in table 3 probably have stabilities of a few tenths of a volt or less. Thus, from the energy

UNIVERSITY OF MICHIGAN LIBRARIES

viewpoint, there is no difficulty in understanding why the heavier hydrocarbons have small molecule ion peaks with a large negative temperature coefficient. It is to be noted, however, that in the mass spectrometer the molecule ions must spontaneously dissociate in less than 10^{-6} seconds to be recorded as fragment ions, and the thermal dissociation energy must come from internal vibrational or rotational energy. Ions undergoing any collisions with walls or other molecules are not recorded. It would not be impossible for an ion of negative energy to be observed provided the transition to the dissociated state involved a long half-life compared with 10^{-6} seconds. Fox and Langer [12] find that in *n*-butane, fragment ions $C_3H_7^+$ and $C_3H_6^+$ appear at the appearance potential of the molecule ion in very low abundance and then increase sharply in abundance at a potential a few tenths of a volt higher. This effect is probably related to the temperature effect discussed in this paper and suggests a serious difficulty in the accurate measurement of appearance potentials.

Berry [4] has pointed out the practical implications of the temperature effect in chemical analysis. Accurate control of the temperature of the ionization chamber is essential for reproducible results, and this is more important for heavy hydrocarbons in the gasoline range than for light gases. In a comparison of results with different instruments, temperature differences can be a more important factor than differences in the other operating conditions. As temperature gradients undoubtedly exist in the ionization chamber, accurate control of the temperature at one point may not be sufficient to insure reproducible spectra. It has been suggested that a better way to maintain reproducibility of spectra is to maintain a constant pattern ratio for the molecule ion of *n*-butane by slight variations in the indicated temperature of the ionization chamber. We have not yet seen experimental evidence, however, to prove that this is better than accurate temperature control at one point.

The authors are grateful to Helen Dean for aiding in the measurement of peak heights in most of the mass spectrograms.

V. References

[1] J. A. Hipple, St. Louis meeting of the Am. Inst. Chem. Eng. (Nov. 1944).
[2] R. E. Fox and J. A. Hipple, J. Chem. Phys. **15**, 208 (1947).
[3] D. P. Stevenson, J. Chem. Phys. **17**, 101 (1949).
[4] C. E. Berry, J. Chem. Phys. **17**, 1164 (1949).
[5] V. H. Dibeler and F. Cordero, J. Research NBS **46**, 1 (1951) RP2169.
[6] Catalog of mass spectral data, Am. Petroleum Inst. Project 44.
[7] H. D. Hagstrum and J. T. Tate, Phys. Rev. **59**, 354 (1941).
[8] A. Hustrulid, P. Kusch, and J. T. Tate, Phys. Rev. **54**, 1037 (1938).
[9] J. Delfosse and W. Bleakney, Phys. Rev. **56**, 256 (1939).
[10] D. P. Stevenson and J. A. Hipple, J. Am. Chem. Soc. **64**, 1588 (1942).
[11] T. Kambara, J. Phys. Soc. Jap. **1** and **2**, 25 and 57 (1946).
[12] R. E. Fox and A. Langer, J. Chem. Phys. **18**, 460 (1950).
[13] M. B. Koffel and R. A. Lad, J. Chem. Phys. **16**, 420 (1948).

WASHINGTON, September 15, 1950.

Journal of Research of the National Bureau of Standards Vol. 46, No. 2, February 1951 Research Paper 2179

Absorption and Emission Spectra of Promethium

William F. Meggers, Bourdon F. Scribner, and William R. Bozman

Five milligrams of promethium ($^{147}_{61}$Pm) separated from fission products at the Oak Ridge National Laboratory, were loaned by the United States Atomic Energy Commission for this investigation. The absorption spectrum of this sample in solution was plotted between 3500 and 10000 angstroms; the principal bands have wavelengths 494.5, 548.5, 568.0, 685.5, 735.5 millimicrons (±0.5 millimicrons). Small portions of the sample were dried on copper electrodes employed in photographing alternating-current arc and spark spectra with a concave grating of 22-foot radius. Excepting Sm, into which Pm decays, no other rare earths could be detected in this sample, but common chemical contaminants were troublesome. Between 2200 and 6900 angstroms the wavelengths and relative intensities of more than 2,200 new spectral lines were determined, but it was not possible to differentiate Pm I and Pm II lines with the light sources employed. The strongest Pm lines have wavelengths 3892.16, 3910.26, 3919.09, 3957.74, and 3998.96 ±0.02 angstroms. Hyperfine structure is suspected in some Pm lines, indicating that the nuclei of $^{147}_{61}$ Pm atoms possess mechanical and magnetic moments. Confirming the findings of the Oak Ridge National Laboratory, both the absorption and the emission spectrum identify this fission product as a new element of rare-earth type; they provide positive proof that the long-sought element with atomic number 61 has been discovered.

I. Introduction

In a paper read before the Bohemian Academy and the Russian Association of Scientists in 1902, Brauner [1] [1] came to the conclusion that only seven elements remained to be discovered. One of these, he said, must lie between neodymium and samarium because the atomic weights of these two elements differed by 6.1 units, whereas the average difference between the atomic weights of two neighboring rare earths is only 3 units. This was undoubtedly the first prediction of a missing rare earth, which ever since has been the object of search and controversy. Moseley's [2] discovery in 1913 of a quantitative relation between Röntgen frequencies and atomic numbers confirmed Brauner's prediction and fixed the atomic number of the unknown rare earth as 61.

In 1926 reports of the concentration and identification of the element with atomic number 61 came practically simultaneously from three different sources. A neodymium concentrate from Brazilian monazite was submitted to X-ray examination by Cork, James, and Fogg [3], who reported that seven L-series lines corresponded to predicted lines of element 61. Harris, Yntema, and Hopkins [4] claimed that the fractionation of cerium group material as double magnesium nitrate concentrated element 61 between 60 Nd and 62 Sm. They based their claim to the discovery of this element on three different lines of evidence: five arc-spectrum lines (3305.8, 3329.1, 3342.5, 3378.0 and 3379.2 A) common to pure Nd and Sm and to intermediate fractions, the presence in intermediate fractions of absorption bands (5,816 and 5,123 A), which became stronger as those of Nd and Sm became weaker, and the presence of two lines (2.2781 and 2.0070 A) in the X-ray spectrum near the theoretical positions for $L\alpha_1$, and $L\beta_1$, of element 61 for which they proposed the name illinium. Rolla and Fernandes [5] reported that experiments with commercial didymium oxide yielded fractions showing variations in absorption spectra and X-ray lines proving the presence of element 61, for which they proposed the name florentium. Up to the present time none of these "discoverers" has substantiated their claims, nor have any other scientists succeeded in separating element 61 from natural sources. Recent application of Mattauch's rule [6] and of considerations [7, 8] on nuclear instability lead to the conclusion that element 61 is either nonexistent in nature or could occur only with extremely low abundance.

Following the discovery of artificial radioactivity in 1934, several attempts have been made to produce isotopes of element 61 by bombarding other rare earths with particles accelerated in cyclotrons. Thus, indications were obtained [9, 10] that an unstable isotope of element 61 may be produced by bombarding praseodymium with alpha particles, but the amounts made in this manner were too small to investigate the atomic weight and properties other than radioactive. The first positive identification of isotopes of element 61 came in 1946 when Marinsky, Glendenin, and Coryell [11] separated and chemically identified 47-hour and 3.7-year half-life isotopes found among uranium fission products. From a fission yield of 1.4 percent the former was judged [12] to have an integral mass of 149, and the latter with a fission yield of 2.6 percent was found [12] with the mass spectrometer to have atomic weight 147. The discoverers of element 61 proposed [13] that this new element be named prometheum (symbol Pm).

The separation of milligram quantities of element 61 from fission was described in 1948 by Parker and Lantz [14]. Portions of this sample were used by Burkhart, Peed, and Spitzer [15] for the measurement of four lines in the Röntgen K spectrum, and by Peed, Spitzer, and Burkhart [16] for the measurement of six lines in the Röntgen L spectrum, thus obtaining evidence that the material was element 61. Three milligrams of sample recovered from the X-ray

[1] Figures in brackets indicate the literature references at the end of this paper.

UNIVERSITY OF MICHIGAN LIBRARIES

tube were then applied to investigations of optical emission and absorption spectra. Part of this sample was used by Feldman [17] to photograph a portion of the arc spectrum in the ultraviolet; seven lines (3366.05, 3377.64, 3391.25, 3418.67, 3427.42, 3441.09, 3449.81 A) characteristic of element 61 were reported, but the five lines previously presented by Yntema [18] were not confirmed. The remainder of this sample was used by Parker and Lantz [19] for an investigation of the absorption spectrum of element 61 in which they found ten principal bands with wavelengths 459.5, 493.5, 548.5, 568.0, 629.0, 685.0, 702.7, 737.2, 785.0, and 810.0 mμ. The spark spectrum of element 61 was first investigated by Timma [20], who published approximate intensities and wavelengths for 59 lines ranging from 3629.8 to 4381.9 A.

At the request of the National Bureau of Standards, the United States Atomic Energy Commission supplied on loan 5 mg of $^{147}_{61}Pm$ for the purpose of studying the optical spectra of this fission product in some detail. The sample was delivered in March 1949, and a preliminary report on the absorption and emission spectra of promethium [21] was given at a meeting of the Optical Society of America on March 11, 1950. In the present paper the authors present the methods and results of their investigations of spectroscopic properties of the last discovered rare-earth element, now called promethium [22].

II. Absorption Spectrum of Promethium

The 5-mg sample of Pm was received in the form of the nitrate; this was dissolved in 0.5 ml (H_2O+HNO_3) to make a concentration of 10 mg Pm/ml, that is, 0.030-molar Pm $(NO_3)_3$ solution. This pink-colored Pm solution was transferred to a 1-cm quartz cell of a Model DU Beckman Quartz spectrophotometer for the observation of absorption bands. A diaphragm limiting the exit light beam to a height of 2 mm was mounted in the filter slide ahead of the solution, and the absorption cell was elevated in its holder so that the light beam could pass unobstructed through the solution. Transmittance measurements were made relative to a blank cell containing water. Before making observations on Pm the instrument was checked with a 0.076-molar solution of $Nd(NO_3)_3$, and then the wavelength scale was carefully calibrated from 253.6 to 1128.7 mμ by using Hg, Ne, and H lines. During the run on Pm, transmittance measurements were made at intervals of 5 mμ or less. The results were plotted, and a curve drawn to represent the absorption spectrum of Pm is reproduced in figure 1. From this curve the wavelengths of at least eight absorption bands characteristic of Pm were estimated with an uncertainty of less than 1 mμ. The wavelengths representing maximum absorption in each band are shown in table 1, where they are compared with similar values (and molar extinction coefficients) reported by Parker and Lantz [19]. The agreement is exceedingly good. In addition to the eight principal bands given in table 1, our absorption observations suggest the existence of five faint bands with approximate wavelengths 403, 450, 590, 628, and 803 mμ. The first of these coincides with 402.5 mμ reported by Parker and Lantz [19], and ascribed to Sm because this is the strongest absorption characteristic of Sm and because Pm naturally transmutes

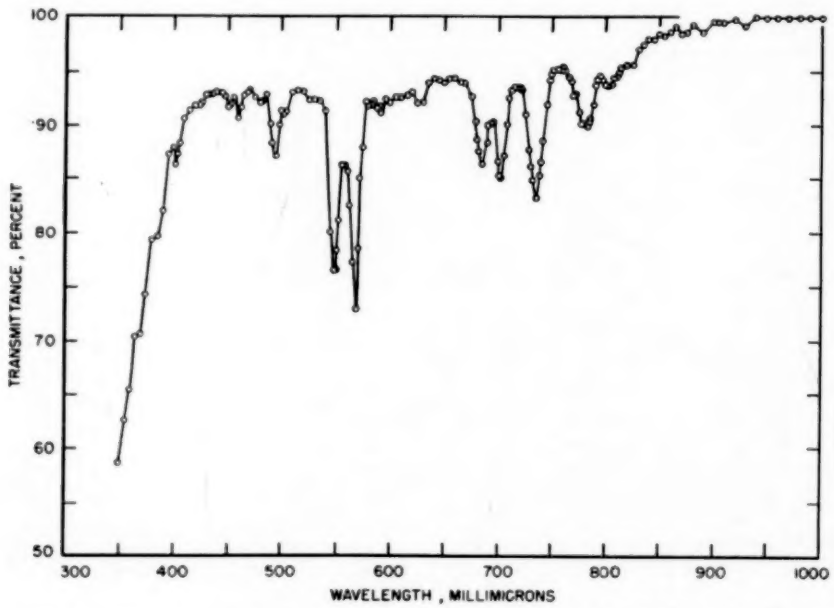

FIGURE 1. *Absorption spectrum of 0.030-molar promethium nitrate solution (10 mg* Pm/*ml).*

to Sm. The faint bands at 450 and 590, although not mentioned by Parker and Lantz [19], are also discernible in their absorption curves, while the last two may correspond to the faintest bands reported by them to have wavelengths 629.0 and 810.0 mμ, respectively. These weak bands probably deserve further investigation to prove that they belong to Pm. These descriptions of the absorption spectrum prove that Pm is a rare earth, resembling Nd or Sm in possessing strong, relatively sharp, bands. These bands are uniquely characteristic of Pm; they cannot be confused with bands belonging to other rare earths, least of all with those reported for illinium [4].

TABLE I. *Principal absorption bands of promethium*

NBS	Parker and Lantz	
Wavelength	Wavelength	Molar extinction coefficient
mμ	mμ	
459.5±0.5	459.5±0.5	0.7
494.5±0.5	493.5±0.5	1.2
548.5±0.5	548.5±0.5	2.3
568.0±0.5	568.0±0.2	2.3
----------	629.0±1.0	0.5
685.5±0.5	685.0±0.2	1.3
702.5±1.0	702.7±0.3	1.6
735.5±0.5	737.2±0.2	1.9
784.0±1.0	785.0±0.2	1.1
----------	810.0±0.1	0.6

III. Arc and Spark Spectra of Promethium

Because Pm is a typical rare earth, like Nd or Sm, its arc and spark spectra could be expected to consist of thousands of lines of moderate to weak intensity. Furthermore, because all rare earths are easily ionized, the second spectrum is strongly excited in arcs as well as in sparks and the first spectrum can be generated strongly in arcs only if ionization can be restrained in some way. In all complex spectra, especially those of rare-earth elements, it is highly desirable to differentiate the first and second spectrum; otherwise it is hopeless or meaningless to find regularities among the spectral lines. Before making any arc or spark spectrograms of Pm, some preliminary tests were made with Sm to determine if two different excitation conditions afforded by the Applied Research Laboratory Multisource unit, and successfully employed by Meggers and Scribner [23] in separating the first two spectra of Tc, could be applied to rare earths. The answer was no.

Previous experience with arc spectra of rare earths on copper and on carbon electrodes showed that the second spectra were somewhat enhanced in carbon spectrograms, but this method was not applied to Pm because the sample was too small and the cyanogen bands would interfere seriously.

Finally, experiments were made to restrain the ionization in the alternating-current arc by adding sufficient cesium to a rare earth. Trials with pure Sm samples admixed with 20, 10, 5, or 2 percent of Cs showed that the addition of Cs actually weakened both Sm spectra, but Sm II more than Sm I. By comparing relative intensities of Sm lines in spark spectrograms with alternating-current arc spectrograms obtained by adding 5 percent of Cs to the sample, it was indeed possible to distinguish between Sm I and Sm II lines. When the same conditions were imposed on Pm, the results were disappointing; the Pm I lines could not be distinguished from Pm II lines by comparing line intensities in juxtaposed spectrograms made with oscillatory arc and spark discharges, even when 5 percent of Cs was added to the arc sample. It was suspected that these efforts to sort Pm I and Pm II were frustrated by the abundance of common chemical impurities, which probably equalized ionization in all the light sources that were tried.

The light sources consisted of oscillatory arc or spark discharges between ¼-in. copper rods bearing 50 to 400 μg of Pm on clean machined ends. These electrodes were mounted in a stainless-steel cylindrical cell provided with a quartz window at one end and with an air exhuast through a glass-wool filter designed to trap the vaporized Pm for future recovery. Although the first electrodes were circular in cross section, the later ones were machined with rectangular ends about 3 mm wide to reduce lateral fluctuations of the discharge and concentrate more light on the spectrograph slit. After the copper electrodes were cut, a thin layer of wax (one drop of a solution of 0.1 g of Apiezon *M* in 100 ml of petroleum ether) was dried on the machined ends. Then with the aid of a remote control pipette, Pm solution was transferred to the electrodes and dried with an infrared heat lamp. The duration of exposure for spectrum photography was limited to 30 or 40 seconds, because successive use of the same loaded electrodes showed that nearly all of the added material was burned off in this time, and a longer time of exposure only enhanced the spectrum of copper.

Spectrograms were made with a concave grating of 22-feet radius and 15,000 lines per inch. In the first order spectrum the resolving power is nearly 50,000 and the reciprocal linear dispersion about 5 A/mm. A slit width of 22 μ was used.

Three positions of the grating and 20-in. plate holder recorded the spectrum between 2,200 and 9,000 A with successive exposures on three types of photographic plates. The region 2,200 to 4,700 A was photographed on Eastman 103-uv sensitized plates, the region 4,400 to 6,900 A on II F sensitized plates, and 6,500 to 9,000 A on I N hypersensitized plates. In the long-wave region, the ARL Multisource unit strongly excited the spectra of atmospheric nitrogen and oxygen, and the spectrum of Pm was disappointingly weak. For that reason we are restricting this report to observations on Pm spectra between the limits 2,200 and 6,900 A.

Because Pm decays by β^- emission to Sm, a spectrogram of pure Sm was recorded beside each Pm spectrogram. By sliding a slotted diaphragm in front of the slit, a series of adjacent spectrograms was made as follows: iron arc, copper spark, samarium spark on copper, promethium spark on copper, iron arc as shown in figure 2. On some spectrograms, exposures to promethium arc on cop-

UNIVERSITY OF MICHIGAN LIBRARIES

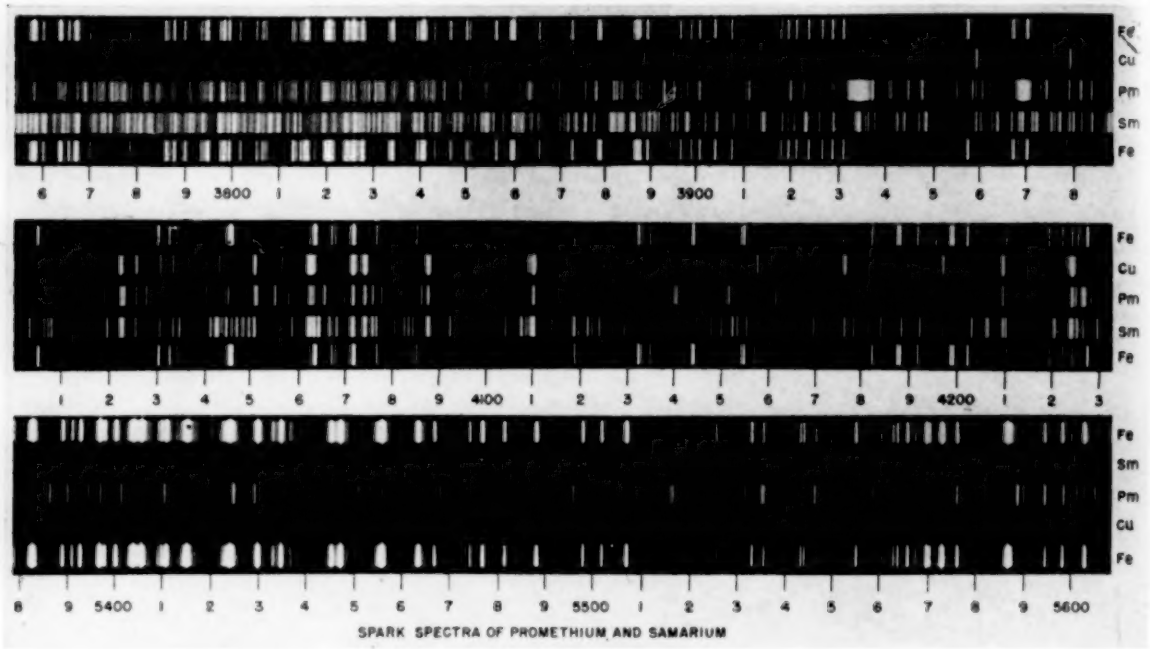

FIGURE 2. *Spark spectra of promethium and samarium.*

per and to copper arc were inserted before the final iron. At least two satisfactory spectrograms were made for each of the first two spectral ranges mentioned above, and the best ones were measured twice. This gave at least six determinations for lines appearing in the overlapping portions of these ranges. The positions of Pm lines relative to iron standards were measured to 0.001 mm with an excellent 50-cm comparator constructed by the Gaertner Scientific Corp. All lines appearing in the Cu plus Pm spectrograms that were not duplicated or masked in the Cu comparison spectra were measured, even though many were easily recognized as impurities. The principal lines of Sm appeared in the Pm spectrograms with about 1 or 2 percent of their intensity in the Sm comparison spectra, and many such lines were measured as internal standards to check the final wavelengths. Incidentally, it appears that accurate measurements of intensity ratios of Pm:Sm lines at intervals of several years could lead to an independent determination of the half life of Pm. These Sm lines are omitted from our Pm table, but a few approximate coincidences are retained because intensity ratios indicate that real Pm lines are present.

Table 2 contains the measured wavelengths and estimated relative intensities of 2,249 new spectral lines believed to belong to Pm atoms and ions. It is most likely that a majority of these lines are characteristic of Pm^+ ions, but some, especially in the visible spectrum, may belong to neutral Pm atoms. Unfortunately, it was not possible with the available sample to differentiate the Pm I and Pm II lines with the light sources employed. Whether or not the impurities in this first sample can be blamed for equalizing excitation in different sources remains an open question. Excepting a trace of Sm, no other rare earths could be detected spectroscopically in this Pm sample, but common chemical impurities were abundant and troublesome. In all, nearly double the number of lines reported in table 2 were measured on Pm spectrograms, but those not reported were identified as belonging to Mg, Ca, Sr, Ba, Li, Na, K, Cr, Mn, Fe, Co, Ni, Si, Zn, Pb, and Al. It is possible that some real Pm lines have been masked by impurity lines, or atmospheric lines, and it is certain that in such a rich spectrum some Pm lines have been obscured by the principal lines of copper, 3248, 3274, 5106, 5153, 5218, 5700 and 5782 A. The agreement of wavelength values derived from different spectrograms, and also the agreement with the wavelengths of impurities, indicates that the values presented in table 2 are rarely uncertain by more than ± 0.02 A.

TABLE 2. *Emission spectra of promethium*

λ=Wavelength; *c*=complex; *d*=double; *h*=hazy; *H*=very hazy; *l*=shaded to longer waves; *s*=shaded to shorter waves; *w*=wide

λ	Intensity	λ	Intensity
6872. 76	2	6661. 25	10
6858. 58	5	6659. 05	40
6857. 21	2	6653. 34	2
6843. 07	2	6652. 50	6
6840. 19	2	6649. 97	8
6837. 08	1	6643. 72	3*h*
6832. 45	3*h*	6639. 55	2*h*
6831. 09	6*h*	6637. 34	2*h*
6824. 06	2	6635. 32	4
6822. 47	1	6635. 07	1
6818. 18	3	6628. 17	1
6811. 68	20	6625. 54	10*h*
6810. 55	2*h*	6623. 14	5*h*
6809. 47	1	6622. 08	3
6802. 95	4*h*+Sm	6614. 45	4*h*
6798. 92	8	6613. 93	5*h*
6798. 25	2*h*	6613. 27	3
6797. 22	2*h*	6598. 11	8
6796. 87	10	6592. 29	10
6793. 56	6	6586. 39	10
6787. 81	2	6576. 03	8
6783. 50	1	6567. 27	10?
6783. 09	10	6558. 48	10*h*
6776. 07	5*h*	6554. 47	4*h*
6774. 66	2*h*	6553. 24	4*h*
6773. 21	2	6550. 58	4
6772. 29	30	6546. 74	1
6771. 00	4*h*	6545. 08	3*h*
6767. 00	1	6544. 33	5*h*
6763. 14	2	6536. 68	6*h*
6762. 01	4	6529. 89	1
6761. 65	3	6529. 49	6
6761. 45	2	6524. 32	3
6758. 91	3	6523. 05	7
6756. 45	20	6522. 03	3
6755. 78	2	6520. 37	5
6755. 11	6	6519. 43	20
6749. 91	5	6518. 18	3*h*
6744. 81	1	6517. 13	3*h*
6742. 30	1	6514. 15	2
6732. 17	4	6509. 74	2
6729. 40	4	6507. 74	2*h*
6727. 93	2*h*	6501. 12	2*h*
6726. 95	8	6490. 36	1*h*
6722. 87	2	6488. 65	1
6720. 30	3	6488. 22	1
6714. 81	5*h*	6475. 93	4
6712. 14	1+Sm	6474. 31	8
6709. 09	2	6469. 91	2*h*
6706. 27	10	6469. 35	1
6698. 82	3	6468. 84	2
6698. 63	4	6467. 36	7
6696. 39	4	6464. 59	2
6692. 65	7	6453. 78	1*h*
6691. 82	3	6452. 20	3
6690. 09	15	6451. 72	1
6686. 2	5*wc*	6450. 98	3*h*
6680. 89	20	6448. 90	2
6668. 94	9	6446. 97	1
6665. 00	2*h*	6446. 05	5

TABLE 2. *Emission spectra of promethium*—Continued

λ	Intensity	λ	Intensity
6443. 27	2*h*	6322. 39	2*hd*
6442. 49	2*h*	6318. 06	2
6440. 74	2*h*	6316. 04	1
6438. 04	4	6314. 20	10
6436. 57	10	6311. 45	2
6433. 98	1	6309. 68	2
6430. 92	5	6306. 77	3
6429. 65	10	6306. 56	5
6428. 61	6	6304. 17	5*l*
6427. 85	2	6302. 42	2
6426. 00	8	6300. 67	2
6425. 71	4	6298. 03	3
6424. 85	5	6294. 20	2
6422. 59	5	6289. 93	8+Sm
6420. 83	6	6287. 31	1
6418. 53	3	6286. 01	2*h*
6416. 25	2	6284. 03	1
6415. 98	5	6280. 65	2*h*
6415. 23	1	6274. 51	4
6413. 15	4	6266. 71	1
6412. 63	2	6264. 54	1*h*
6411. 46	1*h*	6263. 25	10
6409. 99	4	6261. 1	3*Hl*
6401. 53	2	6259. 29	1
6401. 28	6	6257. 94	2
6400. 89	3	6257. 43	2
6399. 87	2*h*	6252. 85	1
6395. 86	1	6251. 64	4*c*
6390. 22	2	6248. 83	3*h*'
6389. 51	2	6244. 52	1
6386. 52	4	6242. 95	3*h*
6383. 74	6	6236. 88	1*h*
6383. 48	3*h*	6234. 32	4*hc*
6379. 89	2	6232. 06	3*hc*
6378. 98	1	6230. 42	2*h*
6378. 24	4	6228. 75	2*h*
6375. 88	2	6226. 58	1
6375. 17	2	6225. 68	2
6373. 62	2	6224. 38	3*h*
6372. 18	2*h*	6223. 01	1
6371. 22	1*h*	6220. 24	1
6369. 47	1	6219. 00	1
6366. 00	5*ld*	6217. 10	1
6360. 57	3	6215. 96	1
6359. 14	2*h*	6211. 97	2*h*
6356. 57	1	6208. 91	20
6356. 01	4	6207. 47	2
6352. 74	1	6206. 53	2*h*
6351. 22	2*h*	6202. 80	2*h*
6348. 79	2*h*	6201. 82	6
6343. 63	2*h*	6201. 13	2
6341. 52	3*c*	6199. 44	1*h*
6339. 14	1	6194. 82	2*h*
6334. 02	6*c*	6191. 81	3
6333. 55	1	6188. 77	1
6332. 99	3	6186. 31	1
6329. 32	3	6184. 52	10
6326. 93	3	6183. 63	2*h*
6323. 74	2*h*	6180. 01	2
6323. 55	3*h*	6179. 36	3*h*

UNIVERSITY OF MICHIGAN LIBRARIES

TABLE 2. *Emission spectra of promethium*—Con.

λ	Intensity	λ	Intensity
6177. 85	3*h*	6027. 11	20
6175. 35	3	6025. 70	8*c*
6173. 41	2*h*	6022. 74	4
6171. 74	2*h*	6022. 12	2*h*
6159. 53	10	6018. 29	5
6156. 14	3*c*	6015. 15	1
6152. 00	4*hc*	6014. 16	1
6151. 70	4	6013. 68	1
6147. 65	1*h*	6012. 73	3*hc*
6134. 64	2*h*	6009. 09	2*h*
6133. 99	2*h*	6008. 04	3
6133. 35	1*h*	6006. 10	1
6132. 05	1	6003. 50	4
6126. 79	3	5997. 74	1
6121. 08	3	5997. 09	15+Ba
6120. 70	1*h*	5996. 03	1
6119. 38	2	5995. 24	1*h*
6117. 35	3	5994. 24	1
6116. 67	2	5992. 44	4
6114. 90	10	5988. 59	2*hl*
6109. 72	2	5987. 13	10*c*
6107. 27	1*h*	5983. 06	3*c*
6101. 10	6	5982. 40	4*c*
6100. 16	6	5981. 71	1
6097. 84	2*h*	5979. 09	3*d*
6097. 23	3	5978. 41	2
6096. 04	2*h*	5977. 44	1*h*
6094. 69	2	5974. 98	1*h*
6094. 11	3*h*	5973. 52	1*h*
6090. 41	2	5972. 19	2
6089. 27	1*h*	5967. 83	6*h*
6087. 41	1	5967. 17	1
6085. 41	20	5963. 00	15
6081. 62	2*h*	5960. 08	10*c*
6079. 64	3	5959. 15	1
6076. 40	10	5956. 65	1
6074. 68	7*dc*	5956. 39	3
6073. 81	4	5955. 33	3
6072. 92	3*c*	5954. 48	2
6070. 09	3+Sm	5950. 82	7
6069. 84	5*c*	5949. 37	1
6069. 00	1	5946. 49	40*c*
6067. 52	1	5943. 29	1*H*
6067. 00	10*c*	5941. 94	3
6060. 96	2*h*	5941. 60	1
6060. 45	1	5939. 62	2
6055. 20	1	5937. 21	1
6054. 31	2	5935. 90	4
6053. 85	2	5934. 99	2*h*
6053. 29	4	5934. 33	2*h*
6052. 57	15*c*	5933. 09	2
6050. 15	8*c*	5930. 85	1
6047. 22	4*c*	5928. 03	3*c*
6043. 33	2*h*	5927. 72	4*c*
6042. 07	2	5927. 17	25*c*
6039. 71	1*h*	5925. 87	1
6038. 31	5*hc*	5925. 08	1
6030. 08	7	5923. 84	2*c*
6028. 69	1*h*	5922. 02	1
6027. 86	3*c*	5917. 39	6*c*

TABLE 2. *Emission spectra of promethium*—Con.

λ	Intensity	λ	Intensity
5915. 73	1	5806. 29	5
5914. 89	2	5804. 13	2
5910. 62	1	5802. 01	1
5907. 42	1	5801. 85	1*h*
5905. 87	1*H*	5801. 38	1
5905. 48	1	5800. 91	1*h*
5904. 67	4	5800. 69	2*h*
5904. 16	4	5798. 26	1
5901. 87	8	5794. 59	1*h*
5899. 76	15	5794. 07	1*h*
5884. 85	1	5793. 32	3
5882. 16	1	5792. 17	1
5881. 24	1	5790. 78	1*h*
5880. 58	1	5789. 30	2
5878. 76	10*c*	5789. 15	3
5876. 51	1*H*	5788. 89	6
5875. 31	20*c*	5785. 74	1
5873. 09	4*h*	5784. 70	1
5872. 56	1*h*	5783. 50	2
5869. 51	1*h*	5780. 75	4
5868. 79	30*c*	5778. 19	3
5868. 14	1	5777. 18	3
5867. 72	2	5774. 03	2
5866. 13	2	5773. 68	3
5863. 65	3	5772. 19	10*c*
5862. 80	2*h*	5769. 32	3
5862. 05	4	5769. 12	2
5861. 16	1*H*	5768. 11	20
5853. 04	1*h*	5766. 92	2
5849. 64	3	5765. 73	2
5844. 67	1	5765. 36	6*c*
5841. 71	1	5764. 73	1*h*
5841. 00	8	5760. 86	3
5837. 32	1	5758. 15	2
5836. 65	1	5756. 80	1*h*
5835. 70	4	5755. 82	2*h*
5834. 96	5*c*	5754. 91	1*h*
5833. 58	1*h*	5753. 72	5*c*
5833. 05	3*c*	5752. 46	1
5831. 54	1	5751. 74	2
5830. 23	1	5749. 75	1
5827. 84	8*c*	5748. 98	1*h*
5825. 90	2	5747. 96	3*c*
5825. 60	1	5747. 36	3
5823. 91	50	5747. 12	4
5823. 52	3*h*	5746. 80	2
5822. 39	1	5746. 17	3*h*
5822. 03	1	5744. 29	1
5821. 72	1	5742. 39	1
5820. 83	2	5740. 81	5
5820. 03	1	5739. 74	2
5818. 31	1	5735. 58	1
5817. 92	1	5734. 75	2
5816. 04	2*h*	5733. 48	1
5815. 92	1	5731. 52	2
5813. 65	1*h*	5730. 79	2
5812. 82	2*h*	5729. 83	2*h*
5812. 01	2*h*	5726. 41	1*h*
5810. 14	6	5725. 05	1
5809. 85	3	5723. 41	1

TABLE 2. *Emission spectra of promethium*—Con.

λ	Intensity	λ	Intensity
5721.01	3*cd*	5604.92	3*h*
5719.38	3	5604.07	3
5718.46	1*h*	5596.58	2*hd*
5714.62	2	5596.22	1
5713.00	2*hd*	5595.74	2*hc*
5712.42	8*s*	5594.87	2*h*
5709.65	2*h*	5591.75	2
5708.83	4	5584.08	2
5704.92	1*H*	5582.62	1*H*
5704.32	1	5580.68	1*h*
5704.12	1*h*	5578.82	3
5702.00	1	5576.46	1
5699.64	2	5576.01	80
5697.06	2*cd*	5573.31	2
5693.28	1	5572.87	1
5692.01	1	5571.03	4*c*
5691.00	1	5569.72	1
5687.34	1	5569.27	1*h*
5686.95	2*h*	5566.56	1
5685.99	2	5565.64	2
5684.92	1*h*	5563.32	4
5681.37	2	5561.72	20
5679.88	1	5560.15	1*h*
5676.23	2	5558.38	15
5674.20	1	5557.61	2*h*
5673.23	2	5556.86	12
5672.57	1*h*	5555.21	1*h*
5671.01	2	5551.28	2*h*
5670.54	1	5549.47	2
5669.45	1	5546.76	5
5668.72	3	5546.09	80
5667.79	2*h*	5543.70	3*h*
5664.95	1*h*	5540.69	1
5662.36	1	5539.75	3
5660.16	2	5539.09	1
5659.70	2	5537.35	1
5657.55	4*c*	5534.95	18
5655.83	1	5531.61	8
5655.04	2	5531.33	3
5654.50	3*c*	5530.70	4*cd*
5651.04	1	5528.59	4
5649.72	6	5528.01	1*h*
5649.07	1*h*	5527.27	1
5645.31	1	5524.91	1
5644.45	1	5524.12	1
5642.83	1*h*	5521.61	5
5641.28	20	5520.84	1
5639.46	4	5518.22	3
5638.32	5	5516.41	10
5636.00	1	5515.79	8
5635.36	1	5514.75	3
5634.45	7	5513.30	6*c*
5634.29	1	5510.21	1
5632.41	1	5508.53	4
5630.72	1	5508.26	2*c*
5616.74	2	5500.84	1
5610.90	7	5500.49	2
5606.50	1*h*	5498.86	4
5605.84	3*c*	5496.21	1
5605.25	3	5495.44	15

TABLE 2. *Emission spectra of promethium*—Con.

λ	Intensity	λ	Intensity
5491.65	5*wc*	5390.48	5
5487.52	2	5389.46	2
5478.36	4	5386.99	4
5477.77	2	5386.79	5
5476.45	2	5382.91	1
5474.85	2	5380.77	1*wh*
5474.16	1	5380.29	2
5473.84	1	5374.27	1
5473.29	1*h*	5371.34	4
5472.14	1*h*	5370.63	1
5471.30	1	5369.06	1*h*
5470.02	1*c*	5365.87	4
5469.45	1*h*	5361.13	2*w*
5468.75	1	5364.65	1
5468.36	1	5362.80	3
5467.62	10	5358.65	1*h*
5466.64	3*h*	5357.67	1*h*
5464.19	1*h*	5354.56	6*sd*
5463.04	2*wc*	5352.28	1*h*
5462.27	1	5351.33	1*h*
5457.45	2	5351.05	1
5456.98	1*h*	5348.26	8
5456.10	1*h*	5347.03	2
5455.50	4	5346.12	8
5453.03	5+*Sm*	5344.83	1
5451.52	3	5344.40	2
5450.81	3	5342.43	1
5450.45	4*cd*	5341.29	2+*Sm*
5447.81	2	5339.18	2*h*
5445.79	1	5335.55	2*h*
5442.44	1	5334.73	2*h*
5441.93	1	5334.02	2
5440.01	3	5333.47	1*h*
5437.38	1	5331.53	1*h*
5436.21	3	5330.50	1
5434.54	2	5327.89	2*wh*
5431.26	1	5320.84	1*h*
5429.03	15	5319.80	8
5428.21	4	5318.58	15
5425.66	1	5314.24	4*hc*
5424.76	18	5311.78	1
5424.52	20	5310.63	1
5422.32	2*h*	5308.84	10
5421.50	1	5305.25	1
5420.33	1*h*	5302.01	8
5419.14	3	5299.89	2
5416.54	2*h*	5296.96	1
5415.29	2	5295.09	2
5414.58	1	5294.62	1
5413.71	1	5293.91	20
5411.30	2*h*	5291.08	1
5410.43	20	5290.79	1
5408.79	2	5289.41	1
5407.06	2*c*	5287.00	1*h*
5406.58	2	5281.40	4
5402.54	1	5280.42	1
5401.60	7	5279.51	1*h*
5398.98	1	5277.26	1
5397.32	8	5276.45	2
5394.83	6	5274.93	1

UNIVERSITY OF MICHIGAN LIBRARIES

TABLE 2. *Emission spectra of promethium*—Con.

λ	Intensity	λ	Intensity
5270. 62	50	5119. 83	1
5263. 10	1	5119. 36	1
5262. 40	15	5116. 92	2*w*
5257. 50	2	5111. 56	1
5257. 09	4	5107. 87	2
5251. 84	5	5100. 73	5
5250. 19	1	5097. 26	15
5249. 27	1	5096. 14	1
5246. 93	2*h*	5094. 80	6
5246. 31	40	5092. 35	1
5242. 35	2*h*	5089. 32	15
5238. 95	1	5085. 79	4
5236. 64	30	5081. 34	1
5236. 25	50	5080. 50	15
5229. 35	1	5074. 99	2
5228. 53	1	5072. 12	1
5225. 10	25	5067. 32	10
5224. 84	8	5060. 68	1
5215. 95	15	5058. 29	15
5214. 67	1	5057. 54	1
5208. 08	50	5054. 93	1
5203. 76	1	5050. 70	1
5203. 24	1	5045. 28	6
5196. 19	1	5044. 84	2*h*
5194. 03	30	5044. 30	5+Sm
5192. 36	1	5039. 58	1
5189. 81	1	5035. 30	1
5188. 16	2	5030. 80	2
5187. 57	1	5028. 75	1
5185. 92	1	5026. 69	1
5185. 01	10	5021. 66	3*c*
5180. 19	1	5016. 14	10
5173. 26	2*h*	5015. 05	2
5171. 57	50	5010. 33	4
5170. 77	1	5007. 50	1
5169. 69	30	5005. 79	1
5165. 65	2	4999. 14	1
5165. 32	3*hc*	4998. 25	2
5164. 62	2	4997. 10	15
5162. 79	2	4993. 63	1
5161. 12	1	4996. 31	2
5158. 74	2	4987. 18	1
5153. 82	40	4984. 47	3
5150. 98	3	4982. 91	1
5150. 30	2	4979. 53	2
5148. 93	1	4975. 36	8
5147. 58	1	4974. 74	3
5146. 27	10	4974. 27	2
5145. 11	8	4972. 44	1
5142. 52	1*h*	4971. 41	10
5140. 53	1*h*	4959. 45	8
5136. 22	1*hc*	4956. 84	1
5135. 38	1	4954. 04	3
5134. 28	1	4950. 80	1
5129. 68	1	4946. 89	3
5127. 33	15	4945. 04	2*d*
5125. 39	2	4943. 28	8
5122. 48	1	4939. 11	1
5121. 44	25	4937. 21	1
5120. 60	4*c*	4932. 99	5

TABLE 2. *Emission spectra of promethium*—Con.

λ	Intensity	λ	Intensity
4918. 29	1	4728. 65	2
4917. 20	1	4728. 37	4
4915. 23	2	4726. 32	1
4913. 18	5*d*	4724. 21	1
4904. 27	1	4720. 98	1
4903. 07	1	4718. 64	1
4902. 05	1	4716. 99	2
4901. 25	2	4714. 90	1
4900. 28	2	4710. 76	2
4892. 51	5	4707. 02	3
4890. 62	2	4703. 93	1
4887. 01	1	4703. 21	1
4882. 60	1	4702. 53	1
4872. 43	2	4697. 48	2
4870. 41	2	4696. 80	1
4869. 80	1	4695. 71	3
4868. 33	1	4694. 64	1
4866. 23	2	4694. 26	1*h*
4865. 72	4	4692. 80	1
4865. 32	3	4691. 02	1
4860. 73	10	4690. 48	1
4858. 89	1	4682. 93	3
4852. 72	2	4682. 24	1
4847. 76	2	4678. 14	1
4846. 59	4	4677. 93	1
4840. 69	5	4675. 98	1
4837. 66	5	4675. 47	1
4831. 14	1	4671. 24	2
4829. 70	2	4666. 85	2*hd*
4829. 48	5*d*	4665. 20	4
4827. 68	1	4663. 47	2
4824. 15	8*c*	4663. 17	1
4813. 44	2	4661. 48	2*h*
4811. 94	5	4660. 76	1
4810. 21	3	4658. 31	2
4809. 54	3	4656. 85	1
4801. 33	7	4656. 10	2
4799. 86	3	4653. 39	2
4798. 97	8	4653. 23	2
4798. 09	3	4651. 90	3*h*
4789. 51	1	4649. 51	1+Sm
4789. 26	4	4647. 03	1
4781. 29	3	4645. 04	1
4779. 36	1	4643. 75	1
4773. 46	6	4643. 35	2
4769. 86	2	4641. 02	2*d*
4764. 46	2	4640. 14	1
4762. 57	15	4638. 34	2
4759. 00	10	4637. 47	3
4758. 36	2	4635. 81	1
4757. 72	2	4633. 46	2
4753. 80	1	4632. 79	2
4745. 12	2	4632. 03	1
4744. 84	1	4630. 17	1
4739. 76	1	4628. 70	7
4739. 08	10	4627. 59	1
4738. 23	1	4625. 97	1
4737. 97	1	4625. 29	3
4734. 26	5	4624. 42	1
4732. 79	1	4623. 68	3

TABLE 2. *Emission spectra of promethium*—Con.

λ	Intensity	λ	Intensity
4623. 11	1*h*	4511. 57	2
4621. 57	1	4509. 37	10+Cu
4620. 30	1	4502. 12	1
4619. 75	1	4500. 14	60
4618. 61	1*h*	4498. 24	3
4617. 01	2	4496. 82	3
4615. 85	10	4492. 05	25
4611. 96	1	4490. 45	1*h*
4609. 83	1	4489. 56	1
4607. 76	1	4485. 02	1
4605. 70	3	4481. 58	2
4602. 07	3	4479. 35	1
4601. 83	1	4477. 46	20
4601. 09	1*h*	4475. 96	1
4600. 24	1	4475. 31	5
4598. 92	2*h*	4475. 05	7
4597. 55	1	4473. 23	30
4591. 29	1	4471. 50	20
4590. 23	3	4470. 61	2
4589. 42	1+Sm	4468. 14	1
4589. 13	1	4465. 80	5*h*
4586. 29	3	4464. 53	2
4585. 49	1	4461. 55	1
4583. 31	1	4459. 95	20
4579. 48	1	4458. 94	5
4578. 60	5	4456. 87	1
4575. 27	2	4453. 96	80
4573. 99	1	4452. 84	10+Sm
4573. 05	1	4451. 81	5
4572. 15	1	4451. 05	1
4570. 37	1	4450. 65	1
4569. 46	2*h*	4450. 26	1
4568. 14	1	4446. 90	60
4565. 58	1	4445. 41	50
4564. 85	10	4443. 67	15
4563. 42	1	4438. 69	1
4560. 35	2	4432. 51	40
4559. 21	1	4430. 58	2
4558. 58	3	4427. 17	1
4557. 02	1	4425. 11	3
4556. 60	4	4423. 99	5
4556. 01	1	4422. 28	1
4549. 80	1	4421. 15	15+Sm
4547. 54	1	4419. 35	10+Sm
4546. 00	1	4418. 15	8
4545. 41	4*h*	4417. 98	100
4538. 51	3	4417. 63	2
4535. 69	3*d*	4414. 09	10
4534. 15	1	4412. 48	1
4531. 70	1	4411. 77	4*d*
4529. 20	80	4406. 73	1
4527. 68	2	4404. 78	1
4526. 07	1	4404. 26	10
4525. 61	1	4403. 07	1+Sm
4525. 19	60	4402. 31	4
4522. 65	8	4401. 97	1
4519. 08	3	4401. 58	1
4517. 92	1	4400. 29	2
4514. 63	2	4400. 17	2
4513. 54	10	4396. 83	1

TABLE 2. *Emission spectra of promethium*—Con.

λ	Intensity	λ	Intensity
4396. 26	1*h*	4310. 36	3
4391. 62	1	4306. 11	3
4389. 68	4	4305. 49	5
4389. 25	2	4303. 86	20
4388. 76	20	4303. 51	5
4388. 51	2	4300. 63	2
4387. 05	5	4300. 32	1
4381. 87	20	4298. 65	1
4381. 17	18+Ca	4295. 70	1
4374. 90	2	4295. 11	7
4374. 41	1	4294. 12	3
4373. 82	1	4293. 38	4
4372. 88	6	4291. 78	2
4372. 52	4	4288. 77	2
4369. 87	1	4287. 78	6
4369. 63	2	4287. 56	1
4367. 23	3	4284. 59	2
4365. 99	5*l*	4281. 97	2
4365. 07	10	4279. 07	1*h*
4364. 58	1	4278. 48	1*h*
4363. 87	1*h*	4277. 83	1
4362 06	4+Sm	4277. 52	10
4360. 79	5*h*	4275. 54	4
4359. 90	4*h*	4273. 29	2
4359. 49	1	4270. 83	1
4356. 97	2	4270. 30	2*h*
4356. 59	2	4265. 32	1
4354. 16	6	4264. 59	3
4353. 48	1*h*	4264. 30	1
4349. 27	1	4263. 33	3
4348. 74	1	4260. 23	3
4346. 92	1	4259. 12	4
4346. 35	3	4254. 93	4
4342. 11	30	4254. 78	6
4340. 52	15	4254. 13	1
4337. 45	20	4249. 38	3*w*
4336. 53	30	4247. 10	1
4334. 87	2	4242. 98	2
4334. 64	2	4241. 93	1
4333. 73	1	4240. 29	5
4333. 40	3	4239. 98	3
4332. 04	20	4238. 26	20*h*
4330. 60	5	4234. 14	15
4330. 06	10	4233. 39	4
4329. 59	1	4231. 74	3
4328. 29	6	4231. 41	1
4327. 41	2	4230. 87	4
4325. 88	25	4228. 74	2
4325. 04	1	4228. 35	10
4324. 84	1	4226. 25	3
4323. 86	1	4225. 06	8
4320. 63	1	4223. 02	2
4319. 46	1	4222. 15	20
4317. 82	1	4219. 08	2
4317. 28	2*h*	4218. 24	1
4315. 65	2	4216. 30	10
4315. 36	10	4214. 61	1
4314. 20	1	4213. 96	2
4313. 12	5	4210. 97	2
4311. 57	2*h*	4208. 42	1

UNIVERSITY OF MICHIGAN LIBRARIES

TABLE 2. *Emission spectra of promethium*—Con.

λ	Intensity	λ	Intensity
4207. 63	1	4129. 33	4
4207. 21	10	4128. 26	1
4206. 37	2	4127. 83	1
4205. 39	1	4125. 46	1
4204. 10	5	4124. 89	2
4201. 56	3	4124. 63	1
4194. 70	20	4123. 97	15+Sm
4192. 92	30	4122. 45	5
4190. 63	3	4119. 97	2
4189. 49	1	4119. 36	2
4188. 96	2	4119. 16	1
4186. 03	2	4116. 16	2*h*
4185. 74	20	4114. 34	1
4180. 06	1	4112. 19	1
4179. 66	5	4111. 32	3
4179. 31	1	4109. 62	2
4178. 93	2	4108. 73	2
4177. 99	1	4108. 27	1
4177. 47	4	4104. 83	6
4174. 74	3	4101. 76	2
4174. 06	1	4100. 55	1
4172. 79	7	4100. 03	5
4171. 46	6	4098. 87	4*h*
4169. 18	1	4096. 72	2*h*
4168. 33	1	4096. 40	2
4167. 69	1	4096. 19	5
4162. 61	1	4095. 72	2*d*
4162. 03	6	4095. 33	3
4161. 50	15	4095. 11	3
4161. 21	10	4094. 76	2
4159. 99	4	4092. 25	3+Sm
4158. 57	2	4090. 79	5
4158. 20	2	4090. 37	3
4157. 45	1	4088. 95	3
4156. 90	1	4086. 10	50*w*
4156. 07	5	4085. 10	3*h*
4155. 67	1	4083. 07	6
4154. 06	3	4082. 49	10
4151. 60	10	4081. 74	10*d*
4151. 40	8	4079. 91	2
4151. 04	3	4079. 56	3
4150. 74	3	4078. 84	2
4149. 45	2	4078. 30	1
4147. 43	1	4075. 85	60
4146. 54	3*l*	4075. 06	2
4143. 85	1	4073. 60	1
4142. 87	10	4070. 48	1
4142. 33	2	4069. 90	10
4140. 46	25*d*	4069. 08	5
4140. 08	3	4067. 92	3
4139. 72	15	4066. 45	5
4137. 98	1	4065. 90	3
4137. 26	2	4065. 65	15
4136. 48	4	4065. 36	2
4136. 16	3	4064. 79	2
4135. 11	9	4063. 27	1
4133. 66	3	4060. 66	2
4131. 87	1*h*	4060. 32	2
4131. 15	1*h*	4059. 72	4
4129. 53	2	4058. 61	3

TABLE 2. *Emission spectra of promethium*—Con.

λ	Intensity	λ	Intensity
4058. 28	1	4000. 83	1
4058. 07	6	4000. 39	1
4057. 07	2	3998. 96	100
4056. 64	3*d*	3997. 83	3
4056. 46	2	3996. 71	3
4055. 20	60*l*	3995. 05	30+N
4053. 63	1	3992. 99	5
4052. 93	4	3987. 90	10
4052. 00	1	3987. 41	1+Sm
4051. 50	30	3987. 10	1
4049. 36	7	3986. 09	2*h*
4048. 55	3	3985. 73	3
4048. 22	2	3983. 71	1
4046. 49	2*h*	3983. 10	10
4045. 37	20	3982. 81	3
4044. 75	4	3982. 23	3
4044. 49	1	3980. 73	50*l*
4042. 89	3+Sm	3980. 41	2
4042. 00	2	3979. 38	2
4040. 74	15*d*	3978. 12	3
4040. 07	4	3976. 98	3*d*
4039. 47	1	3975. 65	4
4038. 94	1	3974. 95	2
4038. 69	1	3974. 38	1
4038. 17	3	3973. 49	5
4036. 48	5	3973. 18	3
4035. 93	2	3972. 63	1
4034. 26	1	3972. 13	6
4032. 45	7	3969. 61	2
4029. 98	1	3965. 64	2
4029. 46	1	3964. 59	1
4028. 84	5*h*	3963. 82	1
4028. 20	25	3961. 98	1
4027. 79	2*h*	3961. 07	2*h*
4026. 98	2	3959. 96	6
4026. 60	4	3959. 74	7
4026. 00	10	3957. 74	100
4023. 70	15	3957. 18	1*h*
4023. 28	5	3955. 88	1
4022. 90	8	3954. 61	3
4021. 75	1	3954. 29	8
4021. 34	5*l*	3953. 97	1
4019. 34	20	3952. 91	2
4018. 68	3	3952. 13	6
4016. 78	1	3950. 65	1*h*
4016. 33	2	3949. 69	10
4015. 54	3	3948. 50	2
4015. 08	1	3947. 79	1+Sm
4014. 81	1	3947. 22	15
4014. 20	25	3946. 85	10
4012. 71	20	3945. 53	1
4010. 55	2	3944. 23	30*h*
4009. 97	50	3943. 95	3+Al
4006. 48	3	3941. 35	2*d*
4006. 31	2	3940. 60	10
4005. 94	4	3940. 13	8
4004. 96	1	3939. 23	1
4004. 22	2	3938. 35	2+Cr
4003. 64	3	3936. 47	80*l*
4002. 86	1	3935. 46	2

TABLE 2. *Emission spectra of promethium*—Con.

λ	Intensity	λ	Intensity
3931. 96	3	3877. 24	3
3931. 55	10	3876. 48	2
3929. 50	1*h*	3876. 15	2
3928. 55	2	3875. 50	2+Sm
3927. 88	2	3875. 34	8
3927. 75	2	3874. 76	2*h*
3926. 81	1*h*	3872. 69	3
3925. 82	2*h*	3871. 84	5
3925. 26	4	3870. 79	2*h*
3924. 99	1	3869. 83	7
3924. 44	2*h*	3869. 62	4
3923. 81	1	3868. 55	6*l*
3922. 33	2	3867. 94	8
3921. 80	15	3866. 79	1
3921. 39	3*h*	3866. 33	4
3919. 09	100*l*	3864. 24	4
3918. 45	2	3863. 62	12*d*
3917. 12	7	3863. 16	8
3915. 94	2	3862. 72	4
3915. 69	1	3861. 15	1
3913. 76	2	3860. 88	1
3913. 48	4	3860. 20	1
3911. 66	1	3857. 98	3*d*
3911. 13	2	3856. 90	1
3910. 76	1	3856. 41	2*h*
3910. 26	100	3854. 62	4*h*
3909. 51	25	3853. 90	3
3907. 83	8	3852. 15	5
3907. 25	5	3850. 84	2*h*
3906. 35	2	3850. 57	2
3904. 40	3	3850. 08	2
3901. 93	3	3849. 46	1
3901. 22	1	3848. 74	15
3900. 99	1	3847. 29	3
3900. 55	1	3846. 30	2*h*
3899. 78	40	3845. 36	25
3899. 36	4	3845. 00	1
3897. 62	2	3844. 33	4*d*
3897. 12	3	3842. 93	40
3896. 35	2*h*	3842. 35	3
3895. 74	6*h*	3842. 22	2
3894. 46	2	3841. 58	2
3894. 11	4*l*	3841. 40	2
3892. 16	100	3841. 21	2
3891. 40	2	3840. 52	8
3889. 71	2	3839. 79	2
3887. 86	1	3835. 76	4
3887. 35	5	3835. 22	3
3886. 56	15	3831. 53	15*d*+Sm
3885. 99	3	3830. 73	9
3885. 69	2	3830. 46	8
3884. 66	2	3829. 08	5
3884. 14	1	3828. 34	8
3883. 05	1	3827. 41	2
3882. 07	10	3825. 90	5+Fe
3881. 37	18*d*+Sm	3824. 83	10
3880. 03	1	3823. 52	8+Cr
3879. 52	1	3823. 00	1
3878. 77	2	3822. 68	2
3877. 63	80*c*	3821. 44	4

TABLE 2. *Emission spectra of promethium*—Con.

λ	Intensity	λ	Intensity
3820. 51	30	3779. 62	2*h*
3820. 07	5	3778. 75	6*l*
3819. 62	5	3777. 35	3
3819. 26	20	3777. 13	5
3818. 26	2*h*	3776. 62	10*h*
3817. 74	1	3776. 02	5
3817. 31	4	3775. 65	6
3816. 36	1	3775. 03	4
3815. 82	10	3774. 58	10*h*
3815. 33	2	3774. 05	3
3813. 73	10	3773. 01	4*d*
3812. 70	2	3772. 61	2+Sm
3812. 36	3	3772. 41	1
3811. 99	2	3771. 98	12
3811. 54	2	3770. 97	9
3811. 33	1	3769. 21	4
3810. 74	2	3768. 97	20
3810. 27	7*h*	3768. 51	2
3810. 05	2	3768. 15	3
3809. 04	5	3767. 49	5
3808. 42	1	3765. 03	1
3806. 92	2*w*	3764. 92	2
3806. 55	1	3764. 62	4
3806. 06	25	3764. 10	3
3805. 78	2	3763. 46	7
3805. 17	1*h*	3762. 32	3
3803. 61	1	3761. 58	3
3802. 99	3*d*	3759. 55	4*h*
3802. 48	15	3758. 98	3*h*
3802. 28	7	3758. 37	5
3802. 08	2	3757. 85	2
3801. 75	1	3756. 55	2+Sm
3801. 31	1	3755. 36	3*d*
3800. 68	2	3754. 88	4*d*+Sm
3800. 30	3	3754. 47	3*h*
3799. 49	5	3753. 76	10*d*
3798. 39	10*h*	3753. 25	10
3798. 17	15	3752. 45	1
3797. 66	2	3751. 59	6
3795. 66	40	3750. 64	1*h*
3794. 54	4	3750. 08	50
3793. 60	3	3748. 54	4
3792. 73	1	3747. 64	3+Sm
3791. 20	15	3747. 10	30
3789. 53	4	3745. 86	50
3788. 46	3	3744. 36	1
3787. 60	1	3743. 90	4*d*+Cr
3787. 33	3	3743. 42	4
3786. 07	2*d*	3742. 51	30
3785. 29	1	3741. 98	2
3785. 03	1	3741. 40	4
3784. 71	4	3740. 56	3
3784. 20	6	3739. 81	2
3783. 82	3	3739. 44	2
3782. 99	1	3735. 53	2
3782. 39	5	3734. 31	10
3781. 98	2*h*	3733. 62	1*h*
3781. 57	6	3733. 03	3
3781. 38	2	3732. 79	3
3780. 40	3	3732. 51	10

UNIVERSITY OF MICHIGAN LIBRARIES

TABLE 2 *Emission spectra of promethium*—Con.

λ	Intensity	λ	Intensity
3730. 46	5*h*	3673. 08	4
3728. 97	2	3670. 02	1
3728. 26	10*d*	3669. 86	6
3727. 79	4	3669. 11	1*h*
3727. 11	2	3668. 47	1
3725. 62	1*h*	3667. 31	7
3724. 87	6+Sm	3667. 04	3
3723. 11	10	3666. 26	10
3722. 71	1	3665. 50	9
3721. 96	8	3664. 94	3
3721. 72	20	3664. 57	1
3719. 62	1	3662. 59	2
3719. 35	2	3661. 08	2
3718. 88	10+Sm	3660. 71	3
3718. 39	1	3660. 54	3
3715. 73	20	3660. 03	4
3714. 54	2	3659. 39	30
3713. 60	1	3658. 63	2
3713. 28	2*h*	3658. 40	10
3712. 59	3	3658. 04	4
3711. 72	80	3657. 59	8
3709. 02	2	3657. 08	2
3708. 34	15*sd*	3655. 80	8
3706. 68	2*h*	3654. 87	2
3705. 22	2*h*	3653. 78	2
3704. 90	1	3652. 13	8
3704. 53	15	3651. 76	2
3704. 21	2	3651. 25	10
3702. 64	40	3650. 54	1
3702. 38	4	3649. 98	10
3701. 65	4	3648. 75	2
3699. 00	15	3648. 35	2
3698. 39	4	3647. 72	2
3697. 50	30	3647. 23	5
3695. 70	1	3646. 29	3
3694. 78	10	3644. 99	2
3693. 49	1	3643. 84	2*h*
3692. 52	30	3643. 58	2*h*
3691. 70	10	3642. 50	1
3691. 11	5	3642. 26	4
3689. 78	40	3641. 65	10+Sm
3689. 47	7	3641. 22	1
3688. 76	1	3640. 74	3*s*
3687. 65	20	3637. 40	2
3687. 26	10	3636. 96	2
3686. 77	8	3636. 48	1
3685. 62	3	3634. 26	30+Sm
3685. 41	5	3632. 25	4*d*
3684. 43	1	3630. 86	3
3683. 67	6	3629. 85	20
3681. 73	6+Sm	3628. 53	3
3680. 89	4	3628. 03	1
3680. 41	10	3626. 28	3
3679. 59	3*h*	3625. 84	1
3679. 14	3	3625. 31	1*h*
3678. 63	18	3622. 94	3*h*
3678. 49	20	3622. 28	5
3675. 86	3	3621. 79	4
3675. 16	1	3620. 90	2
3673. 79	3*h*	3620. 14	15

TABLE 2. *Emission spectra of promethium*—Con.

λ	Intensity	λ	Intensity
3619. 19	1	3574. 52	3
3619. 02	2	3573. 86	4
3618. 13	3	3572. 99	5
3617. 95	1	3572. 45	1
3617. 52	2*d*	3571. 46	1
3615. 58	1	3570. 85	1
3613. 86	2	3570. 54	1
3613. 29	15	3569. 75	2
3612. 15	1	3569. 25	1
3611. 80	6	3569. 02	2
3611. 21	4*d*	3568. 70	1
3610. 74	20	3567. 77	2
3610. 21	4	3567. 01	2
3608. 59	1	3566. 05	1
3608. 09	3	3565. 65	1
3607. 79	2	3565. 32	20
3607. 00	8	3562. 99	8
3606. 73	1	3562. 13	7
3606. 46	1	3561. 62	6
3605. 86	3	3560. 11	1*h*
3604. 09	8	3559. 47	10
3602. 75	2*d*	3557. 83	1
3602. 33	2	3557. 13	3
3601. 43	2	3556. 95	1
3600. 56	5	3555. 89	1*h*
3600. 16	1	3554. 60	1
3598. 79	1	3553. 82	2
3598. 58	2	3553. 61	4
3598. 34	2	3552. 81	1
3598. 26	2	3551. 97	2
3597. 87	2	3551. 63	2
3596. 20	1	3551. 13	5
3595. 50	1	3550. 38	2
3595. 11	5	3550. 17	2
3594. 20	3	3549. 74	1
3592. 93	3	3548. 97	1
3592. 32	2	3547. 52	1*h*
3591. 94	1	3546. 81	1
3591. 65	3	3546. 59	3*d*
3591. 17	3	3546. 33	1
3589. 98	1	3545. 78	3
3589. 56	3	3544. 91	6*d*
3589. 31	2	3544. 03	5*d*
3588. 44	1	3543. 72	1
3587. 81	2	3541. 70	6
3587. 65	1	3540. 72	1
3587. 10	1*h*	3540. 31	1*h*
3586. 42	1	3539. 99	2*h*
3585. 70	6*d*	3538. 80	4
3583. 90	2	3537. 52	2
3583. 04	4	3536. 64	4
3582. 41	3	3532. 26	1
3581. 51	2	3528. 84	2
3580. 11	15	3528. 47	3
3578. 36	1	3528. 01	1
3578. 06	4	3525. 93	1
3577. 43	2	3525. 65	1*h*
3576. 47	1	3525. 00	1
3576. 15	5	3522. 88	3
3575. 94	2	3522. 35	1

TABLE 2. *Emission spectra of promethium*—Con.

λ	Intensity	λ	Intensity
3521.04	2*h*	3412.30	1
3519.14	1	3411.70	1
3518.75	1	3408.67	8+Sm
3517.82	1	3408.06	10
3516.59	1	3404.29	1
3514.84	10	3404.04	2
3512.97	2*d*	3401.32	2
3511.42	3	3400.88	1
3510.88	3*h*	3400.16	1
3509.78	1	3399.81	3
3509.07	1	3398.42	1
3508.58	2*h*	3397.65	2
3508.30	1	3396.67	1
3505.90	3	3396.26	3*d*
3502.47	3*h*	3395.85	2
3501.50	2*h*	3395.15	3
3501.06	2*hd*	3394.17	1
3499.42	2*h*	3393.44	1
3494.06	1	3392.56	2
3490.08	2	3391.28	10
3487.41	3+Sm	3390.66	1
3482.65	4	3387.34	1
3482.14	1	3386.97	1
3481.97	8	3386.76	1
3480.62	20	3386.14	2
3478.62	15+Ca	3384.68	6+Sm
3478.13	3	3383.15	1
3471.98	1	3381.10	2
3471.84	1	3380.23	1
3468.62	1	3379.67	1
3467.20	5*h*	3377.68	9
3462.91	20	3377.02	2
3462.25	2	3376.56	2
3460.25	25	3374.47	2*h*
3456.81	1	3374.17	2*h*
3454.06	1	3371.20	2
3449.81	40	3367.06	2
3448.57	1	3366.05	5
3447.52	1	3364.44	8
3446.89	1	3363.33	1
3442.80	2*h*	3363.02	2
3441.97	1	3360.21	8
3441.16	12	3359.65	3
3439.02	2	3359.29	1
3435.85	3*h*	3359.00	1
3433.21	1	3358.14	10
3432.12	1	3355.84	2
3431.64	2	3354.46	1
3431.19	1	3352.23	4
3430.88	3*h*	3350.48	2
3430.34	1	3345.99	3
3429.49	1	3340.88	4
3428.89	1	3339.18	1
3427.40	50	3336.80	1
3426.99	1	3333.79	3*h*
3422.24	2*h*	3331.73	2
3420.12	1	3331.22	1
3419.06	1	3330.47	1
3418.71	5	3327.64	1
3417.53	1	3327.03	2

TABLE 2. *Emission spectra of promethium*—Con.

λ	Intensity	λ	Intensity
3325.30	3+Sm	3194.64	2
3321.70	1	3192.25	4
3321.21	15+Sm	3187.20	8+Sm
3319.97	1	3186.82	1
3318.85	2	3185.18	6
3318.44	1	3183.88	8+Sm
3314.85	1	3182.54	6
3314.48	3	3174.51	6
3313.40	1	3172.77	10
3311.76	6	3171.47	1
3310.66	8+Sm	3170.58	1
3308.46	1	3169.08	6
3307.05	20+Sm	3167.59	1
3305.39	4	3162.89	3
3304.53	1	3161.48	1
3304.08	1	3161.10	3*w*
3300.42	1	3158.39	4
3299.04	1	3157.27	6
3296.69	1	3145.51	1
3295.65	1	3144.54	4*h*
3294.98	2	3139.34	3
3291.21	1	3133.47	2
3289.68	2	3131.85	1
3287.84	3	3129.53	1
3284.41	1	3126.55	3
3278.79	4	3122.81	1
3271.96	1	3118.76	10
3271.71	1	3117.22	10
3269.59	1	3115.36	10
3268.79	1	3114.36	1
3268.66	2	3108.11	15
3266.39	1	3104.24	6
3265.69	2	3099.46	4
3265.24	1	3096.21	2
3253.00	2	3091.86	15
3252.04	1	3090.19	12
3251.49	1	3089.61	2
3249.98	1	3088.37	4
3241.43	1	3087.83	3
3240.46	3	3086.02	15
3239.86	1	3085.08	4
3239.62	6	3077.70	1
3238.57	4	3077.52	1
3237.29	1	3074.25	4*w*
3236.63	6+Sm	3072.41	30
3232.79	1	3070.08	1
3219.92	1	3067.99	2
3218.61	5	3066.34	5
3211.79	5	3064.05	1
3211.38	2*w*	3061.20	6
3210.37	2*w*	3060.48	8
3207.89	4	3056.06	1
3205.67	4	3054.14	7
3204.51	3	3052.01	1
3203.00	1	3050.59	1
3202.15	3	3050.20	1
3200.79	1	3049.68	1
3200.08	3	3049.53	2
3198.77	1	3047.99	8
3197.95	2	3047.16	1

UNIVERSITY OF MICHIGAN LIBRARIES

TABLE 2. *Emission spectra of promethium*—Con.

λ	Intensity	λ	Intensity
3046.07	2	2843.90	4*w*
3042.12	1	2841.86	15*w*
3041.88	2	2840.82	10*w*
3036.94	1	2839.05	2
3035.50	1	2830.99	5*h*
3033.72	2	2829.63	1
3030.79	1	2826.63	1
3029.52	2	2825.32	3
3029.34	2	2822.15	8*h*
3027.21	3	2820.10	10*h*
3026.23	1	2811.95	2*h*
3025.43	1	2808.05	4
3024.66	1	2794.02	3*w*
3023.54	3	2787.72	5*w*
3019.58	3	2723.17	1
3018.47	8	2671.05	10
3010.31	1	2642.38	1
3008.85	10	2641.93	1
3007.85	2	2638.46	7
3004.59	10	2632.00	15
2990.24	1	2628.87	2
2982.84	6	2610.20	1*h*
2979.58	1	2608.24	4
2963.10	3	2596.04	3
2959.22	2	2589.50	1*h*
2952.25	5	2581.20	1
2946.73	3*h*	2556.18	1
2927.33	2	2502.12	4*w*
2919.36	2	2471.94	3*h*
2916.38	2	2460.86	1
2900.92	1	2453.94	1*h*
2898.02	1*w*	2437.90	2
2889.56	1	2437.45	1
2888.02	1	2429.66	1
2886.89	1	2428.30	2
2885.08	5	2428.16	1
2879.07	2	2420.96	1
2871.78	3	2419.59	1
2860.97	12*d*+Cr	2402.39	2*h*
2857.46	20*c*	2397.44	1
2850.80	5	2385.82	1
2848.21	8*w*	2379.68	1
2846.96	2*c*	2341.17	1*h*
2845.82	1*c*	2337.28	1
2844.99	2*c*		

It is highly desirable that the arc and spark spectra of promethium be reobserved in a greater range with a purer sample, with greater spectrographic dispersion and resolving power, and with a guarantee that Pm I and Pm II lines can be sorted. Until this is accomplished, all attempts to find regularities and recognize atomic energy levels in these spectra will be futile. In the meanwhile, the data presented in table 2 may be regarded as a preliminary description of the spark spectrum of promethium providing positive proof, in addition to that previously obtained at the Oak Ridge National Laboratory [17, 20], that the long-sought element with atomic number 61 has been truly discovered [11]. Although Röntgen spectra were thrice reported as proof of earlier discovery [3, 4, 5] they were never supported by convincing evidence of optical spectra. Both the absorption and the emission spectral data here presented for promethium not only identify this fission product as a new element, but also as one that possesses unmistakable characteristics of a "rare-earth". The strongest emission lines, probably Pm II, have wavelengths 3892.16, 3910.26, 3919.09, 3957.74, and 3998.96 A. These will be important for spectrochemical identification and for testing whether or not Pm can be detected in nature before fission products become abundant and widespread. Hyperfine structure is suspected in some Pm lines, namely, 5868.89, 5875.31, 5927.17, and 5946.49 A, indicating that the nuclei of $^{147}_{61}$Pm atoms possess appreciable mechanical and magnetic moments. This hyperfine structure will be investigated with interferometers at this Bureau.

The authors acknowledge the generous cooperation of the United States Atomic Energy Commission in lending the sample of promethium with which the present investigation was prosecuted.

IV. References

[1] B. Brauner, Nature **118,** 84 (1926).
[2] H. J. G. Moseley, Phil. Mag. **26,** 1024 (1913); **27,** 703 (1914).
[3] J. M. Cork, C. James, and H. C. Fogg, Proc. Nat. Acad. Sci. **12,** 696 (1926).
[4] J. A. Harris, L. F. Yntema, and B. S. Hopkins, J. Am. Chem. Soc. **48,** 1594 (1926).
[5] L. Rolla and L. Fernandes, Z. Anorg. Chem. **157,** 371 (1926); **160,** 190 (1927).
[6] J. Mattauch, Z. Physik **91,** 361 (1934).
[7] H. Jensen, Naturwiss. **26,** 381 (1938).
[8] N. E. Ballou, Phys. Rev. **73,** 630 (1948).
[9] H. B. Law, M. L. Pool, J. D. Kurbatov, and L. L. Quill, Phys. Rev. **59,** 936 A (1941).
[10] C. S. Wu and E. Segré, Phys. Rev. **61,** 203 A (1942).
[11] J. A. Marinsky, L. E. Glendenin, and C. D. Coryell, J. Am. Chem. Soc. **69,** 2781 (1947).
[12] Plutonium Project, J. Am. Chem. Soc. **68,** 2411 (1946).
[13] J. A. Marinsky and L. E. Glendenin, Chem. & Eng. News **26,** 2346 (1948).
[14] G. W. Parker and P. M. Lantz, ORNL–75 (June 1948); AECD–2160 (May 27, 1949).
[15] L. E. Burkhart, W. F. Peed, and E. J. Spitzer, Phys. Rev. **75,** 86 (1949).
[16] W. F. Peed, E. J. Spitzer, and L. E. Burkhart, Phys. Rev. **76,** 143 (1949).
[17] C. Feldman, J. Am. Chem. Soc. **71,** 3841 (1949).
[18] L. F. Yntema, J. Am. Chem. Soc. **46,** 37 (1924).
[19] G. W. Parker and P. M. Lantz, J. Am. Chem. Soc. **72,** 2834 (1950).
[20] D. L. Timma, J. Optical Soc. Am. **39,** 898 (1949).
[21] W. F. Meggers, B. F. Scribner, and W. R. Bozman, J. Opt. Soc. Am. **40,** 262 A (1950).
[22] International Union of Chemistry, XV Conference, Amsterdam (July 1949); Chem. & Eng. News **27,** 2996 (1949).
[23] W. F. Meggers and B. F. Scribner, J. Research, NBS **45,** 476 (1950) RP2161.

WASHINGTON, August 29, 1950.

Journal of Research of the National Bureau of Standards Vol. 46, No. 2, February 1951 Research Paper 2180

A Statistical Solution of a Problem Arising in the Sampling of Leather

John Mandel and Charles W. Mann

The evaluation of the relative merits of different tanning procedures requires that a number of hides or sides [1] of each tannage be subjected to a variety of physical and chemical tests. The destructive nature of these tests makes it desirable to keep to a minimum the number of hides or sides required for test purposes. Moreover, the total number of test specimens for each property should be kept as small as practicable for reasons of economy in leather and labor. Because of the nature of a leather hide, a considerable saving can be realized through a judicious choice of the location on the side from which test specimens for any given property are cut. In this paper a criterion is developed for the evaluation of the suitability of any given side location as a source of test specimens for a given property. It is shown that the coefficient of correlation between the test result on a given location and the average of the test results, on the same property, over the entire side, determines the suitability of this location as sampling location, both from the viewpoint of economy in the number of hides or sides and in the number of specimens required. It is further shown that for any particular property, the number of sides required to detect a given difference between two tanning procedures is inversely proportional to the square of the coefficient of correlation corresponding to the block chosen as sampling location and directly proportional to the square of the coefficient of variation of side averages for the property considered.

I. The Problem

The evaluation of the relative merits of different tanning procedures requires that a number of sides of each tannage be subjected to a variety of physical and chemical tests. It is known, however, that the results of such tests vary appreciably from location to location on the same side, and also, of course, from side to side for the same relative location.

Studies of this variability have been made by Beek [1] [2] and by Beek and Hobbs [2]. Their studies, however, did not include an attempt to define, on the basis of the observed variability, an optimum sampling location on the side. Moreover, their work was limited to a single physical property, namely tensile strength.

For any particular test, the problem naturally arises of finding the "best" location on the side for the selection of a test specimen, or, more generally, of evaluating every location on the side with regard to its suitability for that purpose. As the various physical and chemical tests reflect different properties of the leather, it is reasonable to treat this problem individually for each test.

Information of this type is needed as a basis for sampling leather for research, for specification purposes, and for general testing.

This paper is concerned with the theoretical aspects of the problem of sampling leather. More specifically, the following three parts will be discussed:

1. The planning of an experiment designed to furnish the data, for each of the tests considered, from which the desired information can be extracted. Such an experiment was performed at the National Bureau of Standards.

2. The development of a statistical criterion for the characterization of different positions on the side from the viewpoint of their suitability as test specimen locations.

3. The determination of the number of sides required for the detection, with a prescribed degree of confidence, of variations in the hide properties arising from variations in the tanning procedure.

While the discussion is mainly concerned with the leather problem described above, the statistical development may well apply to a variety of sampling problems in other fields. As this paper deals with principles only, no data will be presented. These will be found, together with the conclusions drawn from them, in a publication that has been submitted to the Journal of the American Leather Chemists Association.

II. The Experimental Plan

Thirty sides were tanned by the same chrome tanning procedure. Each side was then cut into 21 blocks in a rectangular pattern of three rows, parallel to the backbone, and seven columns, perpendicular to the backbone (see fig. 1). Each of the 21 blocks was cut into a number of specimens, such that one or two test specimens of appropriate size

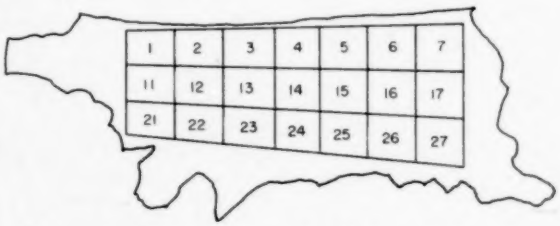

FIGURE 1. *Locations of sampling blocks on leather side*

[1] A side is either one of the halves obtained by cutting a hide along the backbone line.
[2] Figures in brackets indicate the literature references at the end of this paper.

UNIVERSITY OF MICHIGAN LIBRARIES

were available for each property. A total of 10 tests was included in the project. Each specimen was subjected to the test for which it was intended. Thus the data represented the results of 10 tests, on each of 21 blocks of 30 sides.

III. Criteria for the Ranking of Locations

The data from each of the 10 tests were treated separately, inasmuch as a location may be "good" for one test and "poor" for another. Thus the following discussion applies to each test individually. The first object consists in defining a good location. One might think that the best location is the one for which the result varies least from side to side. However, a criterion based on such a consideration disregards an essential desideratum, namely that the characteristic, when measured on the selected location, bear some relationship to the relevant value of this characteristic for the entire side. If, in practice, all 21 locations, that is, the entire side, could be tested, it would be reasonable to characterize the side by the average of the 21 results thus obtained.[3] Such an average will be denoted in this paper by h and referred to as a "side average". Then, the average of a set of h-values, corresponding to a random sample of sides from the lot, is a reasonable measure for the value, characterizing the lot, for the test under consideration.

On the other hand, if it is impractical to carry out the test on all 21 positions, so that a single position must be selected, it seems logical to choose the particular position that best represents the average of the side from which it is taken. Let us denote the result of the test on a particular position P as p. Then, according to this principle, for a good position P, p must represent h in the best possible way.

Consequently the first task is to determine, on the basis of the experimental results, what type of relationship exists between p and h, for each of the 21 positions. Such a study was made, using the data obtained in the experiment described in the preceding section, and it revealed the existence of two types of cases. For some positions, a plot of p versus h, for the 30 sides, shows a mere scattering of points without any discernible pattern or trend. For other positions, however, a definite linear trend is apparent.

Figure 2 shows a typical example taken from the stitch-tear data for each of these two cases. The lower plot represents location 22 and shows a mere random scattering of points, while the upper plot, representing location 14, clearly suggests the existence of an approximate straight-line relationship.

It is evident that locations belonging to the first category are undesirable for sampling purposes, as the position value does not represent in any way the quality of the side for the test under consideration. Attention will therefore be focused on the locations belonging to the second category.

[3] Which value is relevant (e. g. average, largest, smallest) depends primarily on the use of the side in which one is interested. In view of the general nature of our problem the relevant value was taken to be the average of the test results of all 21 locations.

It appears intuitively plausible to select for sampling purposes the position of this category for which the scatter of the experimental points on the p versus h graph is smallest. This, however, is not a sufficient criterion for an adequate sampling position; indeed, in order to detect relatively small differences between side values, the corresponding differences between the values for the selected sampling location should be relatively large; that is, the p versus h straight line should be steep.

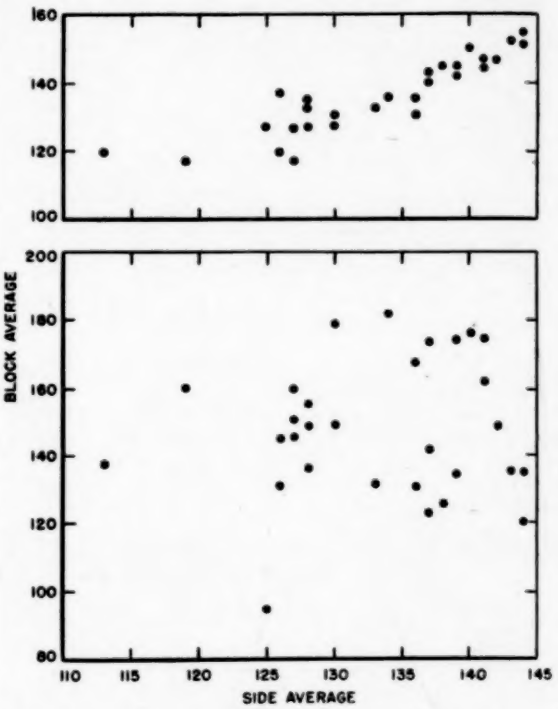

FIGURE 2. *Observed relationship between block average and side average.*

Upper graph, good sampling position: relationship is distinctly linear; lower graph, poor sampling position: no definite relationship exists.

Summarizing, it can be stated that a desirable sampling location P should fulfill the conditions (1) the slope of the p versus h line should be relatively large, and (2) the scatter of the experimental points (h, p) about this line should be small.

IV. Statistical Analysis

In comparing the merits of the various possible sampling locations, the question arises as to how the two criteria formulated in the preceding section should be weighted. For example, the choice between two locations P and P' will appear difficult if P has the higher slope, while P' has the smaller scattering around the p versus h line. It will now be shown that for each physical or chemical test, a single index can be defined for each location that

entirely determines its suitability for sampling purposes. To this end the following definition will be adopted.

A sampling location is said to be better than another if it requires a smaller number of sample sides, for an equal certainty in the final results.

Besides this definition the derivation requires the assumption that the relationship between p and h is linear.

In figure 3, the (p, h) plot is shown for a particular position P. Let p be the value observed, in position P, on a side for which the average value of the characteristic under consideration is h_0. Among all the sides for which the value h happens to be the same (h_0), the values p, in position P, will nevertheless vary, because of biological differences, tanning effects, and test errors. Geometrically, this will result in the fact that p will, in general, not lie exactly on the line, but rather at a variable distance e from it. Likewise, the average h_0 of any particular side will, in general, not be identical with the lot average M. Let us denote by d, the difference between h_0 and M; that is, $d=h_0-M$. The relation between the observed position value p, and the lot average M for which it is the experimental estimate, can be found by noting that the straight line has the equation

$$p_0=b+mh_0$$

where b is the intercept, m the slope, and p_0 the "theoretical" value of p corresponding to the value h_0, that is the value corresponding to the point on the line.

Now, since $p=p_0+e$, we have

$$p=b+mh_0+e$$

and since $h_0=M+d$, we obtain the desired relation

$$p=b+m\ (M+d)+e$$
$$p=b+mM+(md+e) \qquad (1)$$

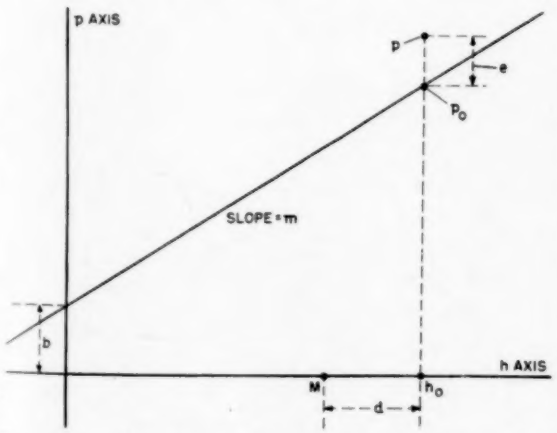

FIGURE 3. *Theoretical relationship between block average, side average, and lot average.*

In this expression, the quantity $(md+e)$ represents the total random fluctuation, analagous to the "error" in the theory of errors. Indeed, if this quantity were known, the value M could be derived from p on the basis of the two parameters b and m. The order of magnitude of this random part is characterized by its standard deviation, which, in accordance with the laws of propagation of errors [3] is given by the relation

$$\sigma=\sqrt{m^2(\sigma_d)^2+(\sigma_e)^2},$$

where σ_d and σ_e are the standard deviations associated with the random fluctuations d and e, respectively.

Suppose now that N sides are taken from a lot, and that the test is carried out in position P of each of these N sides. Then the average of these N test results, which we will denote by $\overline{p}_1$, has a standard deviation equal to $\sigma/\sqrt{N}$, that is

$$\sigma_1=\sqrt{\frac{m^2(\sigma_d)^2+(\sigma_e)^2}{N}}.$$

If, for the purpose of comparing tanning procedures, a sample of N sides is also taken from a second lot, of different tannage, and the test carried out in the same position P on each of these sides, an average $\overline{p}_2$ will be obtained, with a standard deviation:

$$\sigma_2=\sqrt{\frac{m^2(\sigma_d)^2+(\sigma_e)^2}{N}}.$$

It is seen that $\sigma_1=\sigma_2$, provided that the slope m, corresponding to position P, is the same for the two lots and that the fluctuations d and e in the second lot have the same statistical distributions as the corresponding fluctuations in the first lot. Although there is no conclusive evidence for the validity of these assumptions, it seems reasonable to accept them on a tentative basis. It is readily seen that the general principle of the proposed statistical procedure is not dependent on these assumptions, and that situations in which these simplifications do not apply will require only slight modifications in the formulae.

The difference $\overline{p}_1-\overline{p}_2$ constitutes the experimental evidence for any effect of tannage on the test considered. According to the laws of propagation of errors [3], the standard deviation for this difference is given by

$$\sigma_{\overline{p}_1-\overline{p}_2}=\sqrt{\sigma_1^2+\sigma_2^2}=\sqrt{\frac{2}{N}\left[m^2(\sigma_d)^2+(\sigma_e)^2\right]}. \qquad (2)$$

This relation shows that for any observed difference between two lots, the precision of this difference increases (the standard deviation decreases) as the number of sides, N, taken from each lot, increases. From our definition of a "better" sampling location it then follows that the most suitable position is that one for which the quantity $\overline{p}_1-\overline{p}_2$ is known with the greatest relative precision, that is the position for which the ratio of the standard deviation of $\overline{p}_1-\overline{p}_2$

UNIVERSITY OF MICHIGAN LIBRARIES

to its expected value, for any given N, is smallest. The problem thus becomes that of finding the position P for which the ratio

$$\frac{\sigma_{\bar{p}_1-\bar{p}_2}}{\text{Expected value of } (\bar{p}_1-\bar{p}_2)}$$

is a minimum.

The numerator of this expression is given by eq 2. In order to calculate the denominator, let us denote the lot averages of the two lots by M_1 and M_2, respectively. Then, in accordance with eq 1, the expected value of $\bar{p}_1-\bar{p}_2$ is equal to $(b+mM_1)-(b+mM_2)=m(M_1-M_2)$.[4] Accordingly, the ratio that must be made a minimum is equal to

$$\frac{\sigma_{\bar{p}_1-\bar{p}_2}}{\text{Expected value of } (\bar{p}_1-\bar{p}_2)}=\frac{\sqrt{\frac{2}{N}\left[m^2(\sigma_d)^2+(\sigma_e)^2\right]}}{m(M_1-M_2)}$$

$$=\frac{\sqrt{\frac{2}{N}}}{M_1-M_2}\sqrt{(\sigma_d)^2+\left(\frac{\sigma_e}{m}\right)^2}. \qquad (3)$$

Now, for a given number of sides N, the only quantity of this expression that depends on the position P is $(\sigma_e/m)^2$, as M_1 and M_2 are lot values and, σ_d represents the variability of side averages. The minimum of the expression corresponds to a minimum of the quantity σ_e/m.

It is clear now that the single index σ_e/m is the criterion according to which positions must be classified in terms of their suitability as sampling locations. Remembering that σ_e is a measure of the scatter of the (p, h) points about the straight line, and that m represents the slope of that line, it is seen that the statistical analysis confirms the adequacy of the two criteria formulated in the preceding section, and at the same time provides the manner in which they are to be combined for the selection of the best sampling location.

It can also be observed in the expression just given that the larger the index σ_e/m, the larger will have to be the number of sides N to obtain the same relative precision. Thus, the index σ_e/m actually determines the amount of testing required in order to detect tanning effects with a given degree of confidence.

V. The Coefficient of Correlation as a Criterion

It is interesting to note that the index, σ_e/m, which must be chosen as small as possible, is closely related to the coefficient of correlation ρ between p and h.

For a chosen sampling location P, every pair of p and h values can be considered as a random selection from a population of such pairs, since it corresponds to a side selected at random from a population of sides.[5] If it is assumed that this two-variable population is of the Gaussian type, then the coefficient of correlation ρ between p and h can be expressed by the relation ([4])

$$\rho=m\,\frac{\sigma_h}{\sigma_p},$$

where m has the same meaning as above. The standard deviation σ_h refers to the variability of side averages in the lot, that is, $\sigma_h=\sigma_d$, as defined above. The standard deviation σ_p, on the other hand, refers to the total variability of the p values, that is, $\sigma_p=\sqrt{m^2(\sigma_d)^2+(\sigma_e)^2}$ as shown earlier. Thus,

$$\rho=m\,\frac{\sigma_d}{\sqrt{m^2(\sigma_d)^2+(\sigma_e)^2}}=\frac{\sigma_d}{\sqrt{(\sigma_d)^2+\left(\frac{\sigma_e}{m}\right)^2}}. \qquad (4)$$

This relation shows that to a small value of σ_e/m corresponds a large value of ρ. The best sampling location, according to our criterion, is therefore that for which ρ is largest.

VI. Ranking of Sampling Locations

If, for every physical and chemical test, the coefficient ρ were known for every location on the side, there would be a simple solution to the problem of the selection of the most suitable sampling location for each such test. An experiment such as the one described in this paper, based on the testing of 30 sides, permits the calculation of a correlation coefficient for each test and each position. However, the coefficient thus computed, which we will denote by r, is only an estimate for the "true" coefficient ρ, and this estimate will vary from experiment to experiment, because of the chance fluctuations of the p,h points and therefore of the exact location of the p,h line and of the average scatter about this line. Consequently, in comparing positions on the basis of these observed coefficients of correlation, account must be taken of the sampling fluctuations of these estimates, when based on such a limited number of points as 30. This can be done most effectively by grouping the correlation coefficients, for any given property, into a number of groups, such that within each group the differences would not be considered statistically significant, while the differences between successive group averages are significant. One of the difficulties arising in this problem lies in the fact that the precision of an estimated coefficient of correlation depends not only on the sample size (number of points) but also on the value of the corresponding true coefficient. For large values of ρ, the

[4] Indeed, the term $(md+e)$ occurring in eq 1, being a random fluctuation, has an expected value equal to zero.

[5] The randomness in the selection of sides from the lot is essential for the applicability of the method presented in this paper. As has been pointed out by Berkson [5], a coefficient of correlation calculated on a systematically selected sample will depend on the range of values encompassed by the sample, and increase with this range. A coefficient of correlation thus obtained is devoid of any sensible interpretation as a measure of the real degree of interdependence.

precision of r is considerably larger than for small values of ρ. This difficulty can be overcome to a large extent by transforming each r-value into a z-value by means of the transformation ([4])

$$z=\frac{1}{2}\log_e\frac{1+r}{1-r}.$$

It is known that for any value ρ the sample estimates r, when transformed into z-values, have an approximately Gaussian frequency distribution, the mean of which corresponds to the transformed ρ-value and the standard deviation of which is equal to $1/\sqrt{N-3}$, where N is the size of the sample from which r was computed. Since a positive r-value [6] can lie anywhere between 0 and 1, the corresponding z-value can lie anywhere between 0 and ∞. Thus, for any value of ρ, it is theoretically possible to obtain a sample estimate r such that the corresponding z-value will be exceedingly large. However, even for relatively large values of ρ, the sample estimate r will rarely exceed 0.99, and therefore the corresponding z-value will rarely exceed $1/2\log_e(1+0.99)/(1-0.99)=2.65$. Consequently, from a practical viewpoint, this value can be considered as an upper limit for z.

On the other hand, the standard deviation of z, regardless of the value of ρ, is always equal to $1/\sqrt{N-3}$, which for the case of 30 sides, becomes $\sigma=1/\sqrt{30-3}=0.19$.

Consider now, in the range extending from 0 to 2.65, a sequence of z-intervals, S_0, S_1, S_2, . . . the midpoints of which are spaced 2×0.675 standard deviations, that is, $2\times0.675\times0.19$ units apart. Then, in accordance with the properties of the Gaussian distribution assumed to hold for the z's, the probability is 50 percent that a z-value corresponding to a population centered in the midpoint of S_i, will actually fall in the interval S_i. The probability that such a value will fall in S_{i-1} or in S_{i+1}, is, in each case, approximately 23 percent. Thus the probability for such a value to fall in its correct group, or, at worst, in one of the two adjacent groups, is 96 percent. As these probabilities also apply to the corresponding r-values, the z-intervals thus defined can be made the basis of a grouping procedure of correlation coefficients computed on 30 points. To this end it is merely necessary to apply the inverse transformation $r=(e^{2z}-1)/(e^{2z}+1)$ to the end-points of the S-intervals. The values thus obtained will be the endpoints of the groups for the r-values. For the unique determination of the S_i-intervals, the upper limit of S_1 was chosen to be $z=2.65-0.605\sigma$ or $2.65-0.13=2.52$. In this way, an extra interval S_0 is formed extending from $z=2.52$ to 2.65. The probability for a point belonging to the population S_1, to fall in S_0 is 23 percent, and this includes values of the correlation coefficient up to 0.99.

[6] It is unlikely that for any position on the side, the correlation ρ between position value and side average, for any given property, be negative. However, for small positive values of ρ, the sample estimate r will occasionally be negative, due to chance fluctuation. When this occurs, the value of ρ is best taken equal to zero.

The grouping procedure just described is not an ideal solution for the problem outlined at the beginning of this section. In fact, the statistical literature does not seem to contain a satisfactory practical method for a grouping problem of this nature, and it should be noted that any grouping procedure will result in a certain amount of misclassification. The proposed method must be considered as a practical working rule that has some theoretical plausibility.

Table 1 shows the groups into which the r-values were classified, on the basis of the corresponding S-intervals for z. It is noted that the intervals S_0, S_1, S_2, and S_3 were combined to give a single r-group, denoted group zero. This was done because no experimental r-value exceeding 0.94 was found. Furthermore, the lower limit in group 6 has been raised from 0.42 to 0.46, the latter being the 1-percent significance level. It is considered that a value of r that fails to be significantly different from $\rho=0$ at the 1-percent level corresponds to a very poor sampling location.

TABLE 1. *Ranking of sampling location according to r*

z-interval	r-group	Range of r	
		Lower limit	Upper limit
S_0	0	0.988	0.990
S_1	0	.979	.987
S_2	0	.965	.978
S_3	0	.941	.964
S_4	1	.91	.940
S_5	2	.85	.90
S_6	3	.75	.84
S_7	4	.61	.74
S_8	5	.46	.60
S_9	6	Negative [a]	.45

[a] See footnote 6.

VII. Determination of Sample Size

When two lots are compared, with respect to a physical or chemical characteristic, on the basis of a limited number of measurements on each, the conclusions can be affected by two types of error. The effect of chance fluctuations could produce an apparently large difference between the two observed averages, while the real difference between the lots is actually inconsequential. On the other hand, a real difference of practical significance could escape notice if, by the interplay of chance effects, the observed values were sufficiently alike so that one lot would not be considered different from the other. The statistical method of selecting a sample size—in this case, the number of sides N to be tested from each lot—consists in taking predetermined risks with respect to both types of error. (It is obviously impossible to eliminate either type entirely.)[7]

It was shown (eq 3) that the ratio of the standard deviation of $\overline{p}_1-\overline{p}_2$ to its expected value is equal to

$$\frac{\sqrt{\frac{2}{N}}}{M_1-M_2}\sqrt{(\sigma_d)^2+\left(\frac{\sigma_t}{m}\right)^2}.$$

[7] The two types of error in statistical inference are discussed in (6). An example of their use as a basis for the determination of sample sizes is given by Curtiss [7].

UNIVERSITY OF MICHIGAN LIBRARIES

In view of the formula derived for the coefficient of correlation ρ (eq 4), this expression can be written $[(\sqrt{2}/N)/(M_1-M_2)]\cdot\sigma_d/\rho$

Thus

$$\frac{\sigma_{\bar{p}_1-\bar{p}_2}}{\text{Expected value of } (\bar{p}_1-\bar{p}_2)}=\frac{\sqrt{\frac{2}{N}}}{M_1-M_2}\cdot\frac{\sigma_d}{\rho}.$$

In order to simplify the notation, let us write $\bar{p}_1-\bar{p}_2=\delta$ and denote the expected value of any quantity Y by the symbol $E(Y)$.

Then

$$\frac{\sigma_\delta}{E(\delta)}=\frac{\sqrt{\frac{2}{N}}\,\sigma_d}{\rho(M_1-M_2)}.$$

Taking reciprocals, we have

$$\frac{E(\delta)}{\sigma_\delta}=\frac{\rho(M_1-M_2)\sqrt{\frac{N}{2}}}{\sigma_d}. \tag{5}$$

Now, the observed difference δ consists of two portions: a fixed portion, equal to $E(\delta)$; and a variable part, due to chance fluctuations, which we will, for brevity, call "error of δ", and denote by the symbol $\epsilon(\delta)$. Thus

$$\delta=E(\delta)+\epsilon(\delta).$$

Expression 5 thus becomes

$$\frac{\delta-\epsilon(\delta)}{\sigma_\delta}=\frac{\rho(M_1-M_2)\sqrt{\frac{N}{2}}}{\sigma_d}. \tag{6}$$

The values for the risks corresponding to the two types of error mentioned earlier can now be assigned in the following manner:

1. The risk of inferring the existence of a difference between the two lots where there is actually none.

Make $M_1=M_2$ in eq 6 in order to express the fact that no actual difference exists. Then the equation becomes

$$\frac{\delta}{\sigma_\delta}=\frac{\epsilon(\delta)}{\sigma_\delta},$$

that is, the ratio of a chance fluctuation to its standard deviation. It is known that for Gaussian variables the absolute value of this ratio will exceed the value 1.96 only five times in a hundred. (Cf. any table giving the "areas", i. e. the cumulative frequencies of the "normal" curve, e. g. [4]). Thus if the risk in question is to be kept at the 5-percent level, the existence of a difference should only be inferred whenever

$$\frac{|\delta|}{\sigma_\delta}>1.96.$$

2. The risk of not detecting a real difference between the two lots.

Suppose that this real difference equals D. Then $M_1-M_2=D$, and eq 6 becomes

$$\frac{\delta}{\sigma_\delta}=\frac{\rho D\sqrt{\frac{N}{2}}}{\sigma_d}+\frac{\epsilon(\delta)}{\sigma_\delta}.$$

Now, in order to keep the risk of the first type at 5 percent, a difference between the two lots was considered to exist only when

$$\frac{|\delta|}{\sigma_\delta}>1.96,$$

that is, whenever

$$\left|\frac{\rho D}{\sigma_d}\sqrt{\frac{N}{2}}+\frac{\epsilon(\delta)}{\sigma_\delta}\right|>1.96,$$

that is, whenever the first member is either smaller than -1.96 or greater than $+1.96$. The first possibility is remote, as it would require that the standardized error term be considerably smaller than -1.96.

Therefore, in practice, the rule will result in detecting the existence of D whenever

$$\frac{\epsilon(\delta)}{\sigma_\delta}>1.96-\frac{\rho D}{\sigma_d}\sqrt{\frac{N}{2}},$$

and consequently in committing the error of failing to recognize its existence whenever

$$\frac{\epsilon(\delta)}{\sigma_\delta}<1.96-\frac{\rho D}{\sigma_d}\sqrt{\frac{N}{2}}.$$

As in the case of the error of the first type, the probability that this inequality will hold can be given any preassigned value, by using the table of areas of the normal curve. For example, if the second member is made equal to -1.64, (the value that has 5 percent of the area under the curve to its left), this inequality will hold five times in a hundred, so that the risk for the error of considering D as negligible is limited to 5 percent. Then

$$1.96-\frac{\rho D}{\sigma_d}\sqrt{\frac{N}{2}}=-1.64,$$

hence

$$N=2\,\frac{(1.64+1.96)^2}{\rho^2D^2}(\sigma_d)^2. \tag{7}$$

This procedure illustrates the general method of determining sample size on the basis of predetermined risks. By changing the numerical values inside the parentheses, the risks can be changed to any desired values.

It should be noted that N is inversely proportional to the square of the coefficient of correlation, a

relation that permits the comparison of different sampling locations from the viewpoint of economy in sampling. Furthermore, the formula shows the rapid increase in the required number of sides as the difference D to be detected becomes smaller.

By dividing in eq 7 both $(\sigma_d)^2$ and D^2 by the square of the average of the lot means M_1 and M_2, it is seen that the number of sides N is proportional, for a given *percentage* difference D to be detected, to the square of the coefficient of variation of side averages, $\sigma_d/\frac{1}{2}(M_1+M_2)$.

VIII. Conclusion

A rational solution to the problem of selecting the best sampling location, for any particular property, on a leather side has been obtained by theoretical considerations combined with facts derived from data obtained in a statistically designed experiment. This statistical method, which may result in considerable savings both in labor and in material, can readily be applied to other situations in which the properties to be measured vary with location on the sampling unit in a systematic way.

IX. References

[1] J. Beek, Jr., The probable error in the measurement of tensile strength of heavy leather, J. Am. Leather Chem. Assoc. **32**, 4 (1937).

[2] J. Beek, Jr. and R. B. Hobbs, Some applications of statistical methods to sampling of leather, J. Am. Leather Chem. Assoc. **36**, 190 (1941).

[3] A. G. Worthing and J. Geffner, Treatment of experimental data (John Wiley and Sons, Inc., New York, N. Y., 1943).

[4] G. W. Snedecor, Statistical methods (The Iowa State College Press, Ames, Iowa, 1946).

[5] Joseph Berkson, Are there two regressions?, J. Am. Statistical Assoc. **45,** 164 (1950).

[6] A. M. Mood, Introduction to the theory of statistics (McGraw-Hill Book Co., Inc., New York, N. Y., 1950).

[7] J. H. Curtiss, Acceptance sampling by variables, J. Research, NBS **39,** 271 (1947) RP 1827.

Washington, July 27, 1950.

UNIVERSITY OF MICHIGAN LIBRARIES

Journal of Research of the National Bureau of Standards Vol. 46, No. 2, February 1951 Research Paper 218

Heats of Combustion, Formation, and Insomerization of Ten C_4 Hydrocarbons

Edward J. Prosen, Frances W. Maron, and Frederick D. Rossini [1]

The heats of combustion of ten C_4 hydrocarbons were measured by combustion of the gaseous hydrocarbon in a flame at constant pressure in a glass reaction vessel in a calorimeter. The calorimeter system was calibrated by means of electrical energy.

The experimental data yielded the following values for the standard heat of combustion, $-\Delta Hc°$, at 25° C and constant pressure, of the gaseous hydrocarbon in gaseous oxygen to form gaseous carbon dioxide and liquid water, with all the reactants and products in their thermodynamic standard reference states, in kcal/mole: *n*-butane, 687.42 ± 0.15; 2-methylpropane, 685.37 ± 0.11; 1-butene, 649.33 ± 0.18; *cis*-2-butene, 647.65 ± 0.29; *trans*-2-butene, 646.90 ± 0.23; 2-methylpropene, 645.19 ± 0.25; 1,2-butadiene, 619.93 ± 0.13; 1,3-butadiene, 607.16 ± 0.18; 1-butyne, 620.64 ± 0.20; 2-butyne, 615.84 ± 0.23.

Values of heats of isomerization, formation, and hydrogenation were derived from these data.

I. Introduction

The present investigation, sponsored by the U. S. Office of Rubber Reserve, is a continuation of the thermochemical investigation of monomeric compounds [1][2] of importance in the national synthetic rubber program, and is also a part of the work of the thermochemical laboratory of this Bureau on the determination of the heats of formation of compounds of importance to industry and science.

Calorimetric measurements have been made of the heats of combustion at constant pressure of *n*-butane, 2-methylpropane (isobutane), 1-butene, *cis*-2-butene, *trans*-2-butene, 2-methylpropene (isobutene), 1,2-butadiene, 1,3-butadiene, 1-butyne (ethylacetylene), and 2-butyne (dimethylacetylene).

Values of heats of isomerization, obtained as the differences in the heats of combustion of corresponding isomers, are also reported. Combination of the heats of combustion with the heats of formation of water and carbon dioxide yields values for the heats of formation of these compounds. The description of the determination of the heat of isomerization of 1-3-butadiene to 1,2-butadiene has been previously published [1]. For that determination it was not necessary to determine the electrical energy equivalent of the calorimeter system. The calorimeter system has been calibrated with electrical energy as part of this investigation, thus yielding new values for the heats of combustion of these two compounds.

II. Method

The units of energy, molecular weights, and method of assigning uncertainties are the same as previously described [1].

The relative values of the heats of combustion of these compounds were determined as described previously [1]. This involved the determination of a constant B (eq 3 of [1]) from a series of calorimetric combustion experiments on each compound, where B is essentially the temperature rise of the calorimeter system per gram of carbon dioxide formed in the combustion of the hydrocarbon. A standard calorimeter system and approximately the same temperature interval were used in all experiments. The temperature rise was measured as the increase in resistance of the given platinum resistance thermometer as determined on the given resistance bridge.

To determine the absolute values of the heats of combustion of these compounds, it was necessary to determine the electrical energy equivalent E_s of the calorimeter system. This was done by using electrical energy to produce the same temperature rise in the standard calorimeter system as was produced in the calorimetric combustion experiments. The experimental value of the heat evolved per mole of hydrocarbon reacting is

$$-\Delta Hc = E_s \cdot B \cdot (44.010) n, \qquad (1)$$

where 44.010 is the molecular weight of carbon dioxide, and n is the number of moles of carbon dioxide per mole of hydrocarbon (n is 4 for these C_4 compounds).

III. Apparatus

1. Calorimeter Systems

The calorimeter assembly, thermometric system, reaction vessel, and sparking system have been described in the paper on the heat of isomerization of the butadienes [1]. Two changes were made in the calorimeter system during the course of this work, necessitating the consideration of three systems, I, II, and III.

The calorimetric combustion experiments on the two butadienes [1] and the two butanes were performed, using system I. After calibration of system I with electrical energy, the Mueller resistance bridge, Number 404, was replaced by a new Mueller resistance bridge, Number 679195. The calorimetric

[1] Present address: Carnegie Institute of Technology, Pittsburgh, Pa.
[2] Figures in brackets indicate the literature references at the end of this paper.

combustion experiments on the two butynes were performed, using this calorimeter system II. After calibration of system II with electrical energy, the Picein-coated calorimeter heater [1] was replaced by a new calorimeter heater. The calorimetric combustion experiments on the four butenes and a series of electrical energy calibration experiments were then performed on calorimeter system III. Platinum resistance thermometer No. 262214 was used throughout this investigation.

The Picein on the old Picein-coated heater would occasionally crack, causing electrical leakage; or would chip off, causing a change in heat capacity, therefore, a new heater was made that was completely encased in copper. The new heater was wound on a thin copper cylinder 3 in. in diameter, 3 in. high, and 0.016 in. thick. This cylinder was covered by a sheet of mica, 0.003 in. thick, over which was wound, noninductively, a heater of about 65 ohms of enameled manganin resistance wire, No. 30 AWG. This wire was covered by another sheet of mica and another close-fitting machined copper cylinder, 0.016 in. thick, was slipped over the assembly, and the two copper cylinders were soldered together at the ends (the inner cylinder having been originally machined with a lip at each end so that the two cylinders fitted very closely together at the ends and with just room enough for the wire and the two sheets of mica in the body). A thin copper tube was soldered onto the outer copper cylinder to carry the enameled copper wire leads, No. 28 AWG, through the water in the calorimeter can. The assembled heater was nickel-plated and polished.

2. Apparatus for Measurement of Electrical Energy

The apparatus and arrangement for measuring the electrical energy during the calibration experiments was essentially the same as that described previously [2]. A new Wenner potentiometer (range 0 to 100,000μv), Number 684695, was used to measure the potential drops across the standard resistors. This potentiometer was calibrated by the Resistance Measurements Section of this Bureau immediately preceding this series of experiments, and the potentiometer ratio was determined [3] at the time of each experiment with electrical energy. The potentiometer ratio was determined by connecting in series a 10-ohm standard resistor, a 100-ohm standard resistor, a variable resistance, and an auxiliary battery. The current through this circuit was adjusted, by use of the variable resistance, so that the potential drop across the 100-ohm standard resistor was equal to the emf of the standard cell. This comparison was made by first adjusting the potentiometer working current, using the standard cell, then replacing the standard cell with the potential leads from the standard resistor. When these were equal, the potential drop across the 10-ohm standard resistor was read on the potentiometer. The ratio of this reading to the true potential drop, as calculated from the known current flowing through the standard resistors, is the potentiometer ratio.

The standard cell and standard resistors used were calibrated by the Electrochemistry Section and Resistance Measurements Section of this Bureau, respectively, at intervals of about 1 year.

The electrical power was computed as the product of the potential drop per ohm across a 0.1-ohm standard resistor in series with the calorimeter heater and the potential drop across the calorimeter heater, corrected for the current through the standard resistors in parallel with the calorimeter heater. The potential drop across the latter was determined from the potential drop across a 10-ohm standard resistor in series with a 10,000 ohm standard resistor, both of which were in parallel with the heater.

The current was diverted from the external "spill" coil to the calorimeter heater and back again with the use of an automatic switch, [4], which was activated by seconds signals obtained from the Time Section of this Bureau.

IV. Chemical Procedure

1. Purity of the Compounds

The source and purity of the 1,2-butadiene and 1,3-butadiene were previously reported [1].

The 1-butyne and 2-butyne were API–NBS samples purified by the American Petroleum Institute Research Project 6 from material supplied by the American Petroleum Institute Research Project 45 at the Ohio State University, through C. E. Boord. The purities of these two samples were reported [5, 6] as follows, in mole percent: 1-butyne, 99.88 ± 0.07; 2-butyne, 99.959 ± 0.038.

The 2-methylpropene (isobutene) was supplied by the Standard Oil Development Co., through W. J. Sweeney, and had a purity of 99.75 ± 0.10 mole percent, as determined from measurements of the freezing point [7] by A. R. Glasgow, Jr., of this Bureau.

The *n*-butane, 2-methylpropane (isobutane), 1-butene, *cis*-2-butene, and *trans*-2-butene were Research Grade hydrocarbons supplied by the Phillips Petroleum Co. through R. C. Alden and F. E. Frey. The purities of each of these samples, except 1-butene, were determined from measurements of freezing points [7] by A. R. Glasgow, Jr., and A. J. Streiff (of the American Petroleum Institute Research Project 6) as follows, in mole percent: *n*-butane, 99.78 ± 0.08; 2-methylpropane (isobutane), 99.88 ± 0.06; *cis*-2-butene, 99.74 ± 0.10; *trans*-2-butene, 99.32 ± 0.08. The purity of the 1-butene was reported by the Phillips Petroleum Co., from measurements of freezing points, supplemented by mass spectral analysis, to be 99.88 mole percent.

It is believed that in each case the impurity was predominantly isomeric and present in such small amount that the value of the heat of combustion was not significantly affected.

2. Purity of the Reaction of Combustion

As a check on the purity of the reaction of combustion, both the water and carbon dioxide were collected and the masses determined for most of the experiments. The results of these determinations

UNIVERSITY OF MICHIGAN LIBRARIES

are given in table 1, in which are listed, for each substance, the number of experiments, the mean value of the stoichiometric ratio, r, of number of moles of carbon dioxide to the number of moles of water collected multiplied by the factor $b/2a$ (where C_aH_b is the empirical formula of the hydrocarbon), and the standard deviation of the mean. "Blank" corrections to the weights of the carbon dioxide and water absorption tubes were taken into account, insofar as their effect on the ratio r was concerned, in conjunction with the procedure described below (section VI, 2) for determining the "ignition" energy. These ignition-energy experiments were performed in the same manner as the combustion experiments, except that the flame was allowed to burn only about 40 sec. instead of about 20 min. as in the regular combustion experiments. The procedure of handling the tubes and length of time of flushing of the reaction vessel with oxygen were made the same. Any blank corrections to the weights of the absorption tubes due to flushing with oxygen or to the absorption of unburned hydrocarbon in the absorption tubes as the result of any incomplete combustion during the ignition and extinction of the flame, were taken into account in the following manner. The deviation of the ratio r from unity for these short-time ignition experiments was translated into an excess or deficiency in the mass of water collected. This correction was applied to the mass of water collected in the regular combustion experiments in calculating the ratio r given in table 1.

TABLE 1. *Stoichiometric ratios of the masses of carbon dioxide to water formed in the combustion of the hydrocarbons*

Substance	Number of experiments	Mean value of the stoichiometric ratio, r	Standard deviation of the mean
1,3-Butadiene	8	1.00024	±0.00022
1,2-Butadiene	6	0.99994	±.00019
n-Butane	6	.99992	±.00009
2-Methylpropane	6	.99991	±.00005
1-Butyne	5	.99952	±.00019
2-Butyne	4	.99880	±.00017
1-Butene	5	.99962	±.00009
cis-2-Butene	4	1.00007	±.00014
trans-2-Butene	5	0.99984	±.00024
2-Methylpropene	5	.99956	±.00021

The heat effect of any possible incomplete combustion during the ignition or extinction of the flame was taken into acount also by the method of determining the ignition energy. With this procedure the heat of combustion was in reality determined from the portion of the combustion when the flame was in a steady state, any constant errors associated with the ignition and extinction of the flame canceling out.

Samples of the products of combustion were analyzed for carbon monoxide, the most likely product of incomplete combustion, by the Gas Chemistry Section of this Bureau [8]. In no case was the total amount of carbon monoxide greater than 0.004 percent of the amount of carbon dioxide formed in the combustion, hence no corrections were applied for this small amount of carbon monoxide.

3. Determination of the Amount of Reaction

For each calorimetric combustion experiment, the amount of reaction was determined from the mass of carbon dioxide formed, taking 1 mole or 44.010 g of carbon dioxide as equivalent to one-fourth mole of these C_4 hydrocarbons. No blank corrections were applied to the weights of the carbon dioxide absorption tubes, since these corrections, if significant, were automatically translated into ignition-energy corrections.

V. Calorimetric Combustion Experiments

1. Procedure

The calorimetric combustion experiments were performed as described in the paper on the heats of isomerization of the butadienes [1]. For each of these different hydrocarbons, it was necessary only to vary the amount of primary oxygen entering the reaction vessel to produce a blue flame with a sharp inner cone to insure complete combustion of the hydrocarbons. The rate of flow of the hydrocarbon was set such as to produce upon combustion the required temperature rise of 4° C in the colorimeter system (equivalent to about 60,000 j of energy) in a period of about 20 min. The secondary oxygen rate was set such that the total oxygen (primary plus secondary) was about 150 percent of that required stoichiometrically for complete combustion.

In the experiments with 2-butyne, which is normally a liquid at room temperature, the vapor was introduced into the calorimeter, using helium as the carrier gas. Any combustible impurities in the helium were removed by passing the helium through a tube packed with copper oxide and maintained at about 600° C, then through separate tubes containing ascarite, magnesium perchlorate, and phosphorous pentoxide. The rate of flow of helium was determined with a bypass flowmeter, and at the proper instant during an experiment, the helium was bubbled through a fritted-glass bubbler into the liquid 2-butyne (at 15° C) and fed directly into the calorimetric reaction vessel.

2. Determination of the "Ignition" Energy

Experiments to determine the energy associated with the ignition and extinction of the flame (ignition-energy experiments [1]) were performed on each compound in the same manner as the regular combustion experiments, except that the flame was allowed to burn for only about 40 sec. The energy contributed by the combustion of the hydrocarbon, as determined from the mass of carbon dioxide collected and an approximate value for the heat of combustion of the hydrocarbon, was subtracted from the total energy liberated in the short-time experiments, to yield the ignition energy.

The mean ignition energies (with their standard deviations) as determined by such experiments were as follows: 1,3-butadiene and 1,2-butadiene,

33.1±2.8 j; *n*-butane, 63.7±3.6 j; 2-methylpropane, 60.0±1.3 j; 1-butyne, 57.2±5.6 j; 2-butyne, 71.8±7.3 j; 1-butene, 51.9±4.2 j; *cis*-2-butene, 46.2±4.4 j; *trans*-2-butene, 48.7±0.2 j; 2-methylpropene, 43.0±2.5 j. The uncertainties in these ignition energies were taken into account in calculating the final uncertainties assigned to the heats of combustion.

3. Results of the Calorimetric Combustion Experiments

The results of the calorimetric combustion experiments are given in table 2, in which are listed for each compound the following quantities: the experiment number; ΔRc, the corrected temperature rise of the calorimeter expressed in ohms; the mass of carbon dioxide formed; q_x and q_s, the quantities of heat evolved in addition to that evolved by the standard calorimetric process [1]; q_i, the ignition energy; B, the temperature rise in ohms of the calorimeter system contributed by the standard calorimetric process per gram of carbon dioxide formed; and the mean value of B, together with its standard deviation. The data on 1,3-butadiene and 1,2-butadiene have previously been published [1], and only the mean value of B, together with its standard deviation, are given here. These values differ from the previously published values [1] of B due to the use here of the actual ignition energy instead of the "sparking" energy and due to a change in the calorimeter system between the time of the combustion experiments and the electrical energy experiments necessitated by repairs to the reaction vessel.

TABLE 2. *The calorimetric combustion experiments*

Compound	Experiment number	ΔRc	Mass of carbon dioxide	q_x	q_s	q_i	B	Mean value of B with its standard deviation
		Ohms	*g*	*j*	*j*	*j*	*Ohms/g* CO_2	*Ohms/g* CO_2
1,3-Butadiene								0.0935614 ±.0000110
1,2-Butadiene								.0955293 ±.0000054
n-Butane	1	0.388961	3.68834	−10.1	−349.5	90.8	0.1059294	.1059307 ±.0000054
	2	.391255	3.71225	−15.9	−376.2	77.2	.1059455	
	3	.389082	3.69052	−26.3	−382.3	90.8	.1059158	
	4	.391074	3.71027	−23.5	−361.7	90.8	.1059175	
	5	.390701	3.70800	−31.0	−364.0	63.7	.1059464	
	6	.391245	3.71410	−35.0	−366.1	63.7	.1059294	
2-Methylpropane	1	0.391093	3.72580	−18.9	−426.1	73.5	0.1056154	.1056143 ±.0000032
	2	.390330	3.71645	−30.2	−372.2	60.0	.1056250	
	3	.390794	3.72068	−34.5	−382.2	60.0	.1056125	
	4	.390511	3.71728	−21.2	−345.1	60.0	.1056152	
	5	.389206	3.70505	−14.5	−375.1	73.5	.1056005	
	6	.388287	3.69483	−18.0	−356.1	73.5	.1056168	
1-Butyne	1	0.389227	4.07049	+19.5	−347.9	57.2	0.0955511	.0955834 ±.0000108
	2	.388306	4.08219	+14.9	−342.9	57.2	.0955518	
	3	.386382	3.84084	+7.6	−286.2	57.2	.0956153	
	4	.386570	4.06392	−2.6	−347.6	57.2	.0955896	
	5	.387494	4.07181	−1.6	−322.4	57.2	.0955896	
	6	.394014	4.13909	−4.6	−314.2	57.2	.0956030	
2-Butyne	1	0.385354	4.09629	+5.0	−585.0	71.8	0.0948779	.0948451 ±.0000117
	2	.393201	4.16628	−3.5	−347.8	71.8	.0948117	
	3	.392782	4.16211	−0.6	−364.3	71.8	.0948273	
	4	.391251	4.14674	−6.5	−383.5	71.8	.0948487	
	5	.394437	4.18146	−3.2	−410.6	71.8	.0948600	
1-Butene	1	0.390078	3.92767	+4.0	−360.3	51.9	0.0998168	.0998454 ±.0000096
	2	.390959	3.93618	−25.8	−343.3	51.9	.0998460	
	3	.391116	3.93653	−18.6	−346.3	51.9	.0998599	
	4	.390408	3.93126	−13.5	−352.2	51.9	.0998251	
	5	.390460	3.93052	−17.6	−337.4	51.9	.0998394	
	6	.389913	3.92383	−8.8	−349.2	51.9	.0998753	
cis-2-Butene	1	0.391148	3.94593	+2.5	−340.9	46.2	0.0990061	.0995899 ±.0000200
	2	.391834	3.95409	+12.6	−316.3	46.2	.0995172	
	3	.391826	3.95239	+13.9	−332.6	46.2	.0995826	
	4	.391001	3.94650	−17.3	−343.9	46.2	.0995917	
	5	.390403	3.93893	−19.8	−364.1	46.2	.0996683	
	6	.391305	3.94849	−28.0	−332.7	46.2	.0996177	
	7	.388294	3.92211	−10.6	−352.8	46.2	.0995245	
trans-2-Butene	1	0.320851	3.94982	+12.5	−351.1	48.7	0.0994200	.0994716 ±.0000163
	2	.391170	3.95104	+12.4	−347.3	48.7	.0994730	
	3	.391794	3.95639	−9.4	−337.8	48.7	.0995162	
	4	.391341	3.95343	−13.8	−346.3	48.7	.0994974	
	5	.390536	3.94809	−12.1	−356.9	48.7	.0994426	
2-Methylpropene	1	0.393353	3.98479	+24.6	−405.8	43.0	0.0992628	.0992089 ±.0000171
	2	.389757	3.95268	+19.9	−412.9	43.0	.0991787	
	3	.389113	3.94302	+14.0	−389.1	43.0	.0992289	
	4	.383724	3.88059	+14.1	−382.0	43.0	.0991691	
	5	.111579	1.13195	+20.7	−174.4	43.0	.0992052	

UNIVERSITY OF MICHIGAN LIBRARIES

VI. Electrical Energy Experiments

1. Procedure

The calorimetric procedure used in the electrical energy experiments was the same as in the combustion experiments [1], except that electrical energy instead of chemical energy was supplied during the reaction period. The voltage across the 65-ohm calorimeter heater was about 60 v, and the time of heating was about 20 min. (about the same length of heating time as in the combustion experiments).

2. Results of the Electrical Energy Experiments

The results of the electrical energy experiments are given in table 3, in which are listed, for the experiments on calorimeter systems I, II, and III, the following quantities: The experiment number; ΔRc, the corrected temperature rise of the calorimeter system expressed in ohms; the amount of electrical energy supplied to the calorimeter; E_s, the electrical energy equivalent of the calorimeter; and the mean value of E_s, together with its standard deviation.

TABLE 3. *The electrical calibration experiments*

Calorimeter system	Experiment number	ΔRc	Electrical energy	E_s	Mean value of Es with its standard deviation
		Ohms	*j*	*j/ohm*	*j/ohm*
I	1	0.401716	61953.5	154222.1	154230.2 ±4.3
	2	.392416	60525.4	154237.8	
	3	.391576	60397.5	154242.1	
	4	.391473	60373.0	154220.1	
	5	.391621	60399.3	154229.0	
II	1	.394433	60867.0	154315.2	154319.6 ±2.5
	2	.395498	61035.7	154326.2	
	3	.391998	60485.3	154311.8	
	4	.394095	60815.3	154316.3	
	5	.394425	60870.3	154326.7	
	6	.394851	60934.0	154321.5	
III	1	.391971	60581.3	154555.6	154562.9 ±3.2
	2	.395233	61086.7	154558.7	
	3	.393619	60837.8	154560.1	
	4	.393612	60839.6	154567.4	
	5	.361159	55825.4	154572.9	

To test for systematic errors, several series of experiments were performed in which the voltage supplied across the calorimeter heater was 35 to 40 v instead of 60 v, thus making the heating period (40 to 50 min) at least twice as long as the usual 20 min. The resulting electrical energy equivalents obtained from three such experiments on calorimeter system I was $E_s = 154253 \pm 41$, from five experiments on calorimeter system II was $E_s = 154341 \pm 5$, and from five experiments on calorimeter system III was $E_s = 154568 \pm 10$ (standard deviation of the mean). Since these experiments were performed under conditions greatly different from the usual electrical energy experiments or the calorimetric combustion experiments, it was concluded that the heat leak corrections were being made properly and that the rate of stirring of the water in the calorimeter vessel was adequate.

VII. Heats of Combustion, Formation, Isomerization, and Hydrogenation

The product of B and E_s multiplied by the molecular weight of carbon dioxide and the number of moles of carbon dioxide per mole of hydrocarbon (eq 1) yields the heat of reaction as expressed by the "standard calorimetric process" [1]. In these experiments, in which approximately 50 percent of excess oxygen was employed, the process may be defined by the equation

$$C_aH_b \text{ (gas, 1 atm, 25° C)} + 3\left(\frac{b+4a}{8}\right) O_2 \text{ (gas, 1 atm, 25° C)} = \left[a\,CO_2 + \left(\frac{b+4a}{8}\right)O_2\right] \text{(gas, 1 atm, 25° C)} + \frac{b}{2}\,H_2O \text{ (liq, 1 atm, 25° C)}. \quad (2)$$

To convert the heat of this reaction, $-\Delta Hc$, to the standard heat of combustion, $-\Delta Hc°$, as expressed by the reaction at 25° C

$$C_aH_b \text{ (gas)} + \left(\frac{b+4a}{4}\right) O_2 \text{ (gas)} = a\,CO_2 \text{ (gas)} + \frac{b}{2}\,H_2O \text{ (liq)}, \quad (3)$$

it is only necessary to take account of the change in heat content for each gas from its given pressure to zero pressure, so that each substance will have the heat content of the thermodynamic standard state. For this calculation the change in heat content, $[H^{P=0} - H^{P=1}]_{298.16}$, was taken as −180 j/mole for the C_4 hydrocarbons, −8.1 j/mole for oxygen, and $-[8.06 + 15.9x + 17.4x^2]$ j/mole [9] for carbon dioxide-oxygen mixtures, where x is the mole fraction of carbon dioxide in the mixture. As seen from table 4, the value of this correction is −0.02 kcal/mole for each of the compounds investigated.

In table 4 are listed for each compound: the mean value of B from table 2; E_s, the mean value of the electrical energy equivalent of the calorimeter system from table 3; $-\Delta Hc$, the heat of combustion for the standard calorimetric process; $-\Delta Hc°$, the standard heat of combustion; $\Delta Hf°$, the standard heat of formation; $\Delta H°$ isomerization; and $\Delta H°$ hydrogenation.

The heats of formation were calculated from the heats of combustion utilizing the values of 68.317 ±0.010 kcal/mole [10] and 94.052 ±0.011 kcal/mole [17] for the heats of formation of water and carbon dioxide, respectively.

The heats of isomerization are the differences in the heats of combustion, but the uncertainty is lower than the combined uncertainties of the heats of combustion since the electrical energy equivalent of the calorimeter system need not be known precisely [11]. These heats of isomerization apply to the reaction of forming the particular isomer from the first isomer listed.

TABLE 4. *The heats of combustion, formation, isomerization and hydrogenation at 25° C*

Compound (gas)	B	E_2	$-\Delta Hc$		$-\Delta Hc°$	$\Delta Hf°$	$\Delta H°$ isomerization	$\Delta H°$ hydrogenation
	Ohms/g CO_2	*j/ohm*	*kj/mole*	*kcal/mole*	*kcal/mole*	*kcal/mole*	*kcal/mole*	*kcal/mole*
1,3-Butadiene	0.0935614 ±.0000220	154230.2 ±8.6	2540.26 ±0.75	607.14 ±0.18	607.16 ±0.18	+26.00 ±0.19	0	−56.37 ±0.24
1,2-Butadiene	.0955203 ±.0000108	154230.2 ±8.6	2593.69 ±.55	619.91 ±.13	619.93 ±.13	+38.77 ±.14	+12.77 ±0.18	−69.14 ±.20
n-Butane	.1059307 ±.0000108	154230.2 ±8.6	2876.09 ±.63	687.40 ±.15	687.42 ±.15	−30.37 ±.16	0	0
2-Methylpropane	.1056143 ±.0000064	154230.2 ±8.6	2867.50 ±.48	685.35 ±.11	685.37 ±.11	−32.42 ±.13	−2.05 ±0.12	0
1-Butyne	.0955834 ±.0000216	154319.6 ±5.0	2596.66 ±.85	620.62 ±.20	620.64 ±.20	+39.48 ±.21	0	−69.85 ±.25
2-Butyne	.0948451 ±.0000234	154319.6 ±5.0	2576.60 ±.97	615.82 ±.23	615.84 ±.23	+34.68 ±.24	−4.80 ±0.28	−65.05 ±.28
1-Butene	.0998454 ±.0000192	154562.9 ±6.4	2716.72 ±.76	649.31 ±.18	649.33 ±.18	−0.15 ±.19	0	−30.22 ±.23
cis-2-Butene	.0995869 ±.0000400	154562.9 ±6.4	2709.69 ±1.23	647.63 ±.29	647.65 ±.29	−1.83 ±.30	−1.68 ±0.32	−28.54 ±.33
trans-2-Butene	.0994716 ±.0000326	154562.9 ±6.4	2706.55 ±.97	646.88 ±.23	646.90 ±.23	−2.58 ±.24	−2.43 ±0.26	−27.79 ±.27
2-Methylpropene	.0992089 ±.0000342	154562.9 ±6.4	2699.40 ±1.04	645.17 ±.25	645.19 ±.25	−4.29 ±.26	−4.14 ±0.28	−28.13 ±.27

The heats of hydrogenation were derived from the heats of combustion of the compounds involved, combined with the heat of formation of water. These heats of hydrogenation apply to the reaction of hydrogenation of the particular unsaturated compound to form the parent saturated hydrocarbon, *n*-butane or 2-methylpropane.

Some additional heats of isomerization, hydrogenation (or dehydrogenation), or both isomerization and hydrogenation (or dehydrogenation) are given in table 5. Hydrogen is one of the reactants (or products) if the reaction involves hydrogenation (or dehydrogenation).

TABLE 5. *Heats of isomerization and/or hydrogenation in the gaseous state at 25° C*

Reactant (gas)	Product (gas)									
	n-Butane	2-Methylpropane	1-Butene	*cis*-2-Butene	*trans*-2-Butene	2-Methylpropene	1,2-Butadiene	1,3-Butadiene	1-Butyne	2-Butyne
	$\Delta H°$, kcal/mole									
n-Butane	0	−2.05	+30.22	+28.54	+27.79	+26.08	+69.14	+56.37	+69.85	+65.05
2-Methylpropane	+2.05	0	+32.27	+30.59	+29.84	+28.13	+71.19	+58.42	+71.90	+67.10
1-Butene	−30.22	−32.27	0	−1.68	−2.43	−4.14	+38.92	+26.15	+39.63	+34.83
cis-Butene	−28.54	−30.59	+1.68	0	−0.75	−2.46	+40.60	+27.83	+41.31	+36.51
trans-2-Butene	−27.79	−29.84	+2.43	+0.75	0	−1.71	+41.35	+28.58	+42.06	+37.26
2-Methylpropane	−26.08	−28.13	+4.14	+2.46	+1.71	0	+43.06	+30.29	+43.77	+38.97
1,2-Butadiene	−69.14	−71.19	−38.92	−40.60	−41.35	−43.06	0	−12.77	+0.71	−4.09
1,3-Butadiene	−56.37	−58.42	−26.15	−27.83	−28.58	−30.29	+12.77	0	+13.48	+8.68
1-Butyne	−69.85	−71.90	−39.63	−41.31	−42.06	−43.77	−0.71	−13.48	0	−4.80
2-Butyne	−65.05	−67.10	−34.83	−36.51	−37.26	−38.97	+4.09	−8.68	+4.80	0

VIII. Comparison with Earlier Data

The results of the present investigation are compared in table 6 with earlier data on heats of combustion and heats of hydrogenation.

TABLE 6. *Comparison of the data of the present investigation with earlier data*

Compound	Value from previous investigation	Value from present investigation	Difference
Standard heat of combustion, $-\Delta Hc°$ at 25° C, in kcal/mole			
n-Butane	687.98 ±0.17 [12]	687.42 ±0.15	0.56 ±0.23
2-Methylpropane	686.34 ± .15 [13]	685.37 ± .11	.97 ± .19
Standard heat of hydrogenation, $\Delta H°$ at 25° C, kcal/mole			
1,3-Butadiene	−56.56 ±0.15 [14]	−56.37 ±0.24	0.19 ±0.28
2-Butyne	−65.19 ± .30 [15]	−65.05 ± .27	.14 ± .40
1-Butene	−30.09 ± .10 [16]	−30.23 ± .23	.14 ± .34
cis-2-Butene	−28.45 ± .10 [16]	−28.55 ± .33	.10 ± .34
trans-2-Butene	−27.41 ± .10 [16]	−27.80 ± .27	.39 ± .29
2-Methylpropene	−28.11 ± .10 [16]	−28.14 ± .27	.03 ± .29

It is to be noted that the earlier data from this laboratory [12, 13] on *n*-butane and isobutane differ from the data of the present investigation by an amount significantly greater than the estimated uncertainty of the difference. One of the authors (Rossini) has carefully reviewed the earlier data but has been unable to discover any reason for the indicated difference other than the possibility that the earlier samples of *n*-butane and isobutane were not as pure as believed. The purity of the earlier samples of *n*-butane and isobutane was not determined from measurements of freezing points but from differential vapor-pressure measurements, quantitative evaluation of which involved assumptions as to the impurities present in the samples.

The accord of the data of the present investigation with the data on heats of hydrogenation by Kistiakowsky and coworkers [14, 15, 16] is very good, except in the case of *trans*-2-butene, for which the difference is only slightly greater than the combined uncertainties.

916783—51——3

UNIVERSITY OF MICHIGAN LIBRARIES

IX. References

[1] E. J. Prosen, F. W. Maron, and F. D. Rossini, J. Research NBS **42,** 269 (1949) RP1968.
[2] E. J. Prosen and F. D. Rossini, J. Research NBS **33,** 255 (1944) RP1607.
[3] N. S. Osborne, H. F. Stimson, and D. C. Ginnings, J. Research NBS **23,** 197 (1939) RP1228.
[4] E. J. Prosen and F. D. Rossini, J. Research NBS **33,** 255 (1944) RP1607.
[5] A. J. Streiff, J. C. Zimmerman, L. F. Soule, M. T. Butt, V. A. Sedlak, C. B. Willingham, and F. D. Rossini, J. Research NBS **41,** 323 (1948) RP1929.
[6] A. J. Streiff, E. T. Murphy, J. C. Zimmerman, L. F. Soule, V. A. Sedlak, C. B. Willingham, and F. D. Rossini, J. Research NBS **39,** 321 (1947) RP1833.
[7] A. R. Glasgow, Jr., A. J. Streiff, and F. D. Rossini, J. Research NBS **35,** 355 (1945) RP1676.
[8] M. Shepherd, Anal. Chem. **19,** 77 (1947).
[9] F. D. Rossini and M. Frandsen, BS J. Research **9,** 733 (1932) RP503.
[10] D. D. Wagman, J. E. Kilpatrick, W. J. Taylor, K. S. Pitzer, and F. D. Rossini, J. Research NBS **34,** 143 (1945) RP1634.
[11] E. J. Prosen and F. D. Rossini, J. Research NBS **27,** 289 (1941) RP1420.
[12] F. D. Rossini, J. Research NBS **12,** 735 (1934) RP686.
[13] F. D. Rossini, J. Research NBS **15,** 357 (1935) RP833.
[14] G. B. Kistiakowsky, J. R. Ruhoff, H. A. Smith, and W. E. Vaughan, J. Am. Chem. Soc. **58,** 146 (1936).
[15] J. B. Conn, G. B. Kistiakowsky, and E. A. Smith, J. Am. Chem. Soc. **61** 1868 (1939).
[16] G. B. Kistiakowsky, J. R. Ruhoff, H. A. Smith, and W. E. Vaughan, J. Am. Chem. Soc. **57,** 876 (1935).
[17] E. J. Prosen, R. S. Jessup, and F. D. Rossini, J. Research NBS **33,** 447 (1944) RP1620.

WASHINGTON, August 29, 1950.

Journal of Research of the National Bureau of Standards Vol. 46, No. 2, February 1951 Research Paper 2182

Effect of a Metal Mast and Guy Wires on the Performance of the 600-Ohm Multiple-Wire Delta Antenna

Harold N. Cones

This report describes the results of measurements made to determine the effect of a metal mast and guy wires on the radiation pattern and the effect of guy wires on the terminal impedance and the radiation efficiency of the 600-ohm multiple-wire delta antenna. Model techniques were used to obtain radiation patterns of identical antennas supported in various ways. Curves are presented showing the terminal impedance over the frequency range 1 to 25 megacycles of full-scale antennas with and without guy wires. A graph of the quasi-radiation efficiency of the antenna as a function of frequency is shown.

I. Introduction

The 600-ohm multiple-wire delta antenna [1] (fig. 1) used in ionosphere studies requires only a single large wooden mast. This mast, which is less than 80 ft. long, can ordinarily be procured and erected in most locations. However, in some locations it may be desirable to use a sectionalized metal mast. As the mast lies in a neutral plane of the antenna, it would appear that if the antenna was electrically and mechanically symmetrical and was fed by a balanced transmitter there would be no radiation from a metal supporting mast. It is quite improbable however that such a completely balanced condition will prevail. Any unbalance in the system will cause a residual current flow in the mast, which at resonance could become quite large causing appreciable radiation. It would also seem desirable to use guy wires to help support either a wooden or metal mast. Because the effects of a metal mast and guy wires on the radiation pattern and impedance of the delta antenna are difficult to predict analytically, experimental measurements were made to determine these effects. This report describes the results of these measurements.

II. Instrumentation

Radiation pattern measurements were made by using model techniques. That is, all dimensions of the antenna were scaled down by a certain factor, in this case 30, and the frequency was scaled up by the same factor. The model antennas were supported by nonconducting or metal masts of a diameter corresponding to 1 ft. in diameter on a full-scale antenna. Since ordinarily a single mast supports one transmitting and one receiving delta antenna mounted at right angles to each other, guy wires when used were spaced as shown in figure 2. In all cases the guy wires were insulated from the pole and from ground. When continuous guy wires were used these were the only insulators. The sectionalized guy wires had insulators at a spacing equivalent to every 7½ ft., or about 0.2 wavelength at 25 Mc. Pattern measurements were made over a ground mat of metallic mesh. When the model was supported by a metal mast, this mast was electrically connected to the ground mat.

The model antenna was used as a receiving antenna. A battery-operated high-frequency transmitter modulated at an audio frequency was mounted at the apex of an A-frame and moved about the model in a semicircular arc of 13 ft. in radius. The angular displacement of the transmitter with respect to ground was transferred to the turntable of a recorder by means of a selsyn system. The signal received by the model was rectified and the resulting audio-frequency voltage passed through a series of selective amplifiers and servomechanisms to cause a radial displacement of a pen on the recorder turntable. Thus as the transmitter was moved through an arc of 180 deg., the vertical radiation pattern of the antenna was automatically plotted.

Figure 3 is a diagram of the model range showing the paths of the target transmitter with reference to the antenna under test. The model antenna was located in the X-Z plane. Radiation patterns were measured in the X-Z and Y-Z planes. In measuring patterns in the X-Z plane the polarization of the transmitting antenna was always such that the electric vector was tangent to the meridian arc XZX'. In measuring patterns in the Y-Z plane, the electric vector was always parallel to the X axis.

The patterns obtained show the relative power that would be radiated by the antenna at different vertical angles in a given plane for a given frequency. The patterns were normalized, that is, the gain of the pattern plotter was adjusted for each frequency to give a full-scale deflection at the point of maximum gain. Pattern measurements were made only for the frequencies equivalent to 14 through 25 Mc because, with the scale factor of 30 which was used, the model range was too small for measurements at lower frequencies.

Impedance measurements of full-scale antennas were made with a balanced recording impedance meter that automatically plots the absolute magnitude of input impedance of an antenna over the frequency range 1 to 25 Mc. A block diagram and brief description of this instrument have been

[1] H. N. Cones, H. V. Cottony, and J. M. Watts, A 600-ohm multiple-wire delta antenna for ionosphere studies, J. Research NBS 44, 475 (1950) RP2094.

UNIVERSITY OF MICHIGAN LIBRARIES

published.[2] Basically, it consists of a sweep frequency generator with a constant-current output, the voltage across the output terminals being, therefore, directly proportional to the impedance impressed across the output terminals. The instrument is calibrated by substituting noninductive resistors for the unknown impedance. The absolute magnitude of the unknown impedance at any frequency can be determined by interpolating between the calibrating lines.

This instrument can also be used to obtain an indication of the radiation efficiency of a nonresonant antenna. The curve plotted by the impedance meter when an antenna is connected to its output terminals shows in arbitrary units the voltage across the antenna imput terminals. The curve also shows the impedance of the antenna, as the voltage is directly proportional to impedance. Since the input voltage and the input impedance of the antenna are known, the input power (in arbitrary units) can be computed for frequencies at which the antenna is purely resistive. These are, for all practical purposes, the frequencies at which the impedance is either a maximum or a minimum. If measurements are made of the voltage across the terminating resistor, the power dissipated in the resistor (in the same arbitrary units) can be determined. Knowing the power input to the antenna and the power dissipated in the terminating resistor, a quasi-radiation efficiency of the antenna (taken as the quotient of the power input less the power dissipated in the terminating resistor and the power input) can be evaluated. This quasi-radiation efficiency always exceeds the true radiation efficency, since it includes the copper, ground, and dielectric losses as power radiated.

III. Results of Radiation Pattern Measurements

Radiation pattern measurements were made of four identical antennas supported by a nonconducting mast, by a metal mast, by a metal mast and continuous guy wires, and by a metal mast and guy wires that were broken up by insulators spaced at distances equivalent to 7½ ft.

Figure 4 shows the radiation patterns obtained in the *X-Z* plane for these four antennas. Referring to the figures, it is seen that at 14 Mc the side lobes that are characteristic of the multiple-wire delta antenna at this frequency are effectively suppressed, at least in this plane, by the continuous guy wires. At 15 Mc, the metal mast causes a marked change in the usual pattern. Here again the continous guy wires suppress the side lobes in this plane. From 16 through 20 Mc, the method of support does not appear to affect the pattern appreciably, although continuous guy wires slightly increase the amount of low angle radiation at 16 Mc and slightly decrease it at 17, 18, 19, and 20 Mc. At 21 Mc, side lobes appear for the antenna with the continuous guy wires. At this frequency the long guy wires are 2 wavelengths long and the short guy wires are 1 wavelength long. Also at this frequency, the metal mast is approximately 1½ wavelengths long. From 22 through 25 Mc the patterns are very nearly alike, although the use of the sectionalized guy wires results in a slight change in the radiation pattern at 24 and 25 Mc.

The difference in the radiation patterns observed at 15 Mc between antennas employing nonconducting and metal masts (both without guy wires) is attributed to the resonance of the mast close to this frequency. This effect would not be observed except for the existence of an exciting voltage that would have to arise from an unbalance incidental to the model antenna system under test. Therefore, as the unbalance is likely to vary in different installations it may be expected that the resonance effects discussed above will likewise vary in magnitude.

Figure 5 shows comparative radiation patterns in the *Y-Z* plane for all four methods of support. At any one frequency the patterns are substantially alike.

It is seen that the use of continuous guy wires is very effective in suppressing side lobes in the *X-Z* plane at 14 and 15 Mc and to some extent effective in reducing low-angle radiation at other frequencies. They do not appear to affect the pattern in the *Y-Z* plane.

IV. Results of Impedance Measurements

Impedance measurements were made of full-scale antennas. As no metal mast was available, tests were limited to determining the effect of continuous guy wires on the terminal impedance of the antenna.

The following impedance measurements were made: 1. Measurements of an antenna without guy wires; 2. measurements of an antenna with long continuous guy wires, that is, guy wires fastened to the top of the mast; 3. measurement of an antenna with long and short continuous guy wires, that is, guy wires fastened to the top of the mast and guy wires fastened to the mast 35 ft above the ground.

Figure 6 shows the results of these measurements. The long guy wires affected the impedance only near the frequency where the guy wires were a half wavelength long. No change is noted at any multiple of a half wavelength. The short guy wires did not appear to have any effect on the impedance.

V. Results of Measurements of Quasi-Radiation Efficiency

Figure 7 shows the results of measurements of the quasi-radiation efficiency of an antenna with continuous guy wires and of an antenna without guy wires. As noted previously the quasi-radiation efficiency always exceeds the true radiation efficiency, as the copper, ground, and dielectric losses are included as power radiated. Although the true radiation efficiency is not known, the lower curve of figure 7 indicates the manner in which the quasi-

[2] H. N. Cones, Impedance characteristics of some experimental broad-band antennas for vertical-incidence ionosphere sounding, J. Research NBS **43**, 71 (1949) RP2006; see also reference listed in footnote 1.

radiation efficiency changes with frequency. The effects of guy wires are apparently very small.

It was shown in a previous paper (see footnote 2) that the value of the terminating resistor was not particularly critical for frequencies above 8 Mc. Figure 7 shows that only a relatively small amount of energy is dissipated in the terminating resistor at frequencies above 8 Mc.

VI. Conclusions

1. The use of a metal mast to support the multiple-wire delta antenna causes little change in the vertical radiation pattern in the frequency range 14 through 25 Mc, except at 15 Mc where large side lobes were observed in the particular model on which measurements were made. (See fig. 4.)
2. In general the use of continuous guy wires appears to improve the vertical radiation pattern of the antenna.
3. Guy wires that are broken up at short intervals by insulators have no measurable effects on the vertical radiation pattern of the antenna except at the highest frequencies in the operating range. Even here the effects are minor.
4. In the case of wooden masts continuous guy wires have no measurable effect on the input impedance of the antenna except near the frequency where the long guy wires are a half wavelength long.
5. In the case of wooden masts the use of guy wires does not appear to affect the efficiency of the antenna as a radiator.

UNIVERSITY OF MICHIGAN LIBRARIES

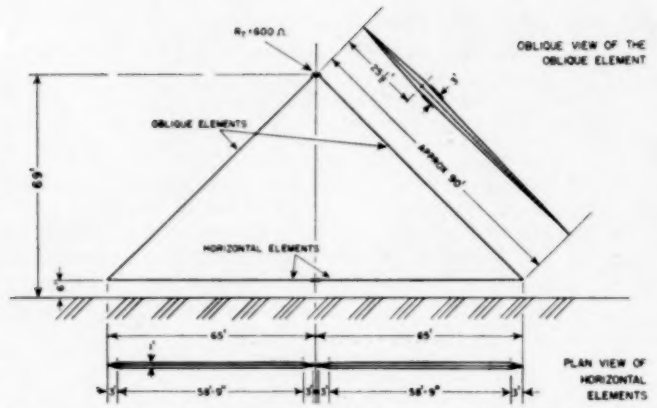

FIGURE 1. *Simplified diagram of the 600-ohm multiple-wire delta antenna.*

No. 12 wire used for all elements.

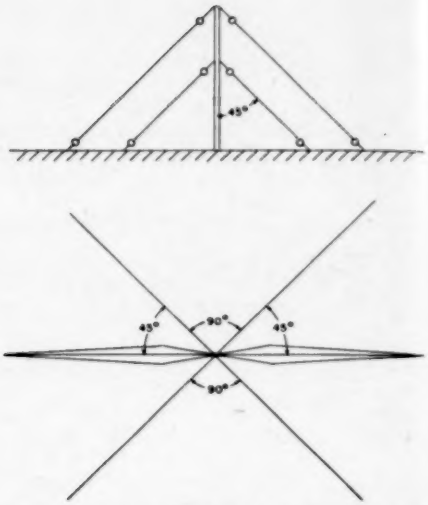

FIGURE 2. *Arrangement of guy wires used with multiple-wire delta antenna.*

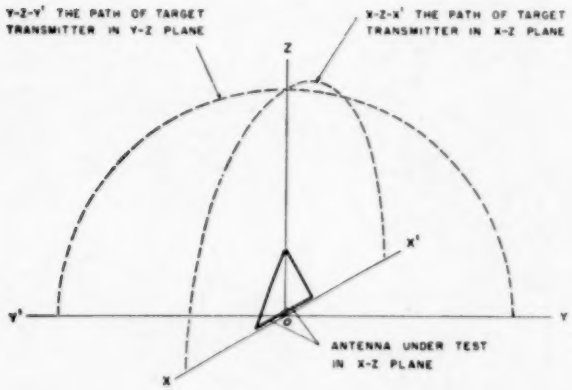

FIGURE 3. *Diagram of the model range showing the paths of the target transmitter with reference to the antenna under test.*

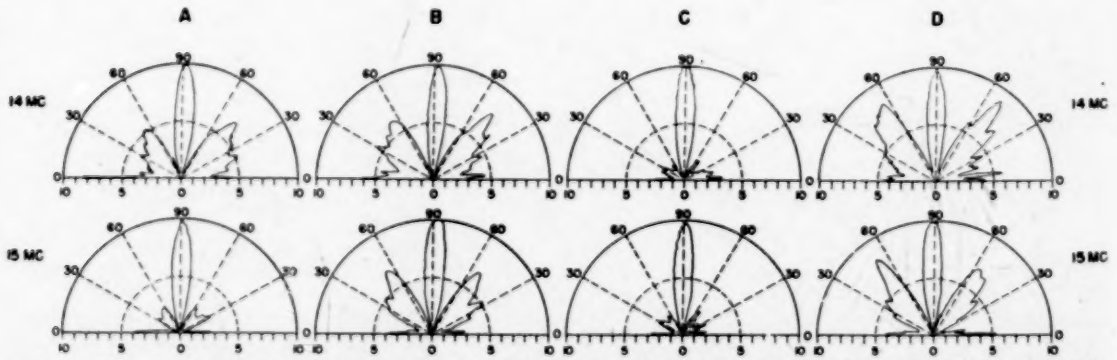

FIGURE 4. *Normalized radiation patterns in space for a multiple-wire delta antenna supported by an insulated mast and for a multiple-wire delta antenna supported by a metal mast with and without guy wires.*

The patterns are taken in the *X-Z* plane, and the antenna is in the *X-Z* plane. The radial displacement is proportional to power. A, Nonconducting mast; B, metal mast; C, metal mast with continuous guy wires; D, metal mast with guy wires that have insulators inserted every 7½ ft.

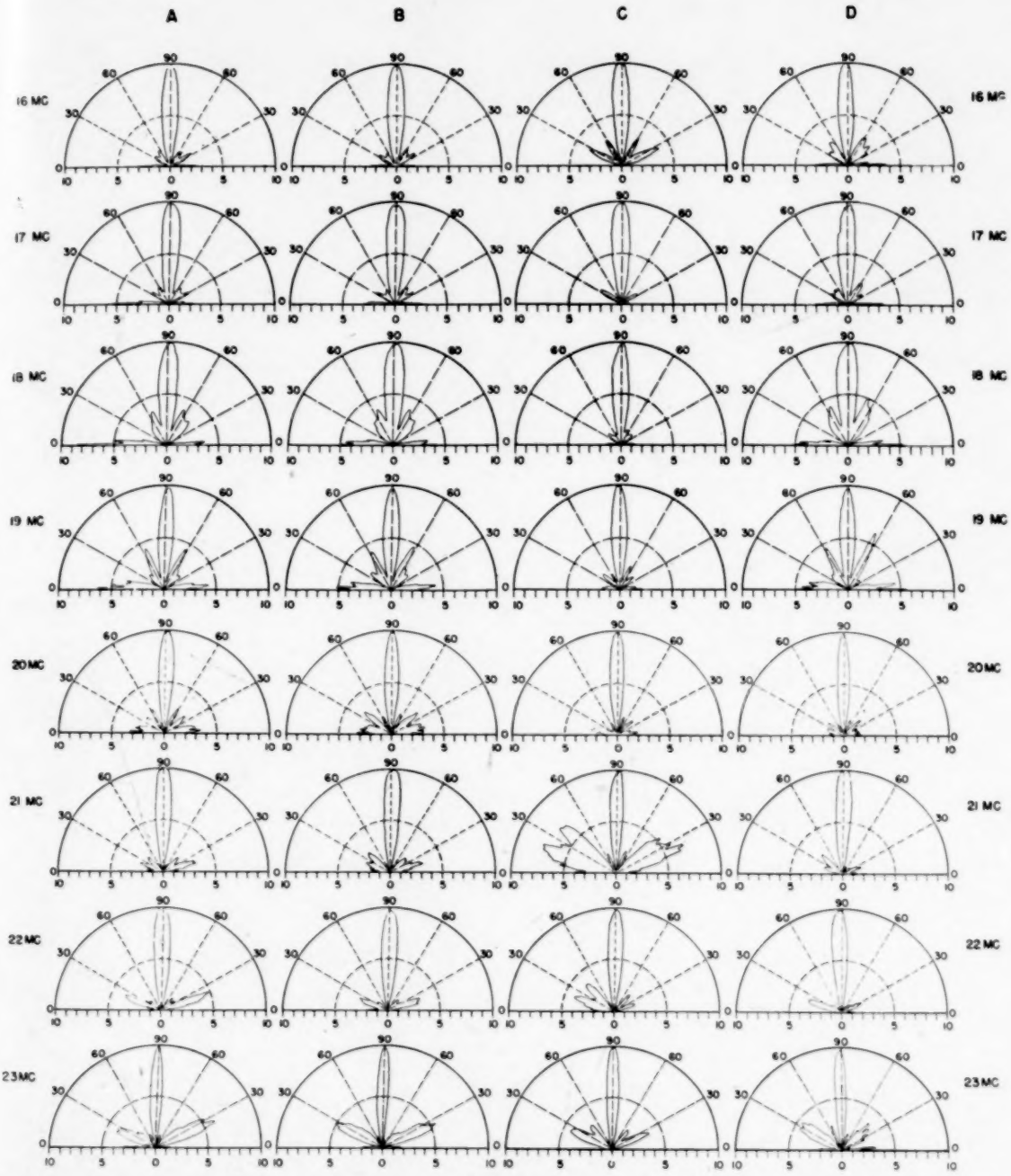

FIGURE 4—*Continued. Normalized radiation patterns in space for a multiple-wire delta antenna supported by an insulated mast and for a multiple-wire delta antenna supported by a metal mast with and without guy wires.*

The patterns are taken in the *X-Z* plane, and the antenna is in the *X-Z* plane. The radial displacement is proportional to power. A, Nonconducting mast; B, metal mast; C, metal mast with continuous guy wires; D, metal mast with guy wires that have insulators inserted every 7½ ft.

UNIVERSITY OF MICHIGAN LIBRARIES

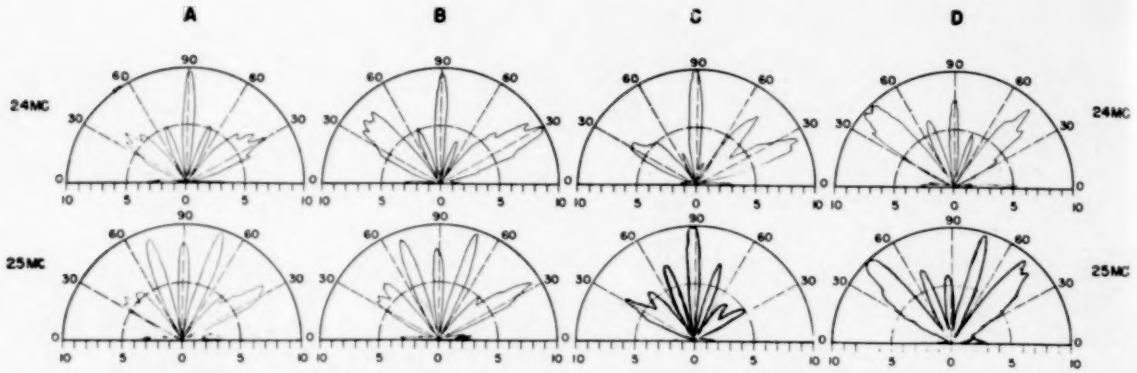

FIGURE 4—*Continued. Normalized radiation patterns in space for a multiple-wire delta antenna supported by an insulated mast and for a multiple-wire delta antenna supported by a metal mast with and without guy wires.*

The patterns are taken in the *X-Z* plane, and the antenna is in the *X-Z* plane. The radial displacement is proportional to power. A, Nonconducting mast; B, metal mast; C, metal mast with continuous guy wires; D, metal mast with guy wires that have insulators inserted every 7½ ft.

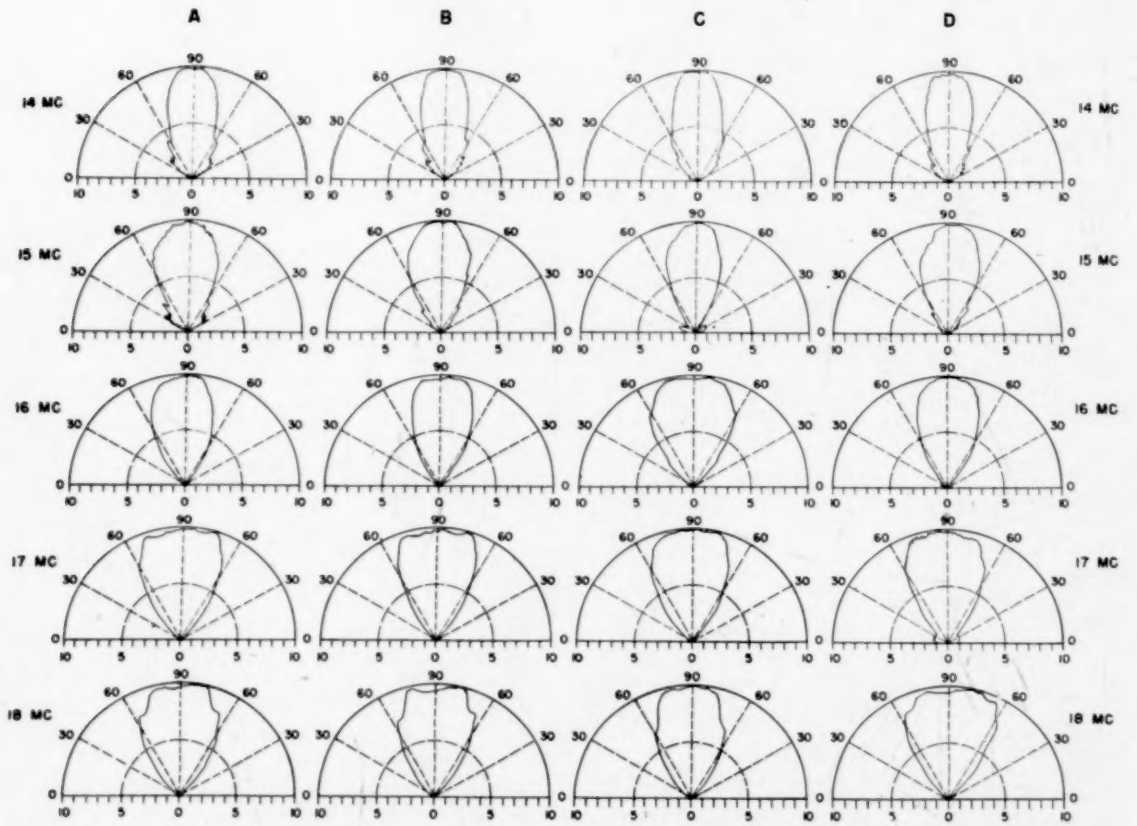

FIGURE 5. *Normalized radiation patterns in space for a multiple-wire delta antenna supported by an insulated mast and for a multiple-wire delta antenna supported by a metal mast with and without guy wires.*

The patterns are taken in the *Y-Z* plane, and the antenna is in the *X-Z* plane. The radial displacement is proportional to power. A, Nonconducting mast; B, metal mast; C, metal mast with continuous guy wires; D, metal mast with guy wires that have insulators inserted every 7½ ft.

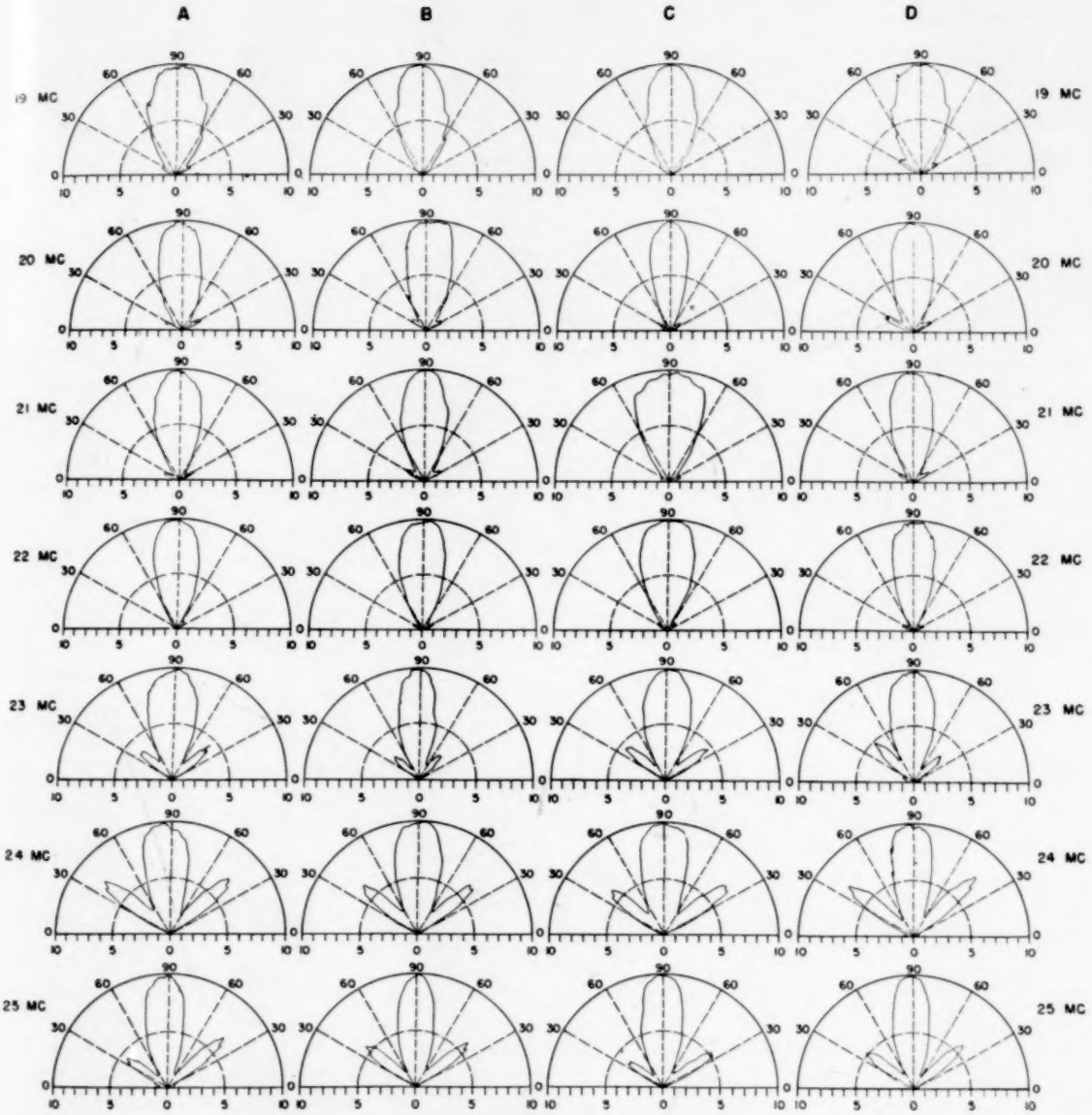

FIGURE 5—*Continued. Normalized radiation paterns in space for a multiple-wire delta antenna supported by an insulated mast and for a multiple-wire delta antenna supported by a metal mast with and without guy wires.*

The patterns are taken in the *Y-Z* plane, and the antenna is in the *X-Z* plane. The radial displacement is proportional to power. A, Nonconducting mast; B, metal mast; C, metal mast with continuous guy wires; D, metal mast with guy wires that have insulators inserted every 7½ ft.

UNIVERSITY OF MICHIGAN LIBRARIES

916783—51——4

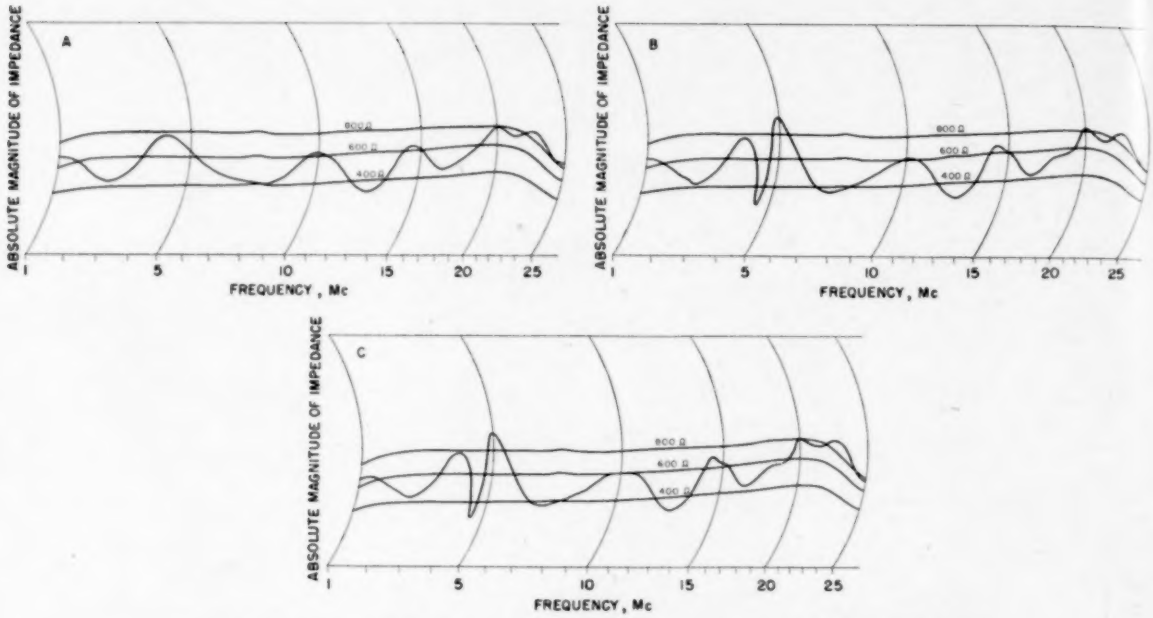

FIGURE 6. *Impedance of 600-ohm multiple-wire delta antenna with and without guy wires.*

A, Impedance of multiple-wire delta antenna without guy wires; B, impedance of multiple-wire delta antenna with long continuous guy wires; C, impedance of multiple-wire delta antenna with long and short continuous guy wires.

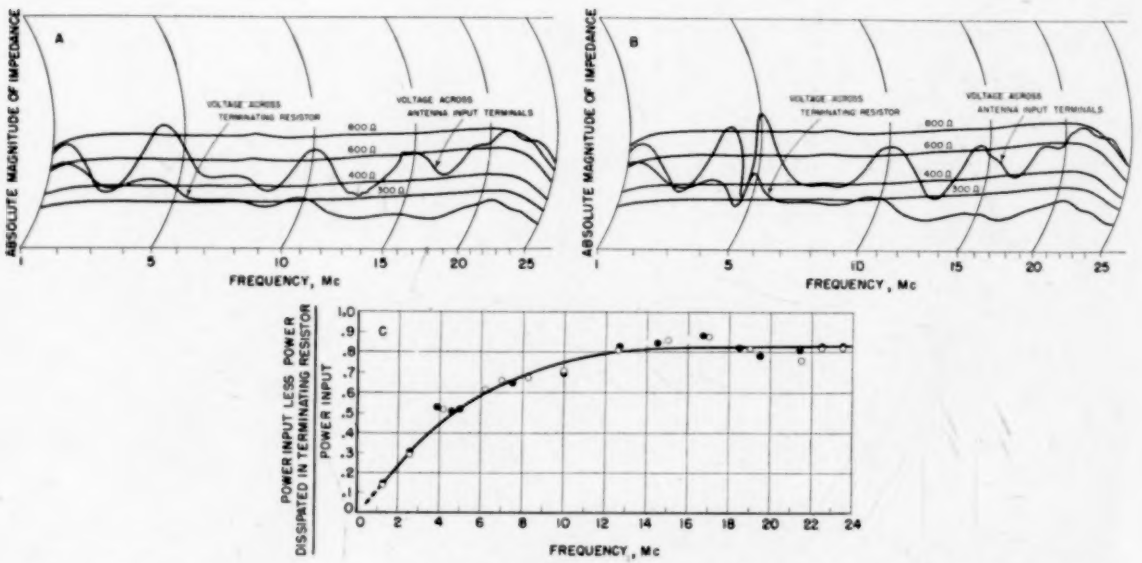

FIGURE 7. *Measurements of the quasi-radiation efficiency of a multiple-wire delta antenna with and without guy wires.*

A, 600-ohm multiple-wire delta antenna supported by a wooden mast, no guy wires used; B, 600-ohm multiple-wire delta antenna supported by a wooden mast, continuous guy wires used; C, ○, without guy wires; ●, with continuous guy wires.

WASHINGTON, October 16, 1950.

Journal of Research of the National Bureau of Standards Vol. 46, No. 2, February 1951 Research Paper 2183

Heat of Solution of Zinc Oxide in 2 *N* Hydrochloric Acid

Richard B. Peppler and Edwin S. Newman

The heat of solution of ZnO in 2 *N* hydrochloric acid was found to vary from 185 to 203 calories per gram, depending on the proportion of ZnO. For 1 gram of ZnO in 640 grams of 2 *N* hydrochloric acid, the heat of solution was found to be 185 calories per gram, in fair agreement with the value[2] of 196 calories per gram calculated from the published heats of formation of ZnO, $ZnCl_2$(aq), and HCl(aq), and the measured heat of mixing of $ZnCl_2$(aq) with HCl(aq).

I. Introduction

Zinc oxide has been found to be a convenient material for determining the energy equivalent (heat capacity) of calorimeters that are to be used for the determination of the heats of solution of acid-soluble materials [1, 2].[1] It has proved to be particularly useful in those laboratories that do not have the relatively elaborate equipment necessary for an electrical calibration.

In the Federal and in the ASTM specifications for measuring the heat of hydration of portland cement, [3, 4], zinc oxide serves as a standard to determine the energy equivalent of the heat-of-solution calorimeter. In the specified procedure, 2 *N* nitric acid solution constitutes 98 percent of the solvent, the remaining 2 percent being hydrofluoric acid. The experimentally determined heat of solution of ZnO in this solvent and the value of the heat of solution of ZnO in 2 *N* nitric acid calculated from available heat-of-formation data are in good agreement.

Some investigators, however, have used hydrochloric acid as a solvent in the determination of the heat of solution of portland cement and other materials [2, 5, 6, 7]. In some investigations of this type at this Bureau, zinc oxide has been used to calibrate the heat-of-solution calorimeters.

The data presented here show fair agreement with the value of the heat of solution of ZnO calculated from published heat-of-formation data, when the heat of mixing of $ZnCl_2$ (aq) with HCl (aq) is taken into account.

II. Apparatus and Reagents

All the determinations were made in a heat-of-solution colorimeter described previously [11]. The energy equivalent of the calorimeter was determined electrically. In each experiment, the calorimeter charge was 640 g of 2 *N* hydrocholoric acid (HCl.26.64 H_2O at 25° C).

Zinc oxide of analytical reagent quality was ground to pass a No. 100 sieve, heated for 1 hour at 900° to 950° C, and stored in the laboratory in a dark screw-capped bottle.

For the determination of the heat of dilution of $ZnCl_2$ in 2 *N* HCl, an aqueous stock solution of $ZnCl_2$, 53.28 H_2O was prepared from $ZnCl_2$ of analytical reagent quality and of known moisture content. The calorimeter sample was taken from this aqueous solution of $ZnCl_2$.

In order to know accurately the temperature of the calorimeter sample, in the dilution experiments, the $ZnCl_2$ solution was kept in a bottle immersed in the constant-temperature bath of the calorimeter. The pipette with which the sample was transferred to the calorimeter was also kept in the bath in a vertical brass tube closed at the bottom and projecting slightly above the water surface. Thus the temperature of the zinc chloride solution was nearly the same as that of the bath. As the calorimeter was operated so that the final temperature was nearly the same as that of the bath, only a small correction was necessary to account for the heat capacity of the sample.

The final temperatures of the calorimeter in the heat-of-solution experiments were from 24.5° to 27.4° C. No attempt was made to correct the heats of solution to 25° C.

III. Results and Discussion

1. Experimental Measurements

Determinations were made of the heat of solution in 2.00 *N* HCl of samples of ZnO ranging from 0.1 to 20 g in weight. Three determinations were made with each size of sample (see table 1). The results were plotted against sample weight, and a line was fitted to the data by the method of least squares (fig. 1). The equation of this line was found to be $Q=184.7+0.91x$, where Q is the heat of solution in calories per gram, and x is the sample weight in grams.

TABLE 1. *Effect of sample weight on the heat of solution of* ZnO *in 640 grams of 2 N* HCl.

ZnO	Heat of solution			
	1	2	3	Average
g	*cal/g*	*cal/g*	*cal/g*	*cal/g*
0.1	185.4	184.6	184.5	184.8
.5	186.4	183.9	184.6	185.0
1	185.0	185.4	184.4	184.9
2	188.4	186.7	185.8	187.0
3	187.0	188.7	188.1	187.9
4	189.4	186.7	189.8	188.6
7	190.9	190.7	191.7	191.1
10	195.0	195.3	192.7	194.3
14	198.1	197.1	194.1	196.4
20	206.6	202.6	200.8	203.3

[1] Figures in brackets indicate the literature references at the end of this paper.

UNIVERSITY OF MICHIGAN LIBRARIES

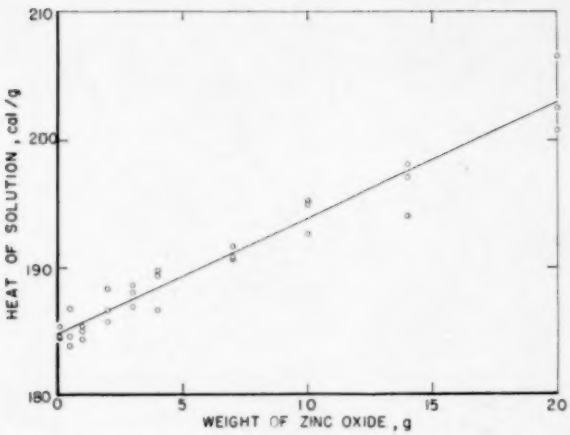

FIGURE 1. *Effect of sample weight on the heat of solution of ZnO in 640 g of 2 N hydrochloric acid.*

The equation of the line is $Q=184.7+0.91x$, where Q is the heat of solution in calories per gram, and x is the weight of the sample in grams.

A sample of 28 g was dissolved, and a value only slightly greater than that of a 20-g sample was obtained, indicating that at higher concentrations, the curve flattens out. An attempt to determine the heat of solution of a 56-g sample failed because of the extreme difficulty in measuring the large and rapid temperature rise, and because the sample would not dissolve completely within a reasonable time, that is, 60 min.

It may be seen in figure 1 that the value of the heat of solution of ZnO in 2 N HCl at infinite dilution is approximately 185 cal/g.

The variation of Q with sample weight, as indicated by the slope of the line in figure 1, is a measure of the change in the heat of dilution for a solution of zinc chloride in hydrochloric acid. The variation of Q also includes the heat of dilution of the hydrochloric acid mix resulting from the formation of water and the removal of HCl as a consequence of the reaction. This heat effect is small relative to the dilution of the zinc chloride solution, except in the case where large samples of zinc oxide are used, in which cases the proportions of HCl removed and of additional H_2O added to the final concentration by the reaction are significant.

2. Method of Calculation

The heat of solution of a 1-g sample of ZnO in 640 g of 2.00 N hydrochloric acid at 25° C may be represented by the following over-all reaction

$$\frac{1}{81.38}\mathrm{ZnO}(c)+\frac{45.18}{36.46}\mathrm{HCl},\frac{594.82}{18.02}\mathrm{H_2O}\rightarrow\frac{1}{81.38}\mathrm{ZnCl_2},\left(\frac{45.18}{36.46}-\frac{2}{81.38}\right)\mathrm{HCl},\left(\frac{594.28}{18.02}+\frac{1}{81.38}\right)\mathrm{H_2O}+Q.$$

Writing this equation in the customary form based on 1 mole of ZnO

$$\mathrm{ZnO}(c)+100.85(\mathrm{HCl},\ 26.64\ \mathrm{H_2O})\rightarrow \mathrm{ZnCl_2}\ [98.85\ (\mathrm{HCl},\ 27.19\ \mathrm{H_2O})]+Q. \quad (1)$$

Equation 1 may be considered as the sum of the following four equations:

$$100.85\ (\mathrm{HCl},\ 26.64\ \mathrm{H_2O})\rightarrow 98.85\ (\mathrm{HCl},\ 26.64\ \mathrm{H_2O})+2\ (\mathrm{HCl},\ 26.64\ \mathrm{H_2O})+Q_1. \quad (2)$$

$$\mathrm{ZnO}\ (c)+2\ (\mathrm{HCl},\ 26.64\ \mathrm{H_2O})\rightarrow \mathrm{ZnCl_2},\ 53.28\ \mathrm{H_2O}+\mathrm{H_2O}\ (l)+Q_2. \quad (3)$$

$$\mathrm{ZnCl_2},\ 53.28\ \mathrm{H_2O}+98.85\ (\mathrm{HCl},\ 26.64\ \mathrm{H_2O})\rightarrow \mathrm{ZnCl_2}\ [98.85\ (\mathrm{HCl},\ 27.18\ \mathrm{H_2O})]+Q_3. \quad (4)$$

$$\mathrm{ZnCl_2}\ [98.85\ (\mathrm{HCl},\ 27.18\ \mathrm{H_2O})]+\mathrm{H_2O}\ (l)\rightarrow \mathrm{ZnCl_2}\ [98.85\ (\mathrm{HCl},\ 27.19\ \mathrm{H_2O})]+Q_4. \quad (5)$$

The heat of the reaction Q[2] is the sum of Q_1, Q_2, Q_3, and Q_4 and may be calculated if the individual heats of reaction are known. The value of Q_1 is zero. The heat of reaction Q_2 (eq 3), calculated from heats of formation [8, 9] is 19.11 kcal/mole of ZnO at 25° C.

The value of Q_3 (eq 4) was found in the heat of dilution experiments with $ZnCl_2$ to be -3.22 ± 0.01 kcal/mole.

The value of Q_4 (eq 5) was calculated from published data on the heat of dilution of HCl [10], assuming that the heat effect of adding 1 mole of H_2O to a solution of 98.85 moles of HCl and 2,688 moles of H_2O would not be appreciably affected by the presence of 1 mole of $ZnCl_2$ in the solution. The value of Q_4 was found to be $+0.02$ kcal/mole.

Thus the heat of reaction Q can be calculated to be

$$Q=19.11-3.22+0.02=+15.91\ \text{kcal/mole}$$

$$=195.5\ \text{cal/g ZnO}.$$

This value differs by 10 cal/g from the value determined experimentally. Part of the discrepancy may lie in the uncertainties in the published heat-of-formation data used to calculate Q_2 (eq 3).

The value of the heat of solution of ZnO in 2 N nitric acid was calculated on the assumption that the $Zn(NO_3)_2$ formed is diluted in water, instead of nitric acid, as is actually the case. This value does not differ appreciably from the value determined in this laboratory in experiments in which ZnO was dissolved in a mixture of 98 percent of 2 N nitric and 2 percent of hydrofluoric acids [12]. However, because of the large endothermic heat effect of the dilution of $ZnCl_2$ in HCl, a corresponding assumption in the case of ZnO dissolving in HCl leads to a great discrepancy (100 cal/g) between the value experimentally determined and the value calculated in this manner.

[2] The heat of the reaction is considered to be positive if heat is evolved, i. e., $Q=-\Delta H$.

IV. Summary

The change of the heat of solution of ZnO in 640 g of 2 *N* HCl with sample weight was investigated in the range from 0.1 to 20 g of ZnO. This relation can be represented by a straight line having a slope of approximately 1 cal/g/g and an intercept on the *Q* axis (*Q* at infinite dilution) of approximately 185 cal/g. For 1 gram of ZnO in 640 g of 2 *N* hydrochloric acid, the heat of solution was found to be 185 cal/g, in fair agreement with the value of 196 cal/g calculated from the published heats of formation of ZnO, $ZnCl_2$(aq), and HCl(aq) and the measured heat of mixing of $ZnCl_2$(aq) with HCl(aq).

V. References

[1] R. W. Stenzel and S. B. Morris, Ind. Eng. Chem. Anal. Ed. **6,** 246 to 249 (1934).
[2] E. W. Reed-Lewis, private communication.
[3] Federal Specifications SS–C–158b for Cements, hydraulic; general specifications (May 20, 1946).
[4] Heat of hydration of portland cement, test for; American Society for Testing Materials, designation C186–47.
[5] S. C. Pierce and H. Mac. Larmour, Eng. News-Record, p. 114 (Jan. 1934).
[6] L. S. Wells and K. Taylor, J. Research NBS **19,** 215 (1937) RP1022.
[7] T. Thorvaldsen, J. Am. Chem. Soc. **51,** 2678 (1929).
[8] F. R. Bichowsky and F. D. Rossini, Thermochemistry of chemical substances (Reinhold Publishing Corp., New York, N. Y., 1936).
[9] Selected values of chemical thermodynamic properties, Series 1, Table 31–2 (NBS, Dec. 31, 1948) and Table 10–3 (NBS Mar. 31, 1947).
[10] F. D. Rossini, BS J. Research **6,** 791 (1931) RP305.
[11] E. S. Newman and L. S. Wells, J. Research NBS **20,** 825 (1938) RP1107.
[12] L. Shartsis and E. S. Newman, Proc. ASTM **43,** 905 (1943).

WASHINGTON, August 29, 1950.

UNIVERSITY OF MICHIGAN LIBRARIES

Journal of Research of the National Bureau of Standards Vol. 46, No. 2, February 1951 Research Paper 218

Bounds for Characteristic Roots of Matrices II

Olga Taussky

This is a continuation of an earlier note (Duke Mathematical Journal, volume **15**, pages 1043–44 (1948)). It deals with bounds for the characteristic roots of matrices with positive (nonnegative) elements, and with bounds for multiple roots.

This note is a continuation of an earlier one [1].[1] There the position of the characteristic roots of an $n \times n$ matrix $A=(a_{ik})$ inside or on the boundary of the n circles C_i with centers a_{ii} and radii $A_i=\sum_{k\neq i}|a_{ik}|$ was studied.

In particular, it was shown in [1] that for $n=2$ the common part of the circles cannot contain a root unless it is a common boundary point. This fact is not true for $n>2$ as is, for example, shown by the matrix

$$\begin{pmatrix} 0 & 1 & 0 \\ 0 & 0 & 1 \\ 0 & -15 & -8 \end{pmatrix},$$

which has the roots $0, -3, -5$. The root 0 is contained in all three circles. It can however be shown that an analogue of the situation for $n=2$ holds if further conditions are imposed on the elements a_{ik}.

Theorem 1. The dominant root of a matrix of positive elements cannot be a common point of all n circles C_i unless it is a common boundary point of at least two of the circles.

Proof. It is known [2] that the dominant root λ of such a matrix is real and positive and that the corresponding characteristic vector $x_1, \cdots, x_n$ can be chosen in such a way that all its components are positive. Consider then the equation

$$a_{i1}x_1+\cdots+(a_{ii}-\lambda)x_i+\cdots+a_{in}x_n=0, \qquad (1)$$

or

$$(\lambda-a_{ii})x_i=\sum_{k\neq i}a_{ik}x_k. \qquad (2)$$

As the right-hand side of (2) is positive, it follows that

$$\lambda-a_{ii}>0. \qquad (3)$$

Equation (2) implies that

$$(\lambda-a_{ii})x_i \geq A_i \min_{k\neq i} x_k. \qquad (4)$$

Let λ be an inner point of all circles C_i, that is,

$$\lambda-a_{ii}<A_i, \qquad i=1, \cdots, n. \qquad (5)$$

It follows from (4) that

$$x_i>\min_{k\neq i} x_k, \qquad i=1, \cdots, n.$$

This is not possible. Hence λ cannot be an inner point of all C_i. Assume then that λ was on the boundary of at least one circle C_i, say C_1, and an inner or boundary point of all other circles. Then relation (4) for $i=1$ implies that

$$x_1 \geq \min_{k\neq 1} x_k. \qquad (6)$$

Let

$$\min_{k\neq 1} x_k = x_2, \text{ (say)} \qquad (7)$$

and consider relation (4) for $i=2$. This implies that either

$$\lambda-a_{22}=A_2 \text{ and } x_2 \geq \min_{k\neq 2} x_k \qquad (8)$$

or

$$\lambda-a_{22}<A_2 \text{ and } x_2>\min_{k\neq 2} x_k. \qquad (9)$$

However, relations (6), (7), (9) lead to a contradiction and so (8) holds which means that λ is on the boundary of C_2.

It can be shown that the dominant root of a matrix of positive elements can lie inside of $n-1$ circles and outside of one circle without touching the boundaries. The following example of this was communicated to the author by A. Ostrowski:

Define a_{ik} $(i\neq k)$ as arbitrary positive numbers. Take λ sufficiently large and positive and define a_{ii} by

$$a_{ii}=\lambda-\frac{1}{2}a_{i1}-\sum_{\substack{k=2 \\ k\neq i}}^{n} a_{ik}>0, \; i>1,$$

$$a_{11}=\lambda-2\sum_{k=2}^{n} a_{1k}>0.$$

It follows that λ is a characteristic root of the matrix (a_{ik}) and that the corresponding vector is $\left(\frac{1}{2}, 1, \cdots, 1\right)$. Hence λ is the dominant root, as the other roots cannot have vectors with positive coordinates only [2].

Two generalizations of theorem 1 are possible, one to matrices with nonnegative elements instead of positive ones. These matrices have as one of their dominant roots a nonnegative real number, and the corresponding vector can be chosen to have nonnegative components. Hence, all the above arguments can be repeated, as long as equations (2) do not involve any equation of the form $0=0$. This

[1] Figures in brackets indicate the literature references at the end of this paper.

could only occur, if the matrix A can be transformed to the form

$$\begin{pmatrix} P & O \\ U & Q \end{pmatrix}$$

by the same permutation of the rows and columns [1] and where P and Q are square matrices, and 0 consists of zeros. Thus the following theorem holds:

Theorem 2. Let A be a matrix of nonnegative elements which cannot be transformed to the form

$$\begin{pmatrix} P & O \\ U & Q \end{pmatrix}$$

by the same permutation of the rows and columns. Then the real dominant root of A cannot be a common point of all n circles C_i unless it is a common boundary point of at least two of these circles.

Consider now matrices whose main diagonal elements are arbitrary real, but whose off-diagonal, elements are positive (nonnegative). It is known [3, 4] that such a matrix has as root with largest real part a real positive (nonnegative) number and the components of the corresponding vectors can be chosen to be all positive (nonnegative). It is clear that theorems 1 and 2 can be generalized to these matrices.

The remaining two theorems concern multiple roots of general matrices. It is easy to find examples of matrices with a multiple root that is contained as inner or boundary point in only one circle C_i. It can, however, be proved that in this case the rank of the matrix

$$(a_{ik}-\lambda\delta_{ik}) \text{ is } n-1.$$

Theorem 3. A characteristic root λ which is an inner or boundary point of only one circle C_i cannot have two independent characteristic vectors corresponding to it.

Proof. Assume that $|a_{11}-\lambda| \leq A_1$ and $|a_{ii}-\lambda| > A_i$ for $i \neq 1$. Consider any characteristic vector $x_1, \ldots, x_n$ which corresponds to λ. Then the relations

$$|a_{ii}-\lambda|\ |x_i| \leq A_i \max_{k \neq i} |x_k| \tag{10}$$

hold. For $i>1$ they imply that

$$|x_i| < \max_{k \neq i} |x_k|. \tag{11}$$

Hence

$$|x_1| = \max_k |x_k| > |x_i| \text{ for } i>1.$$

This eliminates the possibility of a vector $y_1, \ldots, y_n$ that corresponds to λ and is independent of $x_1, \ldots, x_n$, because otherwise a linear combination of both vectors could be found in which the first component is 0 and which does not vanish identically.

Theorem 4. If A has a characteristic root λ of multiplicity $n-1$ and with $n-1$ independent characteristic vectors then λ is contained in at least $n-1$ circles C_i.

Proof. The matrix $(a_{ik}-\lambda\delta_{ik})$ has the same vectors as (a_{ik}) and as roots the numbers $\mu-\lambda$ when μ runs through all roots of (a_{ik}). The circles that correspond to the matrix $(a_{ik}-\lambda\delta_{ik})$ have the same radii as the original ones, but their centers are moved from a_{ii} to $a_{ii}-\lambda$. Hence, we may restrict ourselves to the case where $\lambda=0$. In this case the matrix can be transformed to the form

$$X = \begin{pmatrix} 0 & & & & \\ & \cdot & & & \\ & & \cdot & & \\ & & & 0 & \\ & & & & \alpha \end{pmatrix}$$

by means of a nonsingular matrix $U=(u_{ik})$. Denote by Δ the determinant $|u_{ik}|$ and by U_{ik} the cofactor of u_{ik}. It is then easy to see that the original matrix $(a_{ik})=UXU^{-1}$ is of the form

$$(a_{ik}) = \begin{pmatrix} \alpha u_{1n}U_{1n}/\Delta & \alpha u_{1n}U_{2n}/\Delta & \ldots & \alpha u_{1n}U_{nn}/\Delta \\ \alpha u_{2n}U_{1n}/\Delta & \alpha u_{2n}U_{2n}/\Delta & \ldots & \alpha u_{2n}U_{nn}/\Delta \\ \cdots & \cdots & \cdots & \cdots \\ \alpha u_{nn}U_{1n}/\Delta & \alpha u_{nn}U_{2n}/\Delta & \ldots & \alpha u_{nn}U_{nn}/\Delta \end{pmatrix}.$$

Assume now that 0 lies outside one of the circles, say C_1. This implies

$$|U_{1n}| > \sum_{k \neq 1} |U_{kn}|. \tag{12}$$

This, however, implies that

$$|U_{in}| < \sum_{k \neq i} |U_{kn}|, \qquad i=2, \ldots, n.$$

From this it follows that 0 lies inside all circles C_i, $i=2, \ldots, n$, which proves the theorem.

[1] O. Taussky, Bounds for characteristic roots of matrices, Duke Math. J. **15,** 1043 (1948).

[2] G. Frobenius, Über Matrizen aus positiven elementen, Berlin Sitzb. p. 471 (1908) and 514 (1909); Über Matrizen aus nicht negativen elementen, Berlin Sitzb. p. 456 (1912).

[3] H. Rohrbach, Bemerkungen zu einem determinantensatz, Jahresber. Deut. Math. Ver. **40,** 49 (1931).

[4] Z. Szmydtówna, Sur les racines caractéristiques et sur les directions caractéristiques de certains matrices, Ann. Soc. Pol. Math. **22,** 235 (1949).

WASHINGTON, September 20, 1950.

UNIVERSITY OF MICHIGAN LIBRARIES

Journal of Research of the National Bureau of Standards Vol. 46, No. 2, February 1951 Research Paper 218

Microhardness Tester for Metals at Elevated Temperatures

Abner Brenner

An apparatus has been devised for measuring the hardness of electrodeposited coatings at temperatures up to 900° C in an inert atmosphere. Coatings thicker than about 0.07 millimeter (0.003 inch) may be tested. The main parts of the apparatus are: (1) The indenting mechanism, consisting of a Vicker's diamond mounted on a shaft of fused silica; (2) a mechanical device for raising and lowering the indenter; (3) a micrometer device for orienting the specimen under the indenter; (4) the heating unit. The force on the indenter is varied either by dead-weight loading or by changing the gas pressure inside of the apparatus. Some typical measurements made with the apparatus are given.

I. Introduction

The hot-hardness of a metal may be an important indication of its performance in certain applications at elevated temperatures. As a relation usually exists between the hardness of a metal and some of its other mechanical properties, such as tensile strength, a measurement of hardness may also be useful for obtaining an estimate of those mechanical properties that are more difficult to measure. The development of a microhardness tester that could be used for testing electrodeposits at elevated temperatures was undertaken in connection with studies of electrodeposited metals and alloys.

The hot-hardness of bulk metals has been measured by the same methods as those used at room temperature. These methods utilized a variety of different types of indenters to produce indentations in metals by static or dynamic loading. Other methods were based on mutual indentation procedures, which involved pressing together two cylinders of metal. None of these methods will be discussed in detail because excellent reviews may be found in the literature [1, 2, 3].[1] Of various types of indenters used, the only ones suitable for metal coatings are pointed diamonds, by means of which a micro-indentation may be produced with a small load. Hot-hardness testers with diamond indenters have been designed by P. Bens [4] and E. C. Bishop and M. Cohen [5] for use on bulk metals. However, with these instruments the high loads customary for bulk materials were used in producing the indentations. The procedure consisted in placing the heating unit with the specimen on the platform of a commercial hardness tester and then applying the load on the indenter with that instrument.

The loads ordinarily used in measuring the hardness of bulk metals are too large for use on electrodeposits because they result in too deep an indentation, and in testing electrodeposits at room temperature so-called microhardness testers are used. An ordinary hardness tester and a microhardness tester differ mainly in the magnitude of the load applied to the indenter. The same type of indenter is used for both. Whereas in a Vickers machine the load is usually of the order of 10 kg, in a microtester, the load will range from 25 to 1,000 g. Low loads are particularly necessary in testing hardness at elevated temperatures because metals are considerably softer than at room temperature.

The following example will illustrate the requirement of a low load in the measurement of electrodeposits. A metal that is quite hard at room temperature may have a hardness of only 50 Vickers at an elevated temperature. The impression made with the usual 10 kg-load would have a depth of about 0.087 mm (0.0035 in.). As it is usually considered that the thickness of a coating should be at least 10 times the depth of the indentation to obviate any effect of the basis metal, the coating would have to be about 0.87 mm (0.035 in.) thick for a satisfactory measurement. If a load of 200 g were used, the depth of the impression would be only 0.012 mm. (0.0005 in.). Thus the coating need be only 0.12 mm (0.005 in.) thick. An indentation made with a 10 kg-load would have almost penetrated a coating of this thickness.

II. Design of the Microhardness Tester

The apparatus of Bens and that of Bishop and Cohen were not suitable for measuring the hot-hardness of electrodeposits, because of the high loads used. Some measurements were made by Bens on electro deposits produced in this Bureau; but these deposits were fairly thick, and it is not certain that the effect of the basis metal was obviated. The hot-hardness tester described in this report followed to some extent the designs of Bens and of Bishop and Cohen. Two difficulties are involved in adapting microhardness testing to elevated temperatures. (1) A closed system with an inert atmosphere must be used to prevent oxidation of the specimens. If the specimen were allowed to oxidize, the thickness of the oxide film might be comparable to the depth of the indentation produced with a light load, and the hardness of the film might be quite different from that of the metal. Also, oxidation occurring after a microindentation had been made would obliterate the impression. (2) In order that a light load may be applied accurately, the shaft carrying the indenter

[1] Figures in brackets indicate the literature references at the end of this paper.

must move in a bearing with very little friction. There must be no galling of the bearing at the elevated temperatures. Since a closed system must be used to prevent entrance of air, the clearance between the rod and the bearing must be small.

Bishop and Cohen maintained an inert atmosphere in their apparatus. The shaft carrying the indenter was connected to an annular oil seal. This type of construction is unsuitable for a microhardness tester for several reasons: Small variations in gas pressure would cause large variations in the load on the indenter; the apparatus could not be evacuated for the initial removal of air; the horizontal position of the indenter is not fixed; and cumbersome cooling coils must be used to chill the oil. Bens used an evacuated apparatus, and the shaft of the indenter moved in a closely fitting bearing, lubricated with oil to hold the vacuum. This latter arrangement would not be suitable with the type of apparatus designed at this Bureau, as the bearing became too hot to be lubricated with oil. Also a vacuum was out of the question, as the atmospheric pressure alone would have imposed a load of about 500 g on the indenter.

The problems referred to were met by using in the tester an inert atmosphere slightly above atmospheric pressure. The indenter shaft was a capillary of fused silica, which moved in a dry bearing lubricated with graphite. The clearance between the shaft and the bearing was about 0.001 in., and gas escaped slowly through this space during the test. The friction of the shaft in the bearing was equivalent to 1 or 2 g at room temperature and was probably less at elevated temperatures, as the clearance between the bearing and the indenter shaft increased. Figure 1 shows the details of the construction of the indenter assembly. The indenter fitting, B, was attached to a tungsten rod, A, which passed up through the capillary, G, and was held by a collar and set screw, C. A spring arrangement was provided to hold the tungsten rod under continuous tension and thus allow for its lengthening due to thermal expansion. This indirect method of securing the indenter to the shaft was necessary because a fused silica rod could not be anchored directly to the indenter fitting. A few trials were made to cement a silica rod in the cup of the fitting by using molten potassium bisulphate. Although the rod was satisfactorily anchored on two occasions, after 1 or 2 weeks the rod cracked just above the top of the cup.

It might be of interest to note two other methods of mounting the indenter that were tried without success. A stainless steel shaft was first tried, and although it operated well at room temperature, it would gall and seize at elevated temperatures. A sapphire rod 3 mm (⅛ in.) in diameter was also tried as an indenter shaft, but it was found to be too sensitive to thermal shock, and cracked.

The complete setup used for measuring hot hardness is shown in figure 2. A sketch of the cross section of the hardness tester in figure 3 shows the relation of the working parts. The details of construction of the important parts are shown in figures 1, 4, and 5. The tester is self-contained with the loading mechanism, indenter, and furnace all built into one compact unit. The load is applied to the indenter by dead-weight loading.

The main parts of the tester will now be described briefly. The muffle, before being wound with resistance wire, is shown in figure 4. It was made by welding heavy walled stainless steel pipes together. The anvil was a solid piece of stainless steel welded in tube A. It is provided with a small hole extending to within 3 mm (⅛ in.) of the upper surface to accommodate a thermocouple. The flange, B, was bolted to the top plate of the tester with a silver gasket inbetween to make the apparatus gas tight. A doughnut-shaped disk of insulating brick was placed in the space within the flange to decrease the heat transfer to the top plate of the tester. To provide uniformity of heating, the muffle unit was wound on all four limbs with a continuous length of No. 16 Nichrome wire on an Alundum form. The space between the furnace unit and the main shell was filled with insulation. By making the muffle assembly a single welded unit, and by supporting it from a single point, the relative motion between various parts resulting from thermal expansion was minimized.

The indenter assembly was raised and lowered at the rate of 2 cm (0.75 in.) per minute by a small motor that operated a simple screw mechanism similar to that used on the compound rest of a lathe. The vibration of the motor was damped by a mounting of rubber shock absorbers, and no difficulties were encountered from this source. The disk, E, figure 1, supporting the indenter assembly, rested on two pieces of rubber tubing, which served to make the application of the load more gradual when the supporting frame was lowered away from the assembly.

The indenter assembly weighed about 200 g. This was the maximum load applied in the tests, although larger loads could be applied by placing doughnut-shaped weights on the top of the indenter assembly. Usually lower loads were used at elevated temperatures. These were obtained by increasing the gas pressure in the tester above atmospheric. Each centimeter of mercury was equivalent to a decrease of 7 g in the load applied to the indenter. The smallest load used in the tests was about 30 g.

The assembly for holding and moving the specimens is shown in figure 5. The specimens measure 6 by 6 by 12 mm (0.25 by 0.25 by 0.5 in.) and are polished by metallographic procedures. Six specimens may be indented in one heat. They fit into the carriage, B, which slides in a keyway on the inside of the muffle. The carriage is moved along by a stainless steel micrometer screw, which has been plated with cobalt-tungsten alloy to prevent seizing at elevated temperatures. The micrometer serves to locate an indentation within about 0.2 mm (0.008 in.) of a desired spot.

Because the indentations are microscopic in size, they are difficult to locate in the small field of a microscope when making the subsequent measurements of diagonals. For this reason a fitting (D, fig. 5) was designed to hold the carriage in a definite

UNIVERSITY OF MICHIGAN LIBRARIES

position on the moving microscope stage. By setting the microscope stage at the same reading as that on the micrometer when the indentation was made, the impression appeared in the field.

The temperature of the furnace was measured by a thermocouple that was placed in the cavity extending up through the anvil. In preliminary checking the temperature within the muffle was measured also with a thermocouple inserted through the top bearing of the tester. The two thermocouples agreed within about 5 or 10 deg. centigrade. The temperature was automatically controlled by a commercial pyrometer.

In addition to its use for measuring the hot-hardness of electrodeposits, the microhardness tester may be used for testing bulk metals and has several advantages over the two instruments on which it was based.

1. It is a self-contained instrument, and incorporates within one unit both the furnace and the device for loading the indenter.
2. Six specimens may be tested in one heating cycle.
3. The micrometer screw permits indentation to be made at specified points and enables them subsequently to be readily located in the microscopic field.
4. The small loads are less likely to cause the diamond to shift in its mounting (usually consisting of monel metal) when measurements are made at very high temperatures.

III. Procedure for Making Measurements

The first step in using the hot-hardness tester, after placing the specimens in the instrument, was to evacuate the apparatus and then flush with hydrogen. Nitrogen or argon could also be used. Before turning the current on the furnace, the atmosphere in the apparatus was tested by heating the fused silica tube, G, figure 2, which contained a strip of bright steel. If the steel remained bright on heating and cooling, the tester was heated.

The gas was passed over heated copper (B, fig. 2) to remove oxygen, and then through a drying tube, before reaching the furnace. The flow of gas was measured with a flow meter, A, and was of the order of 60 ml/min, under a pressure of from 3 to 25 cm of mercury. The tester was kept under a positive pressure of gas during the heating, both to regulate the load on the indenter and to prevent the entrance of air, as the apparatus was not vaccum tight.

The pressure in the apparatus was kept constant without difficulty by regulating the needle valve on the gas tank and the needle valve, J, figure 2, on the exit end of the system.

After the heat was turned on the furnace heated up rapidly. About 10 min were required to reach a temperature of 600° C and about 15 min additional were required to reach a temperature of 800° C. The furnace was held at any one temperature for about 15 min before making indentations. At each temperature a set of three indentations were made about 0.01 in. apart, according to preselected micrometer settings. Along with each set of specimens, a molybdenum specimen was used as a check on the precision of the run. The apparatus has been used at 900° C, but most of the data were obtained at a maximum temperature of 800° C.

The accuracy of the hot-hardness tester could be determined only at room temperature. This was done by comparing with a standard type of microhardness tester. Measurements were made with the bot-hardness tester on a variety of different types of specimens, which were then measured with an Eberbach microhardness tester. The agreement of the results, on an average, was within 4 percent.

The reproducibility of the instrument was determined by measurements on a molybenum specimen. In four runs, coverirg the range of room temperature, 400°, 600°, and 800° C, the average deviation from the mean hardness at each temperature was less than 4 percent. Because of the reproducibility of its hardness, the molybdenum specimen was used as a check on the proper functioning of the hardness tester, and a molybdenum specimen was included along with each set of test specimens.

IV. Measurements

Some of the data obtained with the hot-hardness tester, chiefly on electrodeposits, are shown in figures 6, 7, and 8. These data are given to illustrate the use of the instrument and are not presented as part of a systematic investigation of the hot-hardness of metals. Figure 6 shows that soft chromium and hard chromium are about equally soft above 600° C. At 800° C. the hardness of both has dropped to about 100 Vickers, as compared with the high initial values of 600 and 1,000 Vickers.

It will be noted that chromium and nickel become permanently softened as a result of the heat treatment, that is, on cooling to room temperature the hardness is lower than initially. In contrast to this, cobalt and cobalt alloys, figures 7 and 8, regain a large part of their initial hardness on cooling, or may even increase in hardness, provided that the maximum temperature has not been excessive. The maintenance or increase in hardness of a metal after heat treatment cannot be considered as evidence of good hot-hardness. This is demonstrated particularly well by the data on the cobalt phosphorus alloys, figure 7, which have a hardness of only 5 Vickers at 800° C. but which become harder than initially after cooling.

The hot-hardness of the cobalt-tungsten alloys, figure 8, appears to increase with their tungsten content. The alloy containing 31 percent of tungsten is outstanding in hot-hardness. At 800° C. it is as hard as cobalt is at room temperature. Unfortunately, the higher the tungsten content, the more difficult the alloys are to deposit, and the more likely they are to be excessively brittle and to crack on heating, especially when deposited on a steel base.

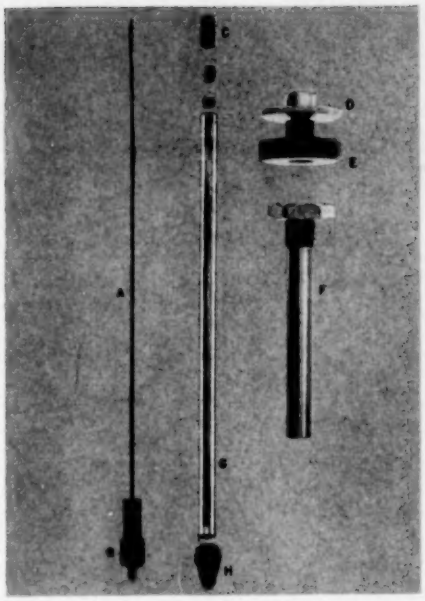

FIGURE 1. *Indenter assembly for hot-hardness tester.*

A, Tungsten rod, 2-mm diameter; B, stainless steel adapter for Vicker's indenter H; C, collar with set screw; D, chuck for gripping silica capillary, G; E, nut for tightening chuck; F, bearing for silica capillary; G, silica capillary, approximately 8 mm in diamter and approximately 2 cm long.

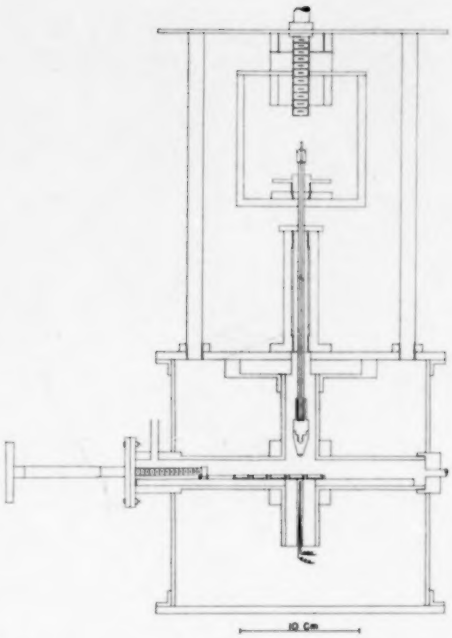

FIGURE 3. *Schematic cross section of hot-hardness tester.*

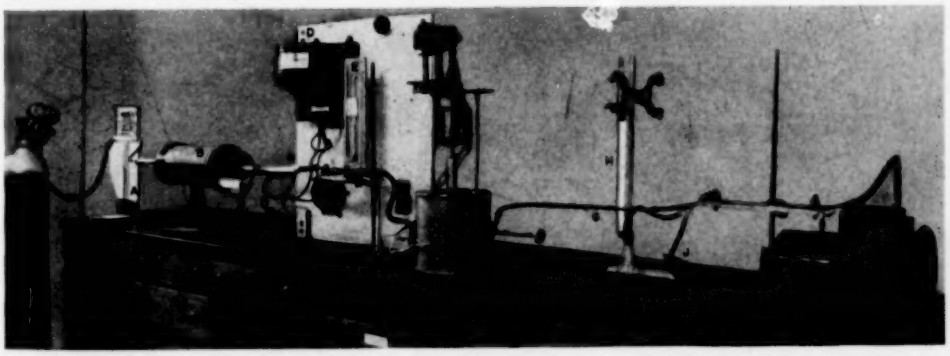

FIGURE 2. *Hot-hardness tester and auxiliary equipment.*

A, Flowmeter; B, apparatus for removing oxygen with hot copper; C, drying tube for gas; D, pyrometer and automatic temperature controller; E, manometer; F, hot-hardness tester; G, transparent silica tube, containing bright steel strip for testing purity of gas; H, open end mercury manometer; J, needle valve at exit of system.

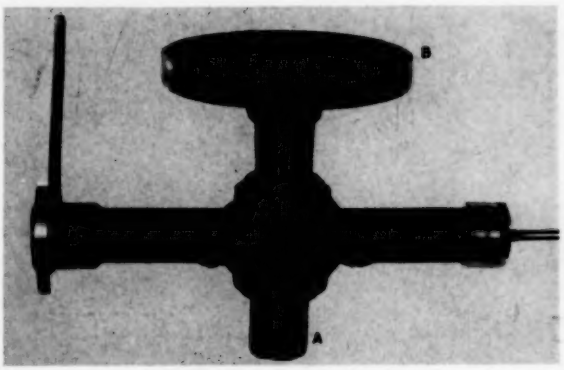

FIGURE 4. *Stainless steel muffle before being wound with heating element.*

A, Anvil; B, flange for bolting to top plate of outside shell.

UNIVERSITY OF MICHIGAN LIBRARIES

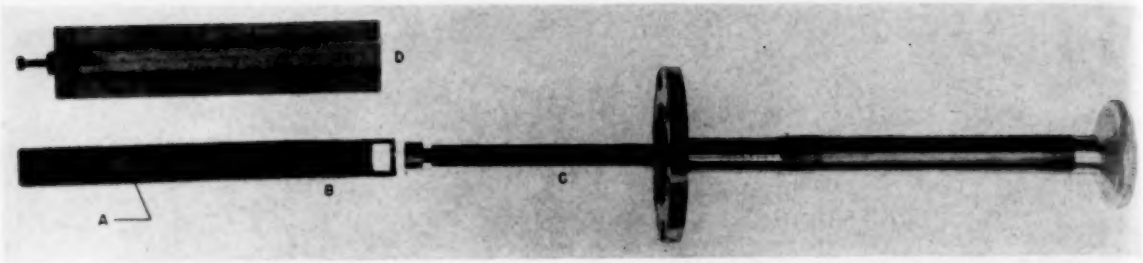

FIGURE 5. *Devices for holding and moving test specimens.*

A, Specimen; B, carriage, 13.3 cm long; C, micrometer screw, plated with cobalttungsten alloy; D, fitting for orienting carriage on moving microscope stage.

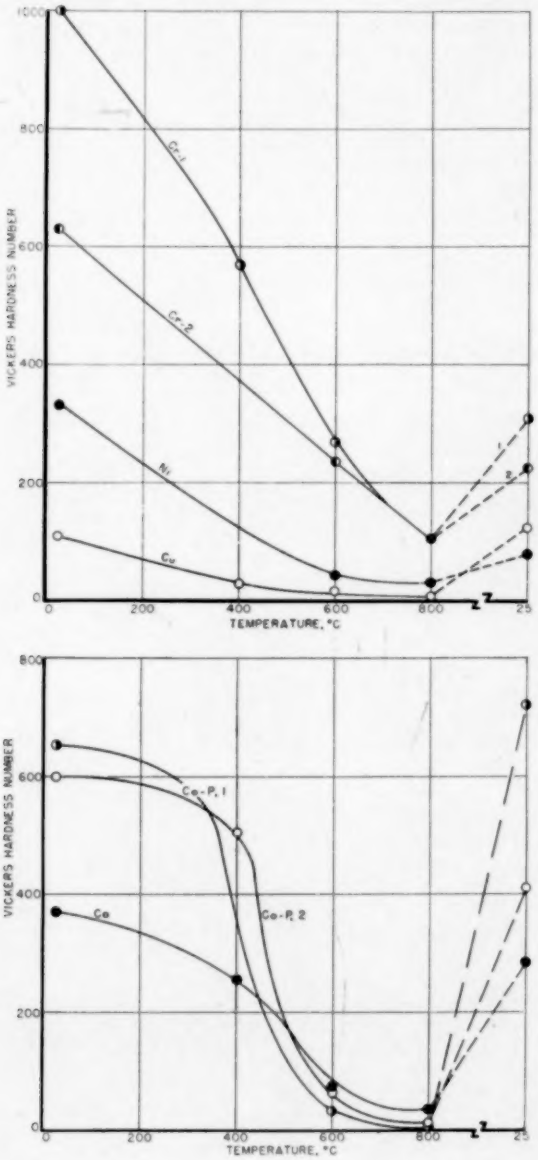

FIGURE 6. *Hot-hardness of electrodeposited chromium and nickel and bulk copper.*

Cr-1, Ordinary bright chromium, deposited from bath containing CrO_3, 250 g/liter; H_2SO_4 2.5 g/liter; current density 20 amp/dm² at 50°C. Cr-2, soft chromium deposited from same bath as Cr-1 but at 85°C and 80 amp/dm². Ni, Nickel deposited from an all-chloride bath, molar in nickel chloride and 0.5 molar in boric acid at 5 amp/dm² and a temperature of 55°C. Cu, Specimen prepared from a commercial bar of copper.

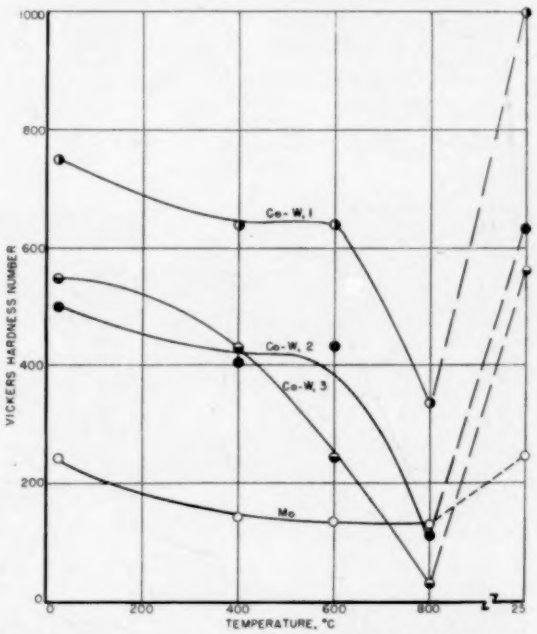

FIGURE 8. *Hot-hardness of electrodeposited cobalt-tungsten alloys and of bulk molybdenum.*

Co-W, Cobalt-tungsten alloy containing about 31 percent of tungsten; Co-W, 2, cobalt-tungsten alloy containing about 15 percent of tungsten; Co-W, 3, cobalt-tungsten alloy containing about 8 percent of tungsten; Mo, commercial specimen of molydenum bar.

FIGURE 7. *Hot-hardness of electrodeposited cobalt and cobalt-phosphorus alloys.*

Co-P, 1, Cobalt-phosphorus alloy containing about 9 percent of phosphorus; Co-p, 2, cobalt-phosphorus alloy containing about 1 percent of phosphorus; Co, cobalt deposited from a cobalt-chloride solution, molar in cobalt.

Acknowledgment is made to M. Sullivan for assisting in the initial design of the instrument; to W. Grote for suggestions in the construction of the apparatus; and to several members of the Electrodeposition Section who assisted in the construction of the tester and in making measurements.

V. References

[1] Oscar E. Harder and H. A. Grove, Hot-hardness of high-speed steels and related alloys, Trans. Am. Inst. Mining and Met. Eng. **105,** 85 (1933).

[2] Erich Fetz, Dynamic hardness testing of metals and alloys at elevated temperatures, Trans. Am. Soc. Metals **30,** 1419 (1942).

[3] George M. Enos, George J. Peer, and James C. Holzwarth, Dynamic hot hardness testing, Metal Progress **54,** 51 (1948).

[4] Frederick P. Bens, Hardness testing of metals and alloys at elevated temperatures, Trans. Am. Soc. Metals **38,** 505 (1947).

[5] E. C. Bishop and Morris Cohen, Hardness testing of high speed steel at high temperatures, Metal Progress **43,** 413 (Mar. 1943).

[6] Abner Brenner, Dwight E. Couch, and Eugenia Kellogg Williams, Electro-deposition of alloys of phosphorus with nickel or cobalt, J. Research NBS **44,** 109 (1950) RP2061.

[7] Abner Brenner, Polly Burkhead, and Emma Seegmiller, Electrodeposition of tungsten alloys containing iron, nickel, and cobalt, J. Research NBS **39,** 351 (1947), RP1834.

WASHINGTON, September 21, 1950.

UNIVERSITY OF MICHIGAN LIBRARIES

Journal of Research of the National Bureau of Standards Vol. 46 No. 2, February 1951 Research Paper 218

Mechanisms for the Mutarotation and Hydrolysis of the Glycosylamines and the Mutarotation of the Sugars

Horace S. Isbell and Harriet L. Frush

A study has been made of the kinetics of the mutarotation and hydrolysis reactions of L-arabinosylamine and a mechanism has been devised to account for the striking sensitivity of the glycosylamines to hydrolysis in a limited pH range. The concepts presented seem applicable for the interpretation of the reactions of other compounds of the aldehyde ammonia type.

I. Introduction

In the development of methods for the preparation of the amides of uronic acids [1] [1] it became necessary to determine conditions whereby the amino group of a 1-amino-uronic amide could be hydrolyzed without alteration of the amide group. It was found that the rate of hydrolysis of the amino group of 1-aminomannuronic amide (I) is extraordinarily sensitive to the acidity of the reaction medium. Thus, when the compound is mixed quickly with one equivalent of a strong acid, hydrolysis requires a period of many hours, but when the acid is added dropwise to the compound in solution, hydrolysis is complete in 15 min or less. Further study showed that 1-aminomannuronic amide is surprisingly stable both to strong acid and to alkali, and that hydrolysis can be effected rapidly only in the pH range 4 to 7. Because of the presence of the hydrolyzable amide group in 1-aminomannuronic amide, the study of the hydrolysis was directed to the 1-aminosugars, more properly designated glycosylamines.

Exploratory experiments with glucosylamine, galactosylamine, and arabinosylamine showed that the glycosylamines in general possess the peculiar sensitivity to hydrolysis in a limited pH range that had been noted for 1-aminomannuronic amide [2]. In this paper, the mutarotation and hydrolysis of L-arabinosylamine are considered in detail. Mechanisms for the mutarotation of the sugars, comparable to those for the mutarotation of the glycosylamines, correlate the properties of the two groups of substances and account for the over-all rate of mutarotation of both the glycosylamines and the sugars as a function of pH.

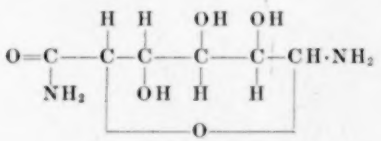

I.

1-Aminomannuronic amide

[1] Figures in brackets indicate the literature references at the end of this paper.

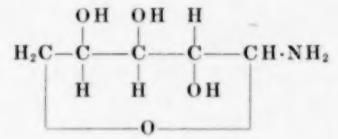

II.

L-Arabinosylamine

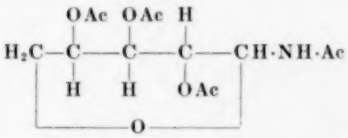

III.

Tetraacetyl-L-arabinosylamine

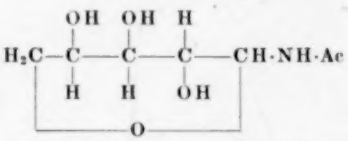

IV.

N-Acetyl-L-arabinosylamine

II. Structure and Chemical Properties of L-Arabinosylamine

L-arabinosylamine (II) was prepared by treating L-arabinose in methanol with ammonia essentially by the method of de Bruyn and Van Leent [3]. Acetylation of the compound with acetic anhydride and pyridine yielded a new tetraacetate (III). Catalytic deacetylation of this substance with barium methylate in methanol gave a crystalline *N*-acetyl-L-arabinosylamine.[2] The latter substance was found to react quickly with 2 moles of sodium periodate, as required for an *N*-acetylpentosylamine having the pyranose structure IV. Since acetylation and deacetylation were carried out by mild reactions that ordinarily cause no change in ring structure, the original L-arabinosylamine and its tetraacetate are tentatively classified as pyranoses.

In a slow titration of L-arabinosylamine, one equivalent of acid was required for neutralization

[2] This compound is analogous to the *N*-acetyl-D-glucosylamine prepared by Brigl and Keppler [4] and shown by Niemann and Hays [5] to be a pyranose.

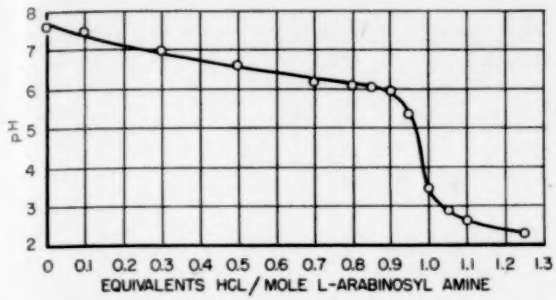

FIGURE 1. *Titration of L-arabinosylamine with acid.*

(fig. 1). Separation of crystalline L-arabinose in nearly quantitative yield from the mixture after titration established the fact that this treatment with dilute acid had caused hydrolysis of the glycosylamine and formation of the free sugar.

When dissolved in water, L-arabinosylamine undergoes spontaneous changes that give rise to a decrease in optical rotation and then to an increase. The changes can be ascribed principally to a mutarotation reaction that establishes equilibrium between the various modifications of the glycosylamine, and hydrolysis of the amino group.[3] The relative rates of the two reactions vary with experimental conditions (fig. 2). Thus, when L-arabinosylamine is dissolved in strong acid, the optical rotation drops almost at once to about +69°, and then increases slowly over a period of several weeks (curve I). However, if it is dissolved in weak acid, for example in water saturated with carbon dioxide, the optical rotation drops immediately to about +70° and then increases rapidly to +105° (curve II). In a weakly alkaline solution prepared by dissolving the substance in carbon dioxide-free water, the specific rotation decreases in the course of a few hours from +86° to a minimum, and then slowly rises (curve III). In strong alkali there is almost no change (curve IV).

These qualitative observations may be summarized as follows:

Solution	Mutarotation reaction	Hydrolysis reaction
Strongly acid	Very rapid	Slow.
Weakly acid	do	Rapid, but measurable.
Weakly alkaline	Rapid, but measurable.	Slow.
Strongly alkaline	Slow	Do.

To obtain quantitative data as to the effect of the oxonium ion concentration, samples of L-arabinosylamine were treated with acids and bases in solutions buffered at various pH values, and the ensuing reactions were followed by optical rotation. Although the mutarotation and hydrolysis reactions of L-arabinosylamine take place simultaneously, they can be studied separately because their rates at a given pH value differ widely, and because the change in optical rotation accompanying each of the two reactions is large. For study, the change in optical rotation was considered to consist of two periods: a short period beginning at zero time and characterized by a decrease in dextrorotation; and a long period beginning when the initial change was complete, characterized by an increase in dextrorotation and extending until the optical rotation reached a value corresponding to complete hydrolysis (+105.2°). The rate of the mutarotation reaction was obtained from the data for the first period and the rate of the hydrolysis reaction from the data for the second period. Suitable data were obtained for the mutarotation reaction in alkaline solutions, in which the hydrolysis is extremely slow, and for the hydrolysis reaction in weakly alkaline or acid solutions, in which the mutarotation reaction is almost instantaneous.

Satisfactory rate constants for the mutarotation of L-arabinosylamine were obtained in the pH range 7.8 to 12 by application of the customary formula[4] for a first-order reaction to the data of table 1. Table 2 gives the mutarotation constants that were obtained for a series of experiments used to evaluate the catalytic effects of the oxonium, hydroxyl, and ammonium ions. The dotted curve of figure 3 represents these mutarotation constants corrected for the catalytic effect of the ammonium ion. The results clearly show that the mutarotation of L-arabinosylamine is strongly catalyzed by acids but not appreciably by bases.[5] The mutarotation differs from

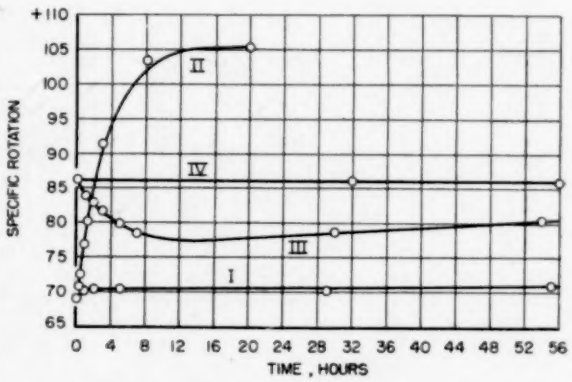

FIGURE 2. *Mutarotation of L-arabionsylamine.*

I, In 2.5 *N* HCl; II, in CO_2-saturated water; III, in CO_2-free water; IV, in 0.01 *N* NaOH.

[3] The process appears to be complicated under some conditions by the formation of the diglycosylamine, and possibly by other reactions that depend on the presence of an intermediate imine cation. See page 142.

[4] The first-order formula is applicable if the concentrations of the acid and base catalysts are held constant.

[5] However, unpublished work has shown that the mutarotation of α-D-galactosylamine is weakly but definitely catalyzed by bases.

UNIVERSITY OF MICHIGAN LIBRARIES

the mutarotations of the sugars in that the latter are catalyzed by bases more strongly than by acids. The reason for this difference will be considered in the next section.

TABLE 1. *Mutarotation and hydrolysis measurements*

0.5 g of L-arabinosylamine dissolved in sufficient acid, base, or buffer to give a volume of 25 ml. Solvents are listed opposite experiment numbers.

Time (minutes)	$[\alpha]_D^{20}$	pH	Mutarotation constant,[a] $k_m=\frac{1}{t_2-t_1}\log\frac{r_{t_1}-r_\infty}{r_{t_2}-r_\infty}$	Hydrolysis rate constant,[a] $k_{hydrol}=\frac{1}{t_2-t_1}\log\frac{r_{t_1}-r_\infty}{r_{t_2}-r_\infty}$
Experiment 1. 0.01 *N* NaOH				
10	+86.4	.....	.....	.....
32	86.1	.....	0.00034	.....
60	86.0	.....	.00040	.....
120	85.1	.....	.00031	.....
270	82.7	12.1	.00040	.....
1,250	77.6	.....	.....	.....
.....	[b] (69.0)	.....	.....	.....
		Avg..	0.00036	
Experiment 2. 0.1 *N* HCl+NH_3 to pH 10.5				
1.7	+85.0	.....	.....	.....
15	84.2	.....	0.0017	.....
60	82.2	.....	.0014	.....
125	79.6	10.5	.0015	.....
300	75.5	.....	.0013	.....
1,290	70.3	.....	.....	.....
.....	[b] (69.0)	.....	.....	.....
		Avg..	0.0015	
Experiment 3. 2.5 *N* HCl+NH_3 to pH 10.5				
3.3	+78.7	.....	.....	.....
4.9	77.2	.....	0.025	.....
10.2	73.1	.....	.026	.....
20.1	67.7	.....	.027	.....
30.2	65.3	10.5	.026	.....
120.0	[c] (61.9)	.....	.....	.....
		Avg..	0.026	
Experiment 4. 0.1 *N* HCl+NH_3 to pH 8.0				
2.2	+82.2	.....	.....	.....
6.1	79.2	.....	0.024	.....
12.1	76.0	8.5	.023	.....
21.1	73.2	.....	.019	.....
145	66.9	.....	.....	.....
		Avg..	0.022	
Experiment 5. 1 *N* HCl+NH_3 to pH 8.0				
1.6	+81.5	.....	.....	.....
6.5	75.6	.....	0.057	.....
8.7	74.0	8.2	.056	.....
17.0	70.7	.....	.056	.....
30.2	69.0	.....	.....	.....
		Avg..	0.056	
Experiment 6. 1 *N* HCl+NH_3 to pH 7.5				
1.9	+78.2	.....	.....	.....
3.8	74.5	.....	0.116	.....
4.8	73.2	7.8	.116	.....
6.9	71.3	.....	.118	.....
21.8	68.9	.....	.....	.....
		Avg..	0.117	

TABLE 1. *Mutarotation and hydrolysis measurements*—Con

0.5 g of L-arabinosylamine dissolved in sufficient acid, base, or buffer to give a volume of 25 ml. Solvents are listed opposite experiment numbers.

Time (minutes)	$[\alpha]_D^{20}$	pH	Mutarotation constant,[a] $k_m=\frac{1}{t_2-t_1}\log\frac{r_{t_1}-r_\infty}{r_{t_2}-r_\infty}$	Hydrolysis rate constant,[a] $k_{hydrol}=\frac{1}{t_2-t_1}\log\frac{r_{t_1}-r_\infty}{r_{t_2}-r_\infty}$
Experiment 7. 1 volume of 1 *M* KH_2PO_4+1 volume of 1 *N* NaOH, pH 10.0				
2.7	+82.4	.....	.....	.....
4.3	81.5	.....	0.019	.....
6.0	80.4	10.0	.021	.....
12.8	76.4	.....	.026	.....
17.1	74.7	.....	.025	.....
60.0	70.3	.....	.....	.....
.....	[b] (69.0)	.....	.....	.....
		Avg..	0.023	
210.0	+72.2	.....	.....	.....
1,750	81.6	.....	.....	0.00009
3,570	84.6	.....	.....	.00006
4,560	85.1	.....	.....	.00005
∞	[d] (105.2)	10.4	.....	.....
		Avg..		0.00007
Experiment 8. 1 volume of 1 *N* Na_2CO_3+1 volume of 1 *N* $NaHCO_3$, pH 9.4				
2.0	+82.2	.....	.....	.....
3.8	79.2	.....	0.060	.....
4.6	78.0	.....	.063	.....
5.5	77.0	9.4	.061	.....
10.1	73.6	.....	.055	.....
30.0	70.9	.....	.....	.....
.....	[b] (69.0)	.....	.....	.....
		Avg..	0.060	
420	+74.5	.....	.....	.....
1,380	78.1	.....	.....	0.000056
2,800	82.6	.....	.....	.000056
4,320	84.3	9.5	.....	.000043
∞	[d] (105.2)	.....	.....	.....
		Avg..		0.000051
Experiment 9. 1 volume of 1 *N* Na_2CO_3+10 volumes of 1 *N* $NaHCO_3$, pH 8.6				
1.6	+79.0	.....	.....	.....
2.4	77.2	.....	0.108	.....
5.5	72.9	8.6	.105	.....
6.6	72.0	.....	.105	.....
12.1	70.4	.....	.....	.....
.....	[b] (69.0)	.....	.....	.....
		Avg..	0.106	
180.0	+72.7	8.7	.....	.....
1,140	77.8	.....	.....	0.000077
4,320	88.4	.....	.....	.000069
8,640	93.1	.....	.....	.000051
∞	[d] (105.2)	.....	.....	.....
		Avg..		0.000066
Experiment 10. 10 volumes of 1 *M* KH_2PO_4+7 volumes of 1 *N* NaOH diluted to 20 volumes, pH 7.0				
1.4	+71.3	.....	.....	.....
6.0	78.1	.....	.....	0.023
10.5	81.5	.....	.....	.018
20.4	87.6	.....	.....	.016
1500.	103.1	7.2	.....	.....
		Avg..		0.019
Experiment 11. 2 volumes of 1 *M* KH_2PO_4+1 volume of 1 *N* NaOH diluted to 4 volumes, pH 6.6				
1.3	+73.9	.....	.....	.....
6.6	84.0	.....	.....	0.033
10.0	87.4	.....	.....	.029
19.9	93.6	.....	.....	.024
110.0	104.3	6.8	.....	.....
		Avg..		0.029

TABLE 1. *Mutarotation and hydrolysis measurements*—Con.

0.5 g of L-arabinosylamine dissolved in sufficient acid, base, or buffer to give a volume of 25 ml. Solvents are listed opposite experiment numbers.

Time (minutes)	$[\alpha]_D^{20}$	pH	Mutarotation constant,[a] $k_m=\frac{1}{t_2-t_1}\log\frac{r_{t_1}-r_\infty}{r_{t_2}-r_\infty}$	Hydrolysis rate constant,[a] $k_{hydrol}=\frac{1}{t_2-t_1}\log\frac{r_{t_1}-r_\infty}{r_{t_2}-r_\infty}$
Experiment 12. 5 volumes of 1 *M* KH_2PO_4+1 volume of 1 *N* NaOH diluted to 10 volumes, pH 5.9				
1.4	+77.1	.....	.....	.....
6.1	89.5	.....	.....	0.057
9.6	94.2	.....	.....	.054
11.3	96.0	.....	.....	.054
60.0	103.9	6.2	.....	.....
			Avg..	0.055
Experiment 13. 10 volumes of 1 *M* KH_2PO_4+1 volume of 1 *N* NaOH diluted to 20 volumes, pH 5.5				
2.9	+80.1	.....	.....	.....
5.6	90.6	.....	.....	0.059
9.7	97.0	.....	.....	.058
60.0	104.2	5.9	.....	.....
			Avg..	0.058
Experiment 14. 5 volumes of 1 *N* acetic acid+3 volumes of 1 *N* NaOH diluted to 10 volumes, pH 4.7				
1.3	+69.4	.....	.....	.....
9.9	100.1	5.0	.....	0.108
12.0	101.6	.....	.....	.105
13.1	102.5	.....	.....	.111
17.9	104.2	.....	.....	.....
			Avg..	0.108
Experiment 15. 5 volumes of 1 *N* acetic acid+2 volumes of 1 *N* NaOH diluted to 10 volumes, pH 4.4				
1.5	+70.8	.....	.....	.....
6.2	92.4	.....	.....	0.095
9.5	99.8	4.6	.....	.108
11.2	101.5	.....	.....	.110
12.9	102.9	.....	.....	.118
21.6	104.4	4.6	.....	.....
			Avg..	0.108
Experiment 16. 1 volume of 5.14 *N* acetic acid+1 volume of 1 *N* NaOH, pH 3.9				
2.3	+76.0	.....	.....	.....
6.6	90.4	.....	.....	0.070
8.2	93.4	.....	.....	.069
10.4	96.3	4.0	.....	.066
41.9	104.7	.....	.....	.....
			Avg..	0.068
Experiment 17. 2 volumes of 5.14 *N* acetic acid+1 volume of 1 *N* NaOH, pH 3.5				
1.9	+70.7	.....	.....	.....
4.7	80.2	.....	.....	0.051
9.7	90.1	3.6	.....	.047
14.5	95.3	.....	.....	.044
150	104.8	3.7	.....	.....
			Avg..	0.047
Experiment 18. 10 volumes of 5.14 *N* acetic acid +1 volume of 1 *N* NaOH, pH 2.7				
1.8	+66.5	.....	.....	.....
2.6	68.0	.....	.....	0.022
9.6	78.3	.....	.....	.021
20.0	87.6	.....	.....	.021
105	104.2	3.1	.....	.....
			Avg..	0.021

TABLE 1. *Mutarotation and hydrolysis measurements*—Con.

0.5 g of L-arabinosylamine dissolved in sufficient acid, base, or buffer to give a volume of 25 ml. Solvents are listed opposite experiment numbers.

Time (minutes)	$[\alpha]_D^{20}$	pH	Mutarotation constant,[a] $k_m=\frac{1}{t_2-t_1}\log\frac{r_{t_1}-r_\infty}{r_{t_2}-r_\infty}$	Hydrolysis rate constant,[a] $k_{hydrol}=\frac{1}{t_2-t_1}\log\frac{r_{t_1}-r_\infty}{r_{t_2}-r_\infty}$
Experiment 19. 1 *N* oxalic acid, pH 0.8				
1.4	[c]+67.1	.....	.....	.....
5.0	69.3	.....	.....	.....
480	72.1	.....	.....	0.000074
1,440	77.7	.....	.....	.000081
1,890	80.6	0.8	.....	.000087
∞	[d] (105.2)	.....	.....	.....
			Avg..	0.000081
Experiment 20. 2.5 *N* HCl				
3.8	[c]+69.0	.....	.....	.....
30.0	[c] 69.9	.....	.....	.....
60.0	70.0	.....	.....	.....
3,300	71.2	.....	.....	0.0000046
35,300	81.2	0.2	.....	.0000047
∞	[d] (105.2)	.....	.....	.....
			Avg..	0.0000047

[a] Symbols are defined in section VII, 5. [b] Postulated equilibrium value.
[c] See page 144. [d] Postulated final value. [e] Value not used in calculations.

TABLE 2. *Mutarotation constants of* L-*arabinosylamine at 20° C*

Experiment	pH	$[H^+]$	$[OH^-]$	$[NH_4^+]$	k_m	k_m corrected [a]
1	12.1	7.94×10^{-13}	1.26×10^{-2}	.....	0.004	0.0004
2	10.5	3.16×10^{-11}	3.16×10^{-4}	0.1	.0015	.0005
3	10.5	3.16×10^{-11}	3.16×10^{-4}	2.5	.026	.001
4	8.5	3.16×10^{-9}	3.16×10^{-6}	0.1	.022	.021
5	8.2	6.31×10^{-9}	1.58×10^{-6}	1.0	.056	.046
6	7.8	1.58×10^{-8}	6.31×10^{-7}	1.0	.117	.107

[a] Mutarotation constant, k_m, was corrected for the catalytic effect of ammonium ion. See page 139.

III. Mechanisms for the Mutarotation Reactions of the Sugars and the Glycosylamines

A satisfactory mechanism for the mutarotation of both the sugars and the glycosylamines must lead to an accurate expression for the rate of mutarotation as a function of the acid and base catalysts present. Years ago Hudson showed that the mutarotation constants for the sugars in the presence of strong acids and bases can be represented by the following empirical equation [6]:

$$k_m=k_{H_2O}+k_H[H^+]+k_{OH}[OH^-], \qquad (1)$$

where k_{H_2O}, k_H, and k_{OH} are constants characteristic of the particular sugar, and $[H^+]$ and $[OH^-]$ represent the concentrations of the oxonium and hydroxyl ions, respectively. More recently it has been established that the reaction is subject to general acid and base catalysis, and consequently the expression has been extended to include terms accounting for the catalytic effect of undissociated acids, anions of weak acids and cations of weak bases [7]. Thus eq 1 is replaced by eq 2:

$$k_m=k_{H_2O}+k_H[H^+]+$$
$$k_{OH}[OH^-]\ \ldots\ +\sum^{i}k_i[HA_i]+\sum^{j}k_j[B_j], \qquad (2)$$

UNIVERSITY OF MICHIGAN LIBRARIES

in which HA signifies any hydrogen acid, neutral or ionic, and B signifies any base, neutral or ionic.

Although several mechanisms have been advanced for the mutarotation reaction, no single mechanism accounts for all of the experimental facts. To account for certain results with acid and base catalysts, including the observation [8] that the mutarotation of tetramethylglucose is negligible in either cresol or pyridine, but rapid in a mixture of the two solvents [6] Lowry [10] advanced a mechanism that involves the addition of a proton at one point in the sugar molecule and simultaneous elimination of a proton at another point. The process may be represented in the following manner:[7]

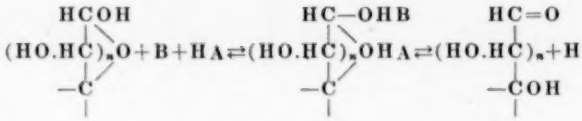

(3)

This mechanism would give rise to a third-order term in the rate expression [11], but as pointed out by Swain [12], this is not detectible because of the relative magnitude of the terms, and hence the rate constant on the basis of this mechanism can be represented within the experimental error by eq 1. The simplicity of the mechanism makes it most attractive for interpretation of the mutarotation reaction, expecially in amphoteric solvents. Certain experimental facts, however, may be explained more satisfactorily by separate acid- and base-catalyzed mechanisms, and such mechanisms have come to be quite generally accepted. It seems probable that they act concomitantly with Lowry's mechanism, and that the extent to which each mechanism is effective is determined by the experimental conditions.

Acid-catalyzed mechanisms

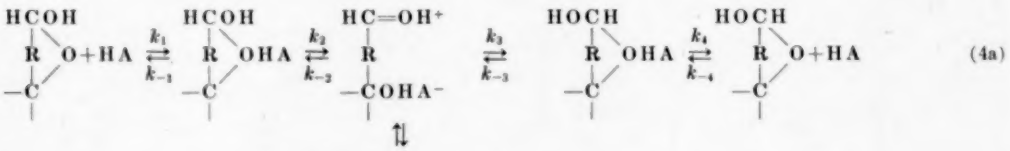

(4a)

all open-chain forms

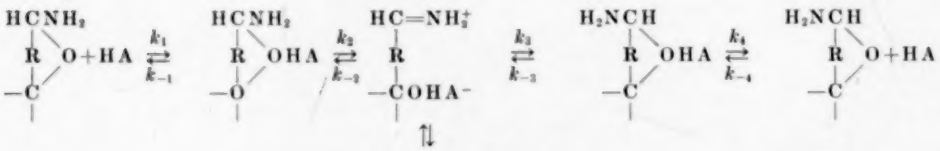

(4b)

all open-chain forms

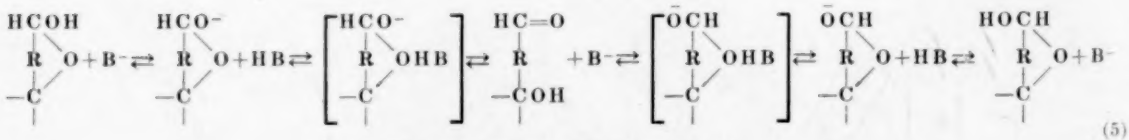

(5)

("Base-catalyzed" mechanism of [14])

[6] Similarly, Butler, Smith, and Stacey [9] have recently observed that the α- and β-tetraacetates of *N*-phenylglucosylamine are extremely stable in dry pyridine, but mutarotate to an equilibrium value on addition of a drop of water.

[7] Although the mechanism of eq 2 was represented in a generic fashion with respect to *HA* and *B*, in eq 3 and succeeding mechanisms charges have been indicated for clarity. Nevertheless, the mechanisms may be regarded as generic. Thus, if *B* in eq 6a is a neutral substance, then HB becomes HB^+.

Base-catalyzed mechanisms

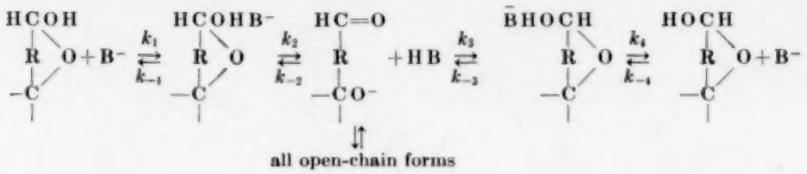

(6a)

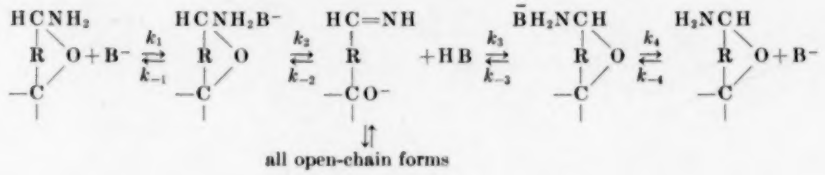

(6b)

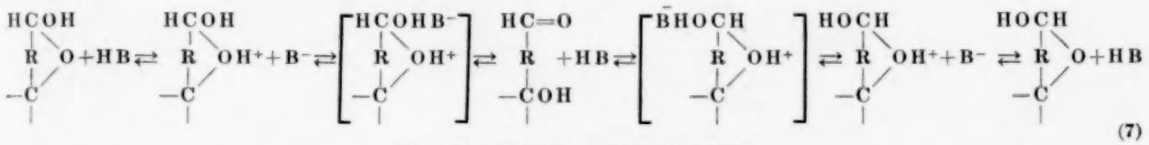

(7)

("Acid-catalyzed" mechanism of [14])

In eq 4 and 6 there are proposed acid- and base-catalyzed mechanisms that we believe represent reasonable courses for the mutarotation of the sugars and the glycosylamines. These mechanisms differ in certain respects from the mechanisms commonly accepted.

The acid-catalyzed mechanism presented here for the mutarotation of the sugars (eq 4a) begins with the addition of an acid catalyst to the ring oxygen. This is followed by rupture of the ring through an electron shift in which a lone electron pair of the glycosyl oxygen facilitates release of electrons to the ring oxygen. The product quickly establishes equilibrium with all species of the open-chain modification. Cyclization can then proceed through combination of carbon 1 with the oxygen of either carbon 4 or carbon 5. This gives rise to the alpha and beta furanoses and pyranoses in equilibrium proportions.

The acid-catalyzed mutarotation of the glycosylamines is formulated in similar manner, as shown in eq 4b. In this case, a shift of a lone electron pair of the amino nitrogen results in the formation of the imonium ion $-\overset{|}{C}=NH_2^+$. Reaction of carbon 1 of the imonium ion with the oxygen of carbon 4 or carbon 5 produces the various ring isomers. A mechanism of this type will account for the striking sensitivity of the mutarotation of the glycosylamines to acid catalysts.

A base-catalyzed mechanism for the mutarotation of the sugars may be represented as shown in eq 6a. Combination of the base with the hydrogen of the glycosidic hydroxyl gives an activated complex that decomposes with separation of the conjugate base and rupture of the ring. By the reversible addition of a proton, the product establishes equilibrium with the open-chain form of the sugar. Restoration of asymmetry on carbon 1 through ring formation, facilitated by combination of the conjugate base with the carbonyl oxygen establishes equilibrium of the cyclic modifications. The glycosylamine, however, does not react to a great extent by a base-catalyzed mechanism (eq 6b) analogous to that of the free sugar because there is less tendency on the part of the amino nitrogen to release a proton.

The above mechanisms differ from those generally accepted primarily in regard to the species of the sugar undergoing reaction. According to Hammett ([13, p. 337]) ". . . the only reasonable mechanisms are the following: for the acid catalysis the mobile and reversible addition of a proton to the ether oxygen followed by a rate-determining reaction with a base . . . for the base catalysis the mobile and reversible removal of a proton, followed by a rate-determining reaction with an acid." These mechanisms, originally advanced by Fredenhagen and Bonhoeffer [14] and based in part on the work of Bonhoeffer and Reitz [15], have been extended to the glycosylamines by Howard, Kenner, Lythgoe, and Todd [16]. The mechanisms of [14] are outlined in eq 5 and 7, in which the steps contained in brackets have been postulated by us. Comparison shows that our acid-catalyzed mechanism of eq 4a resembles the base-catalyzed mechanism of eq 5, and that our base-catalyzed mechanism of eq 6a resembles the prior acid-catalyzed mechanism of eq 7. It will be seen that the two mechanisms classified here under acid-catalysis (eq 4a and 5), operate on different species of the sugar; this is likewise true of the two classified under base-catalysis (eq 6a and 7). The proportions

UNIVERSITY OF MICHIGAN LIBRARIES

of the species are determined by the hydrogen ion concentration and the base strength of the carbohydrate, and hence the relative importance of the several mechanisms in any solution depends on the substance and the pH.

Presumably all of the mechanisms, in addition to Lowry's, are applicable to the sugars, with eq 5 and 6a favored in alkaline solution and 4a and 7 in acid solution. It appears that eq 4b would be the main course for the primary and secondary amines and indeed the only one that is applicable to tertiary amines. The mutarotation of tertiary glycosylamines was observed by Kuhn and Birkhofer [17], who concluded that the reaction involves the formation of a substituted ammonium ion followed by elimination of a proton, to give the imonium ion $-\overset{|}{C}=NH_2^+$. Although eq 4b involves the same imonium ion, we believe that it is produced directly from the amine rather than from the corresponding ammonium ion. It should be pointed out that the mechanism of eq 4a and 4b requires only an acid catalyst and is at variance with the currently held concept that both an acid and a base catalyst are necessary for the mutarotation reaction. As applied to the alkyl glycosides, a mechanism analogous to eq 4a will account adequately for acid-catalyzed interconversion in nonaqueous solvents, a reaction for which mechanisms analogous to those of eq 5, 6a, and 7 are inadequate because the aglycone group does not permit attack by a base catalyst.

Apparently the acid- and base-catalyzed reactions of the sugars take place side by side, and the over-all reaction can be regarded as the sum of the parallel and competing reactions, the rates of which depend on the acid and base catalysts present. It is of interest to examine the newly postulated mechanisms to ascertain whether they will account for the effect of acid and base catalysts on the rate of mutarotation. For this purpose, the mechanisms of eq 4a and 6a can be formulated in the following manner:

Acid-catalyzed system:

$$\alpha + HA \underset{k_{-1}}{\overset{k_1}{\rightleftarrows}} X_1$$

$$X_1 \underset{k_{-2}}{\overset{k_2}{\rightleftarrows}} X_2$$

$$X_2 \underset{k_{-3}}{\overset{k_3}{\rightleftarrows}} X_3$$

$$X_2 \underset{k_{-4}}{\overset{k_4}{\rightleftarrows}} \beta + HA$$

Base-catalyzed system:

$$\alpha + B \underset{k_{-1}}{\overset{k_1}{\rightleftarrows}} X_1$$

$$X_1 \underset{k_{-2}}{\overset{k_2}{\rightleftarrows}} X_2 + HB$$

$$X_2 + HB \underset{k_{-3}}{\overset{k_3}{\rightleftarrows}} X_3$$

$$X_2 \underset{k_{-4}}{\overset{k_4}{\rightleftarrows}} \beta + B$$

In these expressions, HA represents an acid catalyst, B a base catalyst, α and β the modifications of the sugar, and X_1, X_2, and X_3 reaction intermediates. The rate constants and the intermediates are not the same for the two systems. Application of the Christiansen equations ([13, p. 107]) to the acid- and base-catalyzed systems for the sugars, and combination of rate constants, lead to the following expressions, respectively for the rates of reaction:

$$-\frac{d[\alpha]}{dt}=\frac{d[\beta]}{dt}=k_A[HA]\,(k[\alpha]-k'[\beta]),$$

for catalysis by an acid, and

$$-\frac{d[\alpha]}{dt}=\frac{d[\beta]}{dt}=k_B[B]\,(k[\alpha]-k'[\beta]),$$

for catalysis by a base. At equilibrium,

$$-\frac{d[\alpha]}{dt}=0.$$

Thus $k[\alpha]-k'[\beta]=0$ in both cases, and k/k' is fixed by the equilibrium ratio. By adjusting the arbitrary constants k_A and k_B, the same value in the two equations is assigned to k and likewise to k', so that $(k[\alpha]-k'[\beta])$ becomes a common factor for all catalysts. The over-all rate then becomes

$$-\frac{d[\alpha]}{dt}=\Big(\sum^{i}k_i[HA_i]+\sum^{j}k_j[B_j]\Big)(k[\alpha]-k'[\beta]), \qquad (8)$$

for i acid catalysts and j base catalysts. If the only catalysts are oxonium ion, hydroxyl ion, and water eq 8 reduces to

$$-\frac{d[\alpha]}{dt}=(k_{H_2O}+k_H[H^+]+k_{OH}[OH^-])(k[\alpha]-k'[\beta]), \qquad (9)$$

where k_{H_2O} includes both acid and base catalysis by the water molecule. This equation, when integrated and expressed in terms of optical rotation by Hudson's method [18] [8] becomes

[8] At the time that Hudson presented his classical development of the kinetics of mutarotation, it was thought that the equilibrium of lactose was established between a ring form and an open-chain form (referred to in his article as lactone and hydrate, respectively).

$$\frac{1}{t} ln \frac{r_0 - r_\infty}{r_t - r_\infty} = (k_{H_2O} + k_H[H^+] + k_{OH}[OH^-])(k + k').$$

By reducing to common logarithms and combining constants,

$$\frac{1}{t} \log \frac{r_0 - r_\infty}{r_t - r_\infty} = k_{H_2O} + k_H[H^+] + k_{OH}[OH^-] = k_m. \quad (10)$$

This is the familiar expression that Hudson found to represent the mutarotation of glucose in acid, neutral, and alkaline solutions [6]. This derivation shows that the postulated acid- and base-catalyzed reactions are in accord with the previously known, experimentally determined relationship correlating the rate constant for the mutarotation of the sugars with the catalysts present.

The Christiansen equations may be similarly applied to the mutarotation of the glycosylamines (eq 4a and 4b), and the summation then takes the form:

$$-\frac{d[\alpha]}{dt} = \left(\sum^i k_i[HA_i] + \sum^j k_j[B_j]\right)(k[\alpha_{NH_2}] - k'[\beta_{NH_2}]). \quad (11)$$

The expression calls for general acid and base catalysis. It has been found experimentally that the mutarotation rate is increased by the presence of ammonium, phosphate, and carbonate buffers. However, for systems in which the only catalysts are water, oxonium ion, hydroxyl ion, and ammonion ion, eq 11, when treated in the same manner as eq 8, reduces to

$$\frac{1}{t} \log \frac{r_0 - r_\infty}{r_t - r_\infty} = k_{H_2O} + k_H[H^+] + k_{OH}[OH^-] + k_{NH_4}[NH_4^+] = k_m. \quad (12)$$

In the case of the glycosylamines, there is theoretically a complicating factor. In the derivation of the expression for the rate of mutarotation of the sugars, it is possible to assume that a direct relationship exists between the concentrations of the alpha and beta isomers and the optical rotation regardless of the presence of either more or less acid. This assumption is valid because only a minute part of the sugar exists under any given conditions in other than the normal forms. Because of the basic properties of the amino group, however, part of both the alpha and the beta glycosylamine probably exist in solution as the corresponding substituted ammonium ion. The proportion of the free amine in aqueous solutions is determined by the equilibrium:

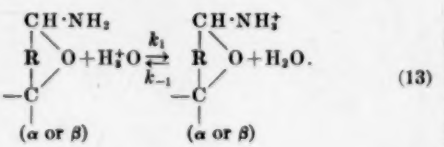

(13)

When this reaction is taken into account, it can be shown by application of the mass law that

$$\frac{1}{t} \log \frac{r_0 - r_\infty}{r_t - r_\infty} = \frac{k_{H_2O} + k_H[H^+] + k_{OH}[OH^-] + k_{NH_4}[NH_4^+]}{1 + K[H^+]} = k_m, \quad (14)$$

where K is the equilibrium constant for eq 13. Application of eq 14 to the data of table 2 gives a series of simultaneous equations that show that in the pH range where the mutarotation is sufficiently slow to be measurable, the effect of the term $K[H^+]$ is less than the experimental error. Consequently, the term can be neglected and eq 12 can be applied to the mutarotation of L-arabinosylamine.

From the data of table 2, numerical values were obtained for the catalytic coefficients of eq 12. At low concentrations of oxonium and ammonium ion, the quantity $k_{H_2O} + k_{OH}[OH^-]$ approaches k_m, and each term must be less than the lowest observed rate (0.0004 at pH 12); hence k_{H_2O} and k_{OH} are less than 4×10^{-4} and 4×10^{-2}, respectively. From experiments 2 and 3, k_{NH_4} was found to be 10^{-2}. Inasmuch as k_{H_2O} and $k_{OH}[OH^-]$ are negligibly small in comparison with the values of k_m in experiments 4, 5, and 6, values of k_H were calculated on the assumption that $k_m = k_H[H^+] + 10^{-2}[NH_4^+]$. The average value of k_H so obtained is 6.9×10^6. The mutarotation constants of table 2, corrected for the catalytic effect of ammonium ion, are given in the last column of the table and are shown by the dotted curve of figure 3.[9] A comparison of the numerical values of the catalytic coefficients for L-arabinosylamine with those for D-glucose is given in table 3. It may be seen that the principal catalyst for the mutarotation of D-glucose is the hydroxyl ion, whereas for the mutarotation of L-arabinosylamine it is the oxonium ion. The striking difference arises primarily from the fact that the glycosyl oxygen has a greater tendency than the nitrogen to release a proton (eq 6a and 6b) and less tendency than the nitrogen to share a lone electron pair (eq 4a and 4b).

TABLE 3. *Catalytic coefficients of mutarotation reactions at 20° C*

Catalyst	Symbol	L-Arabinosylamine	D-Glucose [a]
H_2O	k_{H_2O}	$<4 \times 10^{-4}$	2.6×10^{-4}
H^+	k_H	6.9×10^6	3.6×10^{-1}
OH^-	k_{OH}	4×10^{-2}	8×10^2
NH_4^+	k_{NH_4}	1×10^{-2}	1.2×10^{-2}

[a] Data from [19].

[9] In a preliminary publication [2], an expression was given to represent empirically the rate of mutarotation in experiments 1, 7, 8, and 9. No attempt was made to evaluate the general acid and base catalysis of the buffers used.

UNIVERSITY OF MICHIGAN LIBRARIES

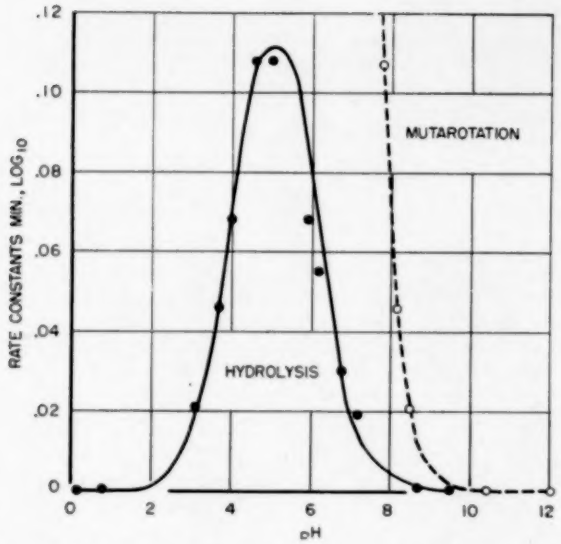

FIGURE 3. *Rate constants for mutarotation and hydrolysis of* L-*arabinosylamine.*

IV. Hydrolysis Reaction

It has already been mentioned that the rate of hydrolysis of L-arabinosylamine was calculated from the increase in optical rotation that follows the initial decrease. The rate of hydrolysis obtained from the data of table 1 is shown in figure 3 as a function of pH. The results bring out clearly the striking sensitivity of L-arabinosylamine to hydrolysis within a limited pH range.[10]

A satisfactory mechanism for this reaction must account for the ease of hydrolysis and the restriction of the reaction to a limited pH range. It follows from the well-known stability of amines to acid hydrolysis [11] that the hydrolytic reaction is not characteristic of the C—NH_2 linkage but must be due to the glycosyl structure. It was mentioned in connection with the acid-catalyzed mutarotation that the glycosylamine is able to form the imonium ion, $-C=\overset{+}{N}H_2$, by rupture of the ring following the addition of a proton to the ring oxygen. A mechanism for hydrolysis including this substance as an intermediate is given in the next column.[12] With this structure (D), addition can take place by attachment of a nucleophilic group to the carbon, and a shift of electrons. If the nucleophilic group is hydroxyl, addition yields an intermediate aldehyde ammonia (F). This grouping is known to be unstable and gives up ammonia readily. Thus the aldehydic properties of the glycosylamine account for the facility with which ammonia is eliminated.

Proposed mechanism for the hydrolysis of glycosylamines:

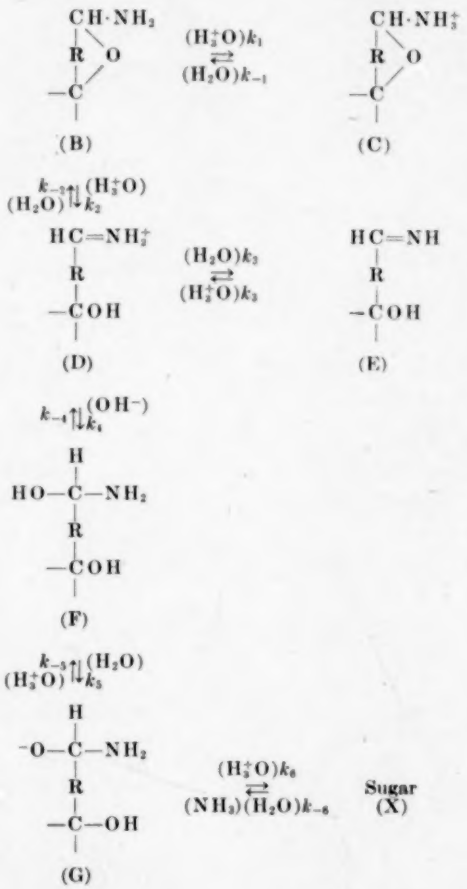

It will be shown next that the proposed reaction mechanism will account for the fact that hydrolysis is rapid only in a limited pH range. Presumably the first step in the hydrolysis is the formation of the imonium ion (D) by acid catalysis; this is accompanied by a side reaction to form the glycosylammonium ion (C). The second step is the addition of a hydroxyl ion to D, to yield the aldehyde ammonia (F); it is also accompanied by a side reaction forming

[10] The reaction-rate–pH curve is similar in shape to many of the enzyme activity–pH curves, among which may be cited those of urease [20], β-glucosidase [21], α-amylase [22], and cellulase [23]. It seems possible that the sensitivity of certain enzyme systems to a change in pH may also arise from equilibria comparable to those cited here.

[11] The stability of the C—N linkage of amines is illustrated by the fact that glucosamine is obtained by treatment of chitin with concentrated hydrochloric acid [24].

[12] The glycosylamines are somewhat analogous to the dialkylaminomethyl alkyl ethers, which have been studied by Stewart and Bradley [25]. These authors found that the compounds are rapidly hydrolyzed by acid and explained the ease of hydrolysis by a mechanism involving the formation of an iminium ion (imonium ion) and condensation of this with hydroxyl ion. Our mechanism includes analogous steps.

the imine (E). The last part of the process covers the elimination of ammonia from the aldehyde ammonia. It is represented as proceeding through the ionization of F (reaction 5), followed by an acid-catalyzed rearrangement of the anion (G) to yield the aldehyde form of the sugar, and ultimately the equilibrium mixture. The ammonia is converted to ammonium ion, thus driving the reaction to completion. In the derivation of the rate constant as a function of the oxonium ion concentration, it is postulated that in the pH range in which hydrolysis occurs, equilibria for all reactions except 6 are established quickly and maintained throughout the reaction. It is also assumed that within this range reaction 6 is irreversible. Inasmuch as equilibrium conditions are postulated for all reactions except 6, the rate of hydrolysis is represented by

$$-\frac{d(A-X)}{dt}=[G]\,[H^+]k_6, \qquad (15)$$

where A is the sum of all components and X is the sugar formed by hydrolysis. From mass law it follows that

$$[F]\,[H_2O]k_5=[G]\,[H^+]k_{-5}$$

$$[D]\,[OH^-]k_4=[F]k_{-4}$$

$$[E]\,[H^+]k_{-3}=[D]\,[H_2O]k_3$$

$$[B]\,[H^+]k_2=[D]\,[H_2O]k_{-2}$$

$$[C]\,[H_2O]k_{-1}=[B]\,[H^+]k_1$$

The equations may be solved for B, C, D, E, and F in terms of G, and the values substituted in the expression $A=B+C+D+E+F+G+X$ to obtain

$$(A-X)=[G]\left(\frac{k_{-5}k_{-4}k_{-2}}{[OH^-]k_5k_4k_2}+\frac{[H^+]k_{-5}k_{-4}k_{-2}k_1}{[H_2O][OH^-]k_5k_4k_2k_{-1}}+\frac{[H^+]k_{-5}k_{-4}}{[H_2O][OH^-]k_5k_4}+\frac{k_{-5}k_{-4}k_3}{[OH^-]k_5k_4k_{-3}}+\frac{[H^+]k_{-5}}{[H_2O]k_5}+1\right).$$

This, when simplified by combining constants, and expressing the results in terms of new constants becomes

$$[G]=\frac{(A-X)[OH^-]^2}{[OH^-]^2+k'[OH^-]+k''}.$$

If the derived value for [G] is substituted in eq 15, it becomes

$$-\frac{d(A-X)}{dt}=\frac{(A-X)[OH^-]^2[H^+]k_6}{[OH^-]^2+k'[OH^-]+k''},$$

which may be simplified by multiplying numerator and denominator by $[H^+]$, and combining constants to obtain

$$-\frac{d(A-X)}{dt}=\frac{(A-X)}{K'+K''[H^+]+K'''[OH^-]}.$$

After integration, evaluation of the integration constant and conversion to common logarithms, the equation becomes

$$\frac{1}{t}\log\frac{A}{(A-X)}=\frac{1}{K_1+K_2[H^+]+K_3[OH^-]}=k_{hydrol},$$

where k_{hydrol} is the hydrolysis rate constant. Inasmuch as the change in optical rotation during the hydrolysis period is a measure of the change in (A−X), the expression in terms of optical rotation becomes

$$\frac{1}{t_2-t_1}\log\frac{r_{t_1}-r_\infty}{r_{t_2}-r_\infty}=\frac{1}{K_1+K_2[H^+]+K_3[OH^-]}=k_{hydrol}. \qquad (16)$$

By use of the data of table 4, nine simultaneous equations corresponding to eq 16 were set up. Combination of these in groups of 4, 2, and 3, and solution by the method of averages gave values of 7.9, 6.1×10^4 and 4.2×10^8, respectively, for K_1, K_2, and K_3. Thus,

$$k_{hydrol}=\frac{1}{7.9+6.1\times10^4[H^+]+4.2\times10^8[OH^-]}.$$

A plot of this expression is shown by the solid curve of figure 3; the experimental results are in good agreement with the curve. Thus, the postulated mechanism and the equation developed from kinetic considerations account for the fact that hydrolysis is rapid only in a limited pH range.

TABLE 4. *Summary of data for the hydrolysis reaction at 20° C*

Experiment	pH	[H+]	[OH−]	k^a_{hydrol}
10	7.2	0.63×10^{-7}	16×10^{-8}	0.019
11	6.8	1.6×10^{-7}	6.3×10^{-8}	.029
12	6.2	6.3×10^{-7}	1.6×10^{-8}	.055
13	5.9	13×10^{-7}	0.8×10^{-8}	.068
14	5.0	1.0×10^{-5}	1×10^{-9}	.108
15	4.6	2.5×10^{-5}	0.4×10^{-9}	.108
16	4.0	1.0×10^{-4}	10×10^{-11}	.068
17	3.7	2.0×10^{-4}	5×10^{-11}	.047
18	3.1	7.9×10^{-4}	1.3×10^{-11}	.021

[a] $k_{hydrol}=1/(t_2-t_1)\log(r_{t_1}-r_\infty)/(r_{t_2}-r_\infty)$, where r_{t_1} is the first measurement in the period used for evaluating the rate of hydrolysis.

In the preceding discussion, it was necessary to omit consideration of the individual reaction constants and of catalysis by acids and bases other than oxonium and hydroxyl ions.[13] Furthermore, it was not possible to consider the several ring isomers of the system separately. In the mechanism on page 140, intramolecular reaction of carbon 1

[13] Inasmuch as equilibrium conditions prevail during the hydrolysis, general catalysis in the formation of the imonium ion does not affect the rate of hydrolysis, although it accelerates the rate of mutarotation.

UNIVERSITY OF MICHIGAN LIBRARIES

of D with the hydroxyl of carbon 4 would give the alpha and beta furanosylamines; reaction with the hydroxyl of carbon 5 would give the alpha and beta pyranosylamines. Hence B and C symbolize all cyclic modifications of the glycosylamine, and the corresponding cation, respectively, and the constants of reactions 1 and 2 represent composite rates. Similarly, F includes both stereomeric modifications of carbon 1, and the constants of reaction 5 represent composite rates.

V. Evidence for the Formation of an Unknown Product, Possibly the Diglycosylamine

In some cases the mutarotation and hydrolysis appear to be complicated further by a side reaction that takes place during the early part of the reaction period and varies in importance with the experimental conditions. Evidence of this complicating factor may be seen from the data of table 5. It will be observed that when an excess of acid is added slowly to L-arabinosylamine, the optical rotation drops to a lower point than when the acid is added quickly. The product having the lower rotation appears to be hydrolyzed more rapidly than the other, as the optical rotation of the solution rises more rapidly and ultimately exceeds that of the solution containing less of the byproduct. It seems probable that the complication is caused by the formation of a diarabinosylamine. Evidence of this reaction is also found in experiments 19 and 20 of table 1. In these, the initial observed rotation is lower than usual, and the early change in optical rotation is too rapid to be due entirely to the hydrolysis of L-arabinosylamine. As the reaction, after the first few minutes, appears to follow the first-order course, the calculations of the rate were made without the use of the early anomalous values. In experiment 18 of table 1, however, although the initial rotation is likewise low, the entire mutarotation follows the first-order course. The side reaction, which under other conditions may become of major importance, is being studied further.

TABLE 5. *Reaction of L-arabinosylamine with acid (evidence for a side reaction)*

0.25 g of L-arabinosylamine dissolved in sufficient 2.5 *N* HCl to give a volume of 25 ml

Time after beginning the addition of acid	Optical rotation after rapid addition of acid	Optical rotation after dropwise addition of acid during 2.5 minutes
Minutes	$[\alpha]_D^{20}$	$[\alpha]_D^{20}$
3.8	69.0	67.2
7.0	69.3	68.2
15.0	69.7	69.4
30.0	69.9	70.5
60.0	70.0	71.0
Change in $[\alpha]_D^{20}$ in 1 hr	1.0	3.8

VI. Role of the Imonium Ion in Other Reactions of Glycosylamines

It is believed that the imonium ion, considered to be an intermediate in the hydrolysis reaction, accounts not only for the formation of the diglycosylamine but for several other reactions. Thus the addition of a nucleophilic substance, as for instance a cyanide ion, would take place most readily through the imonium ion, and the concentration of this cation would largely determine the reaction rate. The imonium ion also plays a part in reactions of the Amadori type; mechanisms for some of these were presented in a prior publication [26].

VII. Experimental Details

1. L-Arabinosylamine

Dry ammonia was passed slowly, at room temperature, into 100 ml of methanol containing 1 g of ammonium chloride and 20 g of L-arabinose in suspension. Addition of ammonia was discontinued when the sugar had entirely gone into solution. Ether was then added to the point of incipient turbidity, and the mixture was allowed to stand in the refrigerator until crystallization of L-arabinosylamine occurred (3 weeks). The crystals were collected on a filter, washed with methanol, and air-dried; the yield was 15 g. Recrystallization was conducted by dissolving the crude arabinosylamine in 30 ml of a 1:10 mixture of concentrated ammonia and water. The solution was filtered and diluted with 60 ml of methanol saturated with ammonia, and then with 150 ml of absolute ethanol. The resulting crystals were separated after 2 hours, washed with methanol saturated with ammonia, and dried at room temperature in a vacuum desiccator containing phosphoric anhydride. The recrystallized product weighed 10.8 g, and melted at 124° C. At a concentration of 2 g/100 ml in CO_2-free water, $[\alpha]_D^{20} = +86.3°$ (5 min); 83.8° (60 min): 78.6° (7 hr); 80.5° (54 hr). De Bruyn and Van Leent [2], who first prepared the compound, reported mp 124° C and $[\alpha]_D^{20} + 83°$ (H_2O, $c = 10$).

Figure 1 shows the titration curve obtained when 0.1 *N* HCl was added portionwise to 75 ml of a solution containing 0.1493 g of L-arabinosylamine. Sufficient time was allowed after each addition of acid for the pH of the solution to reach equilibrium. At the end of the experiment, the optical rotation corresponded to that of L-arabinose, and after the ammonium chloride and excess acid were removed by treatment with ion-exchange resins, 0.14 g of crystalline arabinose was obtained from the solution. This is a nearly quantitative yield.

2. Tetraacetyl-L-Arabinosylamine

A mixture of 4 g of finely powdered L-arabinosylamine, 40 ml of pyridine and 16 ml of acetic anhydride, in a flask equipped with a mechanical stirrer, was

kept in an ice bath and stirred until solution was complete (4 hrs). After 18 hours at 0° C, the solution was poured into a mixture of ice and water, and the product was extracted with chloroform. Evaporation of the chloroform gave a crystalline residue that was recrystallized from hot ethanol. The yield was 3.65 g. After several recrystallizations, tetraacetyl-L-arabinosylamine melted at 177° to 178° C; $[\alpha]_D^{20} = +89.6°$ ($CHCl_3$, $c=1.6$).

Analysis: Calculated for $C_{13}H_{19}O_8N$: C, 49.21; H, 6.04; N, 4.41; $CO{\cdot}CH_3$, 54.26. Found: C, 49.3; H, 6.1; N, 4.4; $CO{\cdot}CH_3$, 52.4.

3. *N*-Acetyl-L-Arabinosylamine

Six grams of tetraacetyl-L-arabinosylamine was dissolved in 100 ml of anhydrous methanol, and 10 ml of 0.1 *N* barium methylate in methanol was added. The alcohol was removed by distillation under reduced pressure, with exclusion of moisture. The residue was dissolved in water and treated successively with a cation and an anion exchange resin to remove barium salts. The resulting solution, after evaporation, gave 3.6 g of crystalline product. To recrystallize, the material was dissolved in 6 ml of hot water, and the solution was treated with a decolorizing carbon. After filtration, the solution, combined with 2 ml of washings, was diluted with 2 volumes of methanol, and the mixture was allowed to stand for several hours at 0° C. The crystalline *N*-acetylarabinosylamine was separated and washed with methanol. Melting point, 222° to 224° C; $[\alpha]_D^{20} = +69.1°$ (H_2O, $c=4$). The constants were unchanged after further crystallization.

Analysis: Calculated for $C_7H_{13}O_5N$: C, 43.97; H, 6.85; N, 7.33. Found: C, 44.1; H, 6.8; N, 7.4.

4. Periodate Oxidation of *N*-Acetyl-L-Arabinosylamine

It was found that the optical rotation of a solution that was 0.1 *M* with respect to *N*-acetyl-L-arabinosylamine and 0.25 *M* with respect to sodium metaperiodate ($NaIO_4$) quickly changed from a dextro to a levo direction and attained a maximum ($[\alpha]_D^{20} = -49°$) in 14 minutes. After this time, there was a very gradual decrease in levo-rotation. At intervals, 10-ml aliquots of the solution were withdrawn, and each sample was treated with 10 ml of a saturated solution of sodium bicarbonate, 25 ml of 0.1 *N* sodium arsenite, and 1 ml of a 20-percent solution of potassium iodide. The excess arsenite was then titrated with a 0.1 *N* solution of iodine. The values in table 6 show that two moles of periodate were consumed per mole of glycosylamine in 10 minutes, and that further consumption of periodate was negligible. These results are in harmony with a pyranoside structure for *N*-acetyl-L-arabinosylamine. The change in optical rotation that takes place during the oxidation is also given in table 6. The levorotatory product, presumably

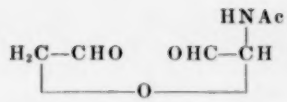

is characteristic of all *N*-acetyl-pentapyranosylamines having the same configuration for carbon 1 as that of *N*-acetyl-L-arabinosylamine.

TABLE 6. *Oxidation of N-acetyl-L-arabinosylamine with sodium metaperiodate*

Reaction time	Optical rotation [a]	Moles periodate per mole amine
Minutes	$[\alpha]_D^{20}$	
2.5	+19.6	.....
3.4	−6.9	.....
5.0	.....	1.92
5.3	−30.9	.....
7.3	−42.8	.....
10.0	.....	1.99
10.7	−47.4	.....
14.2	−49.0	.....
30	.....	2.00
60	−44.8	.....
120	.....	2.01

[a] Based on weight of *N*-acetyl-L-arabinosylamine.

5. Mutarotation and Hydrolysis Measurements

The course of the mutarotation and hydrolysis reactions was followed by measurements of optical rotation on solutions of L-arabinosylamine containing known amounts of acids and bases. In each experiment, 0.5 g of crystalline L-arabinosylamine was placed in a 25-ml volumetric flask. Sufficient acid, base, or buffer solution at 20° C was added rapidly to give a volume of 25 ml, and measurements were made of the optical rotation in a 4-dm tube. Time was measured from the moment the solvent was added to the crystals. At the end of the experiment, and in some cases at intermediate points, the pH of the reaction mixture was measured. As 1 mole of ammonia is liberated during the hydrolysis, it was not possible to maintain the hydrogen ion concentration constant, and in each case the pH of the solution increased somewhat as the reaction proceeded. For purpose of comparison, the values obtained at the end of the experiment were used in the calculations.

In solutions more acid than pH 7.8, the initial decrease in optical rotation that characterizes the mutarotation was too rapid to detect. In the pH range 7.8 to 12, velocity constants for the mutarotation were calculated by the formula

$$k_m = \frac{1}{t_2 - t_1} \log \frac{r_{t_1} - r_m}{r_{t_2} - r_m},$$

where r_{t_1} and r_{t_2} are the specific rotations at times t_1 and t_2, and r_m, the minimum optical rotation, is assumed to be the equilibrium rotation in the absence of hydrolysis. In some experiments the minimum rotation was not reached because the

916783—51——5

UNIVERSITY OF MICHIGAN LIBRARIES

reaction either was too slow, or was complicated by competitive hydrolysis. In these cases, a value of +69°, the minimum rotation found for uncomplicated cases, was used for r_m.

It is noteworthy that the equilibrium rotation obtained in highly alkaline solution in the presence of 2.5 *N* ammonium chloride (experiment 3, table 1), is appreciably lower than that found at the same pH in the presence of only 0.1 *N* ammonium chloride (experiment 2). The cause of the difference is not known, but it may be due to the side reaction mentioned on page 142.

The rate of hydrolysis was calculated from the rise in optical rotation that takes place after the primary mutarotation reaction is complete. In the calculations it is assumed that the second change in rotation is due solely to the hydrolysis reaction and that the optical rotations of both the arabinosylamine and the product, L-arabinose, remain constant throughout the period chosen for the rate measurement.

The values for the hydrolysis rate constant given in table 1 were calculated from the formula

$$k_{\text{hydrol}}=\frac{1}{t_2-t_1}\log\frac{r_{t_1}-r_\infty}{r_{t_2}-r_\infty},$$

where r_{t_1} and r_{t_2} are the rotations at times t_1 and t_2, respectively, and r_∞ is the specific rotation of the fully hydrolyzed material.

VIII. Summary

It has been found that L-arabinosylamine undergoes a mutarotation reaction that is followed or accompanied by hydrolysis of the amino group. The mutarotation takes place at measurable rates between pH 7.8 and 12, but it is too rapid to observe in solutions of higher oxonium ion concentrations. Mechanisms are proposed for the mutarotations of the glycosylamines and of the sugars. The mutarotation of the glycosylamines, in marked contrast to that of the sugars, is not appreciably catalyzed by hydroxyl ion, but is strongly catalyzed by oxonium ion. Apparently mutarotation and hydrolysis of the glycosylamines take place through an intermediate imonium ion.

The rate of hydrolysis of L-arabinosylamine is unusually sensitive to the acidity of the medium, is greatest at pH 5, and is negligible in both alkaline and highly acid solutions. A mechanism is proposed to account for these facts and by application of mass law to the reaction scheme and evaluation of the constants, the following expression is obtained for the rate of hydrolysis:

$$k_{\text{hydrol}}=\frac{1}{7.9+6.1\times10^4[\text{H}^+]+4.2\times10^8[\text{OH}^-]}.$$

To provide information concerning the structure of L-arabinosylamine, the following new compounds were prepared: Tetraacetyl-L-arabinosylamine ($C_{13}H_{19}O_8N$), mp 177° to 178° C, $[\alpha]_D^{20}=+89.6°$ ($CHCl_3$. $c=1.6$); *N*-acetyl-L-arabinosylamine ($C_7H_{13}O_5N$), mp 222° to 224° C, $[\alpha]_D^{20}=+69.1°$ (H_2O, $c=4$). The latter substance was found to react quickly with 2 moles of sodium periodate, as required for an *N*-acetylpentosylamine having the pyranose structure.

The authors gratefully acknowledge the assistance of Nancy B. Holt in various phases of the work, and of Rolf A. Paulson, who analyzed the compounds reported. They also express their appreciation to T. D. Stewart of the University of California for kindly and helpful criticism of the reaction mechanisms.

IX. References

[1] H. L. Frush and H. S. Isbell, J. Research NBS **41,** 609 (1948) RP1943.
[2] H. S. Isbell and H. L. Frush, J. Am. Chem. Soc. **72,** 1043 (1950).
[3] C. A. Lobry de Bruyn and F. H. Van Leent, Rec. trav. chim. Pays-Bas. 14, 129 (1895).
[4] P. Brigl and H. Keppler, Z. physiol. Chem. **180,** 38 (1929).
[5] C. Niemann and J. T. Hays, J. Am. Chem. Soc. **62,** 2960 (1940).
[6] C. S. Hudson, J. Am. Chem. Soc. **29,** 1571 (1907).
[7] J. N. Brönsted and E. A. Guggenheim, J. Am. Chem. Soc. **49,** 2554 (1927).
[8] T. M. Lowry and I. J. Faulkner, J. Chem. Soc. **127,** 2883 (1925).
[9] K. Butler, F. Smith, and M. Stacey, J. Chem. Soc. **1949,** 3371.
[10] T. M. Lowry, J. Chem. Soc. **127,** 1371 (1925).
[11] G. E. K. Branch and M. Calvin, Theory of organic chemistry, p. 404 (Prentice-Hall, Inc., New York, N. Y., 1944).
[12] C. G. Swain, Abstracts of papers, p. 47P (116th Meeting, Am. Chem. Soc., Atlantic City, N. J., Sept. 21, 1949).
[13] L. P. Hammett, Physical organic chemistry (McGraw-Hill Book Co., Inc., New York, N. Y., 1940).
[14] H. Fredenhagen and K. F. Bonhoeffer, Z. physik. Chem. [A] **181,** 392 (1938).
[15] K. F. Bonhoeffer and O. Reitz, Z. physik. Chem. [A] **179,** 135 (1937).
[16] G. A. Howard, G. W. Kenner, B. Lythgoe, and A. R. Todd, J. Chem. Soc. **1946,** 855.
[17] R. Kuhn and L. Birkofer, Ber. deut. chem. Ges. **71,** 1535 (1938).
[18] C. S. Hudson, Z. physik. Chem. **44,** 487 (1903).
[19] T. M. Lowry and G. F. Smith, Rapports sur les hydrates de carbone, p. 116, 10th Conference of the International Union of Chemistry (Liege, 1930).
[20] S. F. Howell and J. B. Sumner, J. Biol. Chem. **104,** 619 (1934).
[21] K. Hill, Ber. Verhandl. sächs Akad. Wiss. Leipzig, Math. phys. Klasse. **86,** 115 (1934). See also, W. W. Pigman and R. M. Goepp, Jr., Carbohydrate chemistry, p. 490 (Academic Press, New York, N. Y., 1948).
[22] E. Ohlsson, Z. physiol. Chem. **189,** 17 (1930).
[23] G. A. Greathouse, Textile Research J. **20,** 227 (1950).
[24] C. S. Hudson and J. K. Dale, J. Am. Chem. Soc. **38,** 1431 (1916).
[25] T. D. Stewart and W. E. Bradley, J. Am. Chem. Soc. **54,** 4172 (1932).
[26] H. S. Isbell, Ann. Rev. Biochem. **12,** 206 (1943).

WASHINGTON, July 25, 1950

Journal of Research of the National Bureau of Standards Vol. 46, No. 2, February 1951 Research Paper 2185

Infrared Studies of Association in Eleven Alcohols

Francis A. Smith and E. Carroll Creitz

This work provides information to facilitate the interpretation of the structures of carbohydrates in terms of their infrared absorption spectra and additional knowledge of the properties of alcohols as associated solvents. The spectra of methanol, 1-dodecanol, 2-methyl-2-propanol (*t*-butyl alcohol), 3-pentanol, 3-methyl-3-pentanol, 2,2,4-trimethyl-3-pentanol, 2,4-dimethyl-3-ethyl-3-pentanol, 2,2,4-trimethyl-3-ethyl-3-pentanol, 2,2,4-trimethyl-3-isopropyl-3-pentanol, 2,2,4,4-tetramethyl-3-*n*-propyl-3-pentanol, and 2,2,4,4-tetramethyl-3-isopropyl-3-pentanol have been studied.

Some of the effects of dilution in nonpolar solvents, and of steric hindrance by branching, on their intermolecular association through the formation of hydrogen bridges have been determined.

Evidence is presented for the existence of a single-bridge type of dimer.

The assignment of the band at 2.86 microns to dimer has been given strong support.

An isobestic point, at which the molar absorbancy index (28.6) is independent of the degree of dissociation, was found at 8.82 microns in the spectrum of 3-pentanol. Others not so well marked appear in the spectra of some of the other alcohols. Such points facilitate the quantitative determination of such alcohols in favorable circumstances.

The absorptions of the monomer and the dimer, separately, appear to obey Beer's law.

Both the monomer and the single-bridge dimer appear to contribute to the free hydroxyl absorption; their relative contributions depend upon the concentration of the solution.

I. Introduction

The interpretation of the infrared spectra of carbohydrates and other hydroxyl-bearing compounds in terms of molecular structure is complicated by the intra- and intermolecular association of such compounds through the formation of hydrogen bridges [1, 2].[1] Many workers have investigated these association phenomena and their effects on the infrared spectrum by means of progressive dilution in solvents [3 to 7]. As the average intermolecular distance increases with dilution, a progressively larger number of bridges are broken, with a corresponding effect upon the spectrum.

A solvent suitable for the study of association between molecules of the solute should (a) dissolve the solute in appreciable quantities; (b) be free from absorption bands of its own in the region to be studied; (c) show no association with the solute. Solvents in which carbohydrates, such as cellulose, are sufficiently soluble usually contain O or N (to which the solute could form hydrogen bridges) and have relatively complex spectra. Consequently, it has not been possible to study such carbohydrates by this method directly. The same situation exists in the case of sugars, although their solubility in otherwise suitable solvents may be increased slightly by partial acetylation. Many monohydric alcohols, however, are sufficiently soluble in such solvents as carbon tetrachloride and carbon disulfide, which have been shown to be otherwise suitable.

Several possible types of aggregation that may result from the association of alcohols are illustrated diagrammatically in figure 1.

The free fundamental valence stretching vibration of the hydrogen-oxygen bond has been shown to result in a sharp absorption band at approximately 2.75μ (3,636 cm^{-1}), which is little affected by the nature of the rest of the molecule to which the hydroxyl is attached. The free hydroxyl of monomer, unaffected by other molecules, may be expected to absorb at a slightly shorter wavelength than the free hydroxyl of single-bridged dimer or the terminal free hydroxyl of polymer. In the latter cases the bridge to oxygen formed by the hydrogen of another molecule absorbs part of the available energy, weakening the free O—H bond and resulting in absorption at a slightly longer wavelength. A band at approximately 2.86μ (3,497 cm^{-1}) has been ascribed [3, 4] to the fundamental stretching vibration of the O—H in dimer in which the hydrogen participates in a bridge between its own oxygen and the oxygen of another molecule. In such cases, represented in figure 1 by the bridged O—H · · · O of the single-bridge dimer and the terminal O—H · · · O of the polymer, the O—H bond is weakened much more than was the case in the change from monomer to the free hydroxyl of dimer. When several molecules are linked together as indicated for polymer in figure 1 (except in the case of the formation of a closed ring), there will be a free hydroxyl group at one end and a bridged hydroxyl group at the other, like those just discussed above. All the internal O—H vibrations will be of the type in which both oxygen and hydrogen, instead of oxygen or hydrogen alone, participate in bridges to other molecules. In this case the O—H bond is weakened even more than in the other cases, and the still lower frequency of the fundamental stretching vibration results in an absorption band centering near 3μ (3,333 cm^{-1}). The skeletal vibrations of long chains of such nature could result in a relatively continuous statistical variation in the lengths, strengths, and frequencies of vibration of the O—H bonds of the intermediate bridges and so account for the breadth of the absorption band and the lack of indication of discrete fine structure even at high resolution. The situation in the case of the

[1] Figures in brackets indicate the literature references at the end of this paper.

UNIVERSITY OF MICHIGAN LIBRARIES

double-bridged type of dimer represented in figure 1 differs from that of the polymer $(\cdots O-H\cdots)_n$ in several respects. The $O-H\cdots O$ angle in the dimer is necessarily much smaller, and consequently the bridge can exert less effect upon the O—H stretching frequency than would be the case if the angle were nearly straight. But both hydrogen and oxygen of both molecules participate in bridges. The combined result of both effects should place the absorption of the O—H bond of double-bridged dimer at a wavelength somewhere between that of free hydroxyl and that of polymer. The quadrangle formed by the doubly bridged pair of hydroxyl groups should be planar, and the in-plane bending vibrations of the O—H bond should be much more affected by the bridges than the out-of-plane bending with a marked difference between the frequencies of the in-plane and out-of-plane vibrations. Available spectra of the liquids, obtained with rock salt prisms, indicate on this basis that, undiluted, the shorter *n*-1-alkanols are almost completely associated. With the higher resolution obtained with the lithium fluoride prism, and at sufficiently slow rates of scanning, some indication of free hydroxyl is sometimes found. Indicatons of any "dimer" that may be present are often obscured by the broad polymer band.

In this work, as a means of improving the basis for the interpretation of the spectra of alcohols of more complex structure, several of the simpler alcohols have been used to study the following:

The effects of progressive dilution in carbon tetrachloride on the relative intensities of the fundamental stretching bands at about 2.75, 2.86, and 3 μ, and of the first harmonic bands from 1.2 to 1.7 μ. 1-Dodecanol, 2-methyl-2-propanol (*t*-butyl alcohol), 3-pentanol, and 2,4-dimethyl-3-ethyl-3-pentanol were used for this purpose.

The effects of dilution on the intensities of the bands of 3-pentanol from 6.65 to 9.7 μ, and of methanol from 2 to 12 μ, in order to identify bands connected with the O—H bending vibration.

The effects on association of the steric hindrance produced by branching. The following series of eight increasingly branched alkyl derivatives of 3-pentanol, undiluted, were used in this study: 3-pentanol, 3-methyl-3-pentanol, 2,2,4-trimethyl-3-pentanol, 2,4-dimethyl-3-ethyl-3-pentanol, 2,2,4-trimethyl-3-ethyl-3-pentanol, 2,2,4-trimethyl-3-isopropyl-3-pentanol, 2,2,4,4-tetramethyl-3-*n*-propyl-3-pentanol, and 2,2,4,4-tetramethyl-3-isopropyl-3-pentanol.

II. Materials

The methanol used was part of a sample of duPont GRX methanol, a catalytic product, prepared as a raw material for the catalytic production of hydrogen by a process in which trace impurities except water were known to poison the catalyst. The portion used was dried by standing over activated silica gel.

The 1-dodecanol, obtained from John D. Hoffman of Princeton Univ., had been purified by crystallization from dry ether followed by five fractional distillations at 1 mm. Freezing point, 23.5° C, [8].

The 2-methyl-2-propanol (*t*-butyl alcohol) obtained from Frank L. Howard, Engine Fuels Section, was recrystallized by freezing.

The 3-pentanol and its seven alkyl derivatives [9] were obtained from Howard, who supplied the following data: All the carbinols except 2,2,4,4-tetramethyl-3-*n*-propyl-3-pentanol were center fractions from the distillation of large quantities through columns with an efficiency of about 30 theoretical plates.

The 3-pentanol was prepared by the fractionation of commercial mixed secondary alcohols in a column of about 110 theoretical plates.

The 3-methyl-3-pentanol was prepared from ethyl-magnesium chloride plus ethyl acetate.

The 2,4-dimethyl-3-ethyl-3-pentanol was prepared from ethyl-magnesium chloride plus diisopropyl ketone. Freezing point, −16.0°C; boiling point, 177.9°C; n_D^{20} 1.4439; D_4^{20}, 0.8588.

The 2,2,4,4-tetramethyl-3-isopropyl-3-pentanol was prepared from *t*-butyl chloride plus ethyl isobutyrate. Boiling point, 234.0° C; n_D^{20}, 1.4646; D_4^{20}, 0.8889; possible impurity, pentamethyl acetone.

The 2,2,4-trimethyl-3-isopropyl-3-pentanol was prepared from methyl trimethyl acetate plus isopropyl chloride. Freezing point, −18.3° C; boiling point, 215.4° C; n_D^{20}, 1.4574; D_4^{20}, 0.8758; possible impurity, pentamethyl acetone.

The 2,2,4-trimethyl-3-pentanol was a byproduct obtained during the preparation of 2,2,4 trimethyl-3-isopropyl-3-pentanol and was formed by reduction of pentamethyl acetone. Freezing point, −11.3° C; boiling point 151.3° C; n_D^{20}, 1.4287; D_4^{20}, 0.8322.

The 2,2,4-trimethyl-3-ethyl-3-pentanol was prepared from ethyl bromide and pentamethyl acetone. Boiling point, 93 to 97° C at 35 mm; n_D^{20}, 1.4479; D_4^{20}, 0.862; purest of the group, no significant quantity of any known impurity.

The 2,2,4,4-tetramethyl-3-*n*-propyl-3-pentanol was prepared from hexamethyl acetone and *n*-propyl chloride, also from methyl-*n*-butyrate and *t*-butyl chloride. Boiling point, 117° C at 22 mm; n_D^{20}, 1.4563; D_4^{20}, 0.8595.

Carbon tetrachloride was several center fractions from a distillation through a Widmer column. n_D^{20}, 1.4574 to 1.4577.

Several of the spectra of the alkyl derivatives of 3-pentanol showed an absorption band at 5.82μ (1,718 cm^{-1}), in the range where carbonyl absorptions might be expected. Ketones and esters were possible impurities in some of the alcohols, and the possible contribution of any of the alcohols to the absorption at this wavelength was unknown. The 2,2,4-trimethyl-3-ethyl-3-pentanol was stated to be the purest of this group of alcohols, and its spectrum showed no marked absorption greater than background at 5.82μ. Consequently, its absorbance index at this wavelength was used as a background value above which to estimate spectrometrically the possible upper limit of carbonyl group impurities in the others. The result is shown in the following tabulation in mole percent.

3-Pentanol	0.4
3-Methyl-3-pentanol	.1
2,2,4-Trimethyl-3-pentanol	2.2
2,4-Dimethyl-3-ethyl-3-pentanol	2.3
2,2,4-Trimethyl-3-isopropyl-3-pentanol	3.4
2,2,4,4-Tetramethyl-3-n-propyl-3-pentanol	.2
2,2,4,4-Tetramethyl-3-isopropyl-3-pentanol	3.8

This estimated upper limit would, of course, be diminished to the extent to which the alcohol is found to contribute to the absorption at this wavelength in any given instance.

III. General Experimental Procedure

The spectra were recorded with a Perkin-Elmer spectrometer model 12–B, using a lithium fluoride prism. The spectra of the solutions of 3-pentanol and methanol were also recorded by using a rock-salt prism, as were those of the series of undiluted alkyl derivatives of 3-pentanol. The characteristics of the spectrometer and the method of operation have been described previously [10].

The temperature of the air at the spectrometer was approximately 25.2°C at all times, and the temperature of the samples during measurement probably did not differ greatly from this.

The cells used were constructed with rock-salt windows and lead or tin spacers cemented with amalgam as described previously [11]. The thickness of the cells was measured by the interference method of Smith and Miller [12]. The spectra of solutions were corrected for cell and solvent losses by using as a blank a cell of nearly identical thickness filled with solvent, and for scattered energy by the use of shutters of glass and lithium flouride. Cell losses were compensated in the case of the undiluted alcohols by the use of a window of double thickness as a blank.

By using the densities of the alcohols and of the solvent, and assuming no volume change on mixing, molar solutions were prepared by weight, the concentrations being adjusted when possible (as dilution progressed) to correspond to successively increasing thicknesses of the fixed cells, so that the weight of a given solute in the absorbing path would remain approximately the same at all concentrations. If possible, the spectrum of each solution was recorded on the day it was prepared, to avoid the preferential loss of the lighter alcohols by evaporation noted by Saier and Coggeshall [13], or of solvent in other cases.

Change of concentration during the process of filling the cells was minimized by the use of the device shown in figure 2. A 30-ml bottle with a standard taper cap, containing the solution, was supported on a platform. The cap was replaced with a dispensing fitting having a short vertical outlet surmounted by a small male standard taper. The fixed absorption cell was supported above it in "ways," or positioning guide slots, like those on the spectrometer housing. The lower cell fitting was provided with a nut containing a tapered teflon packing, which, when lowered upon the small standard taper of the dispenser, provided a reasonably tight connection. The upper cell fitting was provided with another small male standard taper, made tight with a nut and teflon packing, to serve as a sight-glass and to indicate any loss of solution. Air dried over silica gel was forced into the bottle over the solution. When the solution rose into the cell and sight-glass the air was turned off, the upper standard taper was capped, the cell separated from the dispenser, the connecting nut replaced by a teflon sealed cap nut, and the dispenser capped.

IV. Treatment of the Data

Terminology and symbols conform to the usage outlined in NBS Letter Circular LC857.

For undiluted alcohols, T, (transmittance)$=I/I_0$, where I_0 is the intensity of radiation incident on the sample, and I is the intensity of that transmitted. "Transmittance in percent"$=100\ T$. a_M ("molar absorbance index")$=1/bc\ \log_{10}1/T$, where b is the thickness of the cell in centimeters, and c is the concentration or number of moles per liter.

For solutions, $T=I_{soln}/I_{solv}$ and molar absorbancy index differs from molar absorbance index also in that the concentration c is expressed in moles per liter of solution.

Assuming the accuracy of the values of transmittance, concentration, and cell thickness, as well as obedience to Beer's law, an absorption band resulting from C—H should yield a value of molar absorbency index that is independent of concentration. In those cases in which such a band was present adjacent to the spectral range of interest, it was used as an internal standard by which to evaluate a factor, constant for any one solution, with which to adjust the values of molar absorbency index of one or more solutions in a group to give a constant value for the "standard" band. Such deviations from a constant value reflect probable uncertainties in the numerical values, as well as possible deviations from Beer's law. The application of such a correction has resulted in a general improvement of the relative numerical values of the curves of a group, as evidenced by its effect upon several isosbestic points, some of which are reasonably good after the correction.

The data have all been plotted by using a linear wavelength scale reading from left to right, with a corresponding scale in wave numbers.

Certain sections of some curves have been delineated by small dots to indicate that unusual uncertainties exist in the photometric data because of strong bands in the background or solvent, or of the F—H absorption by the lithium fluoride prism.

V. Results

1. Effect of Dilution on the O—H Stretching Vibrations

The spectral changes in the vicinity of the O—H fundamental stretching vibration that accompany the dissociation of 1-dodecanol, 2-methyl-2-propanol,

UNIVERSITY OF MICHIGAN LIBRARIES

3-pentanol, and 2,4-dimethyl-3-ethyl-3-pentanol as each was progressively diluted in carbon tetrachloride are shown in figures 3 to 6, respectively, in which molar absorbency index is plotted aginst wavelength. Letters on the curves correspond with the concentrations and cell thickness indicated in the captions. The number 0 indicates undiluted alcohol.

The coexistence of free hydroxyl, dimer and polymer states of aggregation in 1-dodecanol, 2-methyl-2-propanol and 3-pentanol, is indicated in figures 3, 4, and 5, respectively, by the presence in each of bands at about 2.76, 2.86, and 3.0 μ, respectively.

Undiluted 3-pentanol (curve 0 of fig. 5) shows a little free hydroxyl but any evidence of dimer is unobservable. There is some evidence of dimer in the spectra of all the solutions in all the figures.

It will be noted that there is no progressive shift of the wavelength of the bands connected with the several states of aggregation. Each band is characteristic of a given state of aggregation, and the changes in the relative intensities of the three bands reflect the relative population of the three states of aggregation in the solutions.

Although the molar concentrations represented by curves a in figures 3 and 4 are approximtaely the same (2.914 and 2.416, respectively), the population of free hydroxyl in 1-dodecanol is much less than in 2-methyl-2-propanol. It was necessary to reduce the molar concentration of the former to 0.651 in order to attain the same degree of dissociation, as evidenced by free hydroxyl, as was attained at 2.416 moles/liter in the latter. The less complete association of undiluted 2-methyl-2-propanol and its apparently greater tendency toward dissociation on dilution, as compared to 1-dodecanol, was attributed to the effect of the steric hindrance of the *t*-butyl groups. This led to the study of the series of progressively branched alkyl derivatives of 3-pentanol to be discussed later.

In figure 6 the spectrum of 2,4-dimethyl-3-ethyl-3-pentanol shows little or no evidence of polymer absorption. The dimer band at about 2.85 μ is relatively narrow, as compared with the broad polymer bands of the other alcohols, and much stronger than its counterpart in the other three. The free hydroxyl peak of the undiluted alcohol (curve 0) is much stronger than that of the 3-pentanol (curve 0 of fig. 5) or that of the most concentrated solution of the 2-methyl-2-propanol (curve a of fig. 4).

Most significant is the indication of the doublet character of both peaks in curves 0 and a of figure 6. The dimer peak of curve 0 has a stronger component at 2.842 μ with a shoulder at a slightly longer wavelength, 2.857 μ. The free hydroxyl peak of curve 0 has a stronger component at 2.763 μ with a shoulder at a slightly shorter wavelength, 2.757 μ. A similar situation exists in curve a with the relative intensities of the two components reversed. Curves b, c, d, and e, corresponding to successively more dilute solutions show the shorter wavelength component of the free hydroxyl peak.

This situation is interpreted to mean that in the undiluted alcohol most of the stretching vibration of free O—H is that in a single-bridge type of dimer such as that proposed by Fox and Martin [3] as one possible type of hydrogen bridge (see fig. 1). Such participation of the oxygen would diminish the force constant of its bond to free hydrogen, resulting in absorption at a slightly longer wavelength. In the first solution, (curve a), most of the stretching vibration of the free O—H results from monomer, although a portion is attributable to the free hydrogen of the single-bridge dimer. The relative proportion of monomer to single-bridge dimer increases with dilution.

The splitting of the free hydroxyl absorption was noted by Fox and Martin [14], working with benzyl alcohol, and by Coggeshall [15], working with phenols. Fox and Martin [3] presented evidence, based on equilibrium constants, against a single-bridge type of dimer, but in their later work [14] while suggesting the possibility that the band at 2.765 μ results from the interaction of hydroxyl and phenyl groups, they also consider the possibility of single-bridge dimer. Coggeshall attributes the splitting in 2,6-*t*-amyl-4-*t*-butyl phenol to the presence of an impurity in which a single large group is substituted in the ortho position, and notes the disappearance of the longer wavelength component on dilution.

The two components of the dimer peak noted in figure 6 also suggest the possibility that they result from single-bridge and double-bridge dimers. Additional evidence from the free hydroxyl peaks of the series of branched alkyl derivatives of 3-pentanol will be presented in the discussion of their absorption curves.

The absorptions represented by the shoulders on several of the curves of figure 6 at 2.822 μ probably represent contributions unrelated to the hydroxyl group because they appear to be unaffected by dilution.

The spectral changes in the vicinity of the first harmonic of the O—H stretching vibration that result from the dissociation accompanying dilution of 3-pentanol in carbon tetrachloride are shown in figure 7. The numerical values of molar absorbancy index plotted are 100 times the actual values. The band at 1.7 μ was used as an internal standard as described above. In addition to the changes at 1.4 μ (7,143 cm^{-1}) maximum differences between curves o and e appear at about 1.50 and 1.57 μ, indicating bands connected with the associated molecules. Their wavelengths do not bear the same ratio to the polymer and dimer peaks of figure 5 as do the free hydroxyl peaks of the two figures, so they may not represent absorption of polymer and dimer, as such. An imperfect isosbestic point appears in the vicinity of 1.43 μ (6,993 cm^{-1}) with a molar absorbancy index of about 0.1.

2. Effect of Dilution on O—H Bending Vibrations

The identification of the absorption bands connected with the O—H bending vibrations appears to

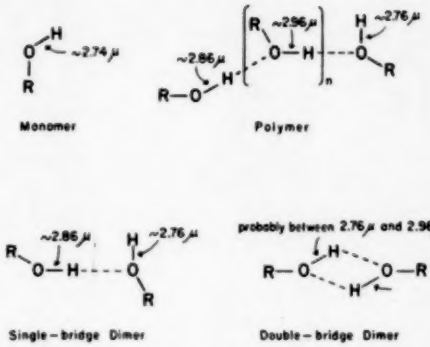

FIGURE 1. *Types of aggregation in the association of alcohols.*

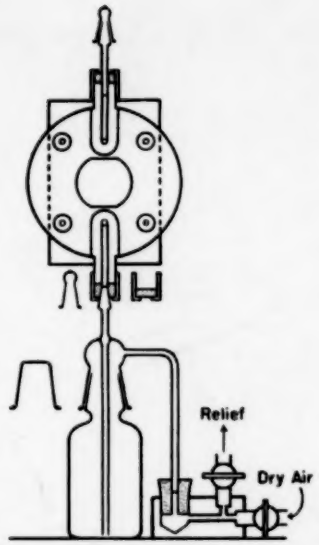

FIGURE 2. *Dispensing device for transfer of volatile solutions from bottle to absorption cell.*

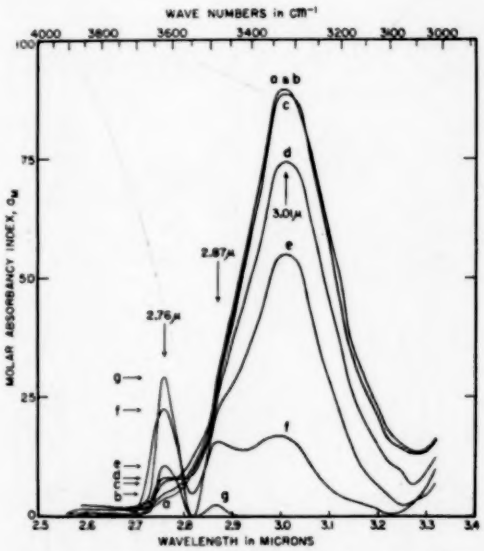

FIGURE 3. O—H *fundamental stretching bands of 1-dodecanol in* CCl_4 *solution.*

LiF prism. Concentrations in moles per liter and cell thicknesses in centimeters are, respectively: Curve (a) 2.914, 0.0108; (b) 1.889, 0.0108; (c) 1.148, 0.0108; (d) 0.651, 0.0108; (e) 0.362, 0.0108; (f) 0.109, 0.0461; (g) 0.0236, 0.200.

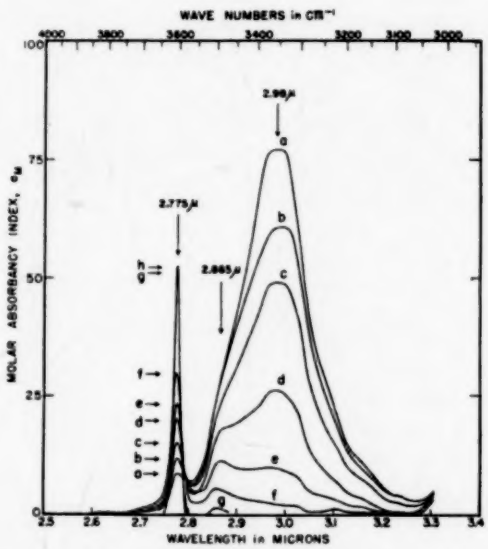

FIGURE 4. O—H *fundamental stretching bands of 2-methyl-2-propanol in* CCl_4 *solution.*

LiF prism. Concentrations in moles per liter and cell thicknesses in centimeters are, respectively: Curve (a) 2.416, 0.0108; (b) 1.308, 0.0202; (c) 0.650, 0.0461; (d) 0.263, 0.100; (e) 0.129, 0.200; (f) 0.065, 0.200; (g) 0.0335, 0.200; (h) 0.0087, 0.200.

UNIVERSITY OF MICHIGAN LIBRARIES

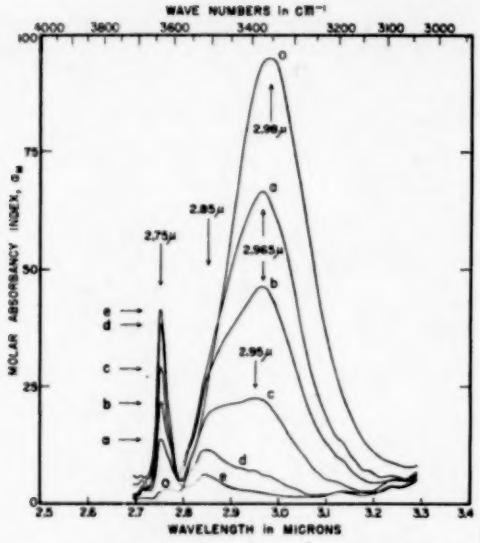

FIGURE 5. O—H *fundamental stretching bands of 3-pentanol in* CCl_4 *solution.*

LiF prism. Concentrations in moles per liter and cell thicknesses in centimeters are, respectively: Curve (O), undiluted, 9.245, 0.0016; (a) 1.587, 0.0087; (b) 0.7068, 0.0190; (c) 0.3253, 0.0427; (d) 0.1408, 0.100; (e) 0.0568, 0.269.

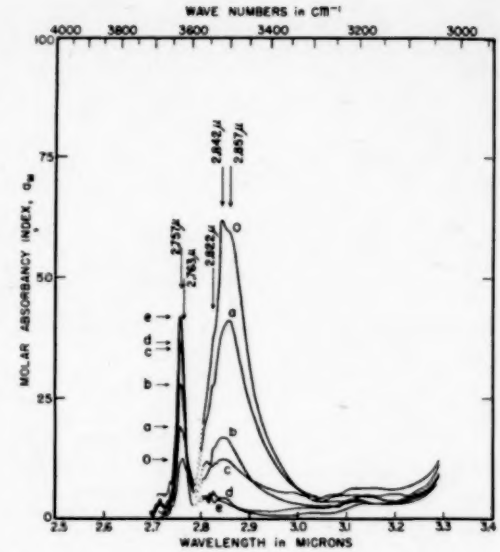

FIGURE 6. O—H *fundamental stretching bands of 2,4-dimethyl-3-ethyl-3-pentanol in* CCl_4 *solution.*

LiF prism. Concentrations in moles per liter and cell thicknesses in centimeters are, respectively: Curve (O), undiluted, 5.924, 0.0015; (a) 2.849, 0.0031; (b) 0.898, 0.0087; (c) 0.468, 0.0190; (d) 0.2010, 0.0427; (e) 0.0864, 0.100.

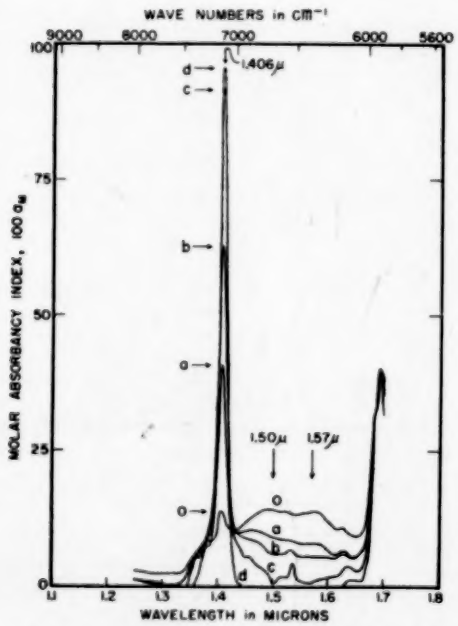

FIGURE 7. *First harmonic of the* O—H *stretching bands of 3-pentanol in* CCl_4 *solution.*

LiF prism. Concentrations in moles per liter and cell thicknesses in centimeters are, respectively: Curve (O) undiluted, 9.245, 0.269; (a) 1.587, 1.196; (b) 0.7068, 1.196; (c) 0.3253, 1.196; (d) 0.1408, 1.196.

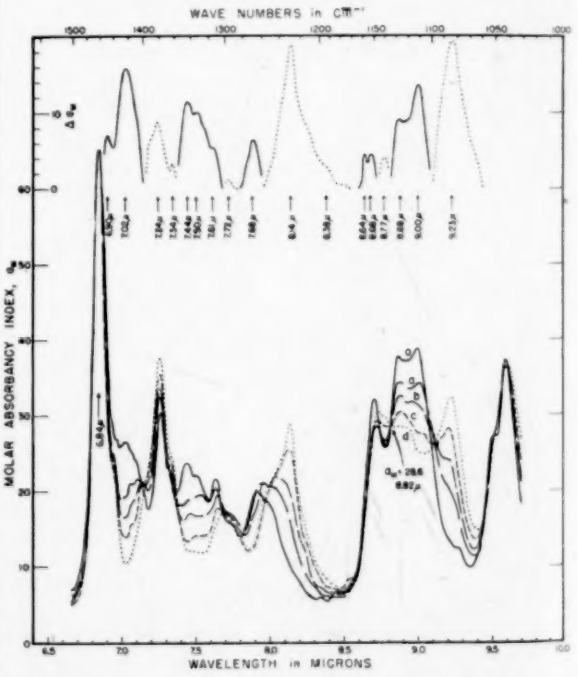

FIGURE 8. *Bands of 3-pentanol in the* O—H *bending region that change in intensity on dilution in* CCl_4 *solution.*

NaCl prism. Concentrations in moles per liter and cell thicknesses in centimeters are, respectively: Curve (O) undiluted, 9.25, 0.0015; (a) 1.597, 0.0089; (b) 0.7068, 0.0192; (c) 0.3253, 0.0423; (d) 0.1408, 0.100.

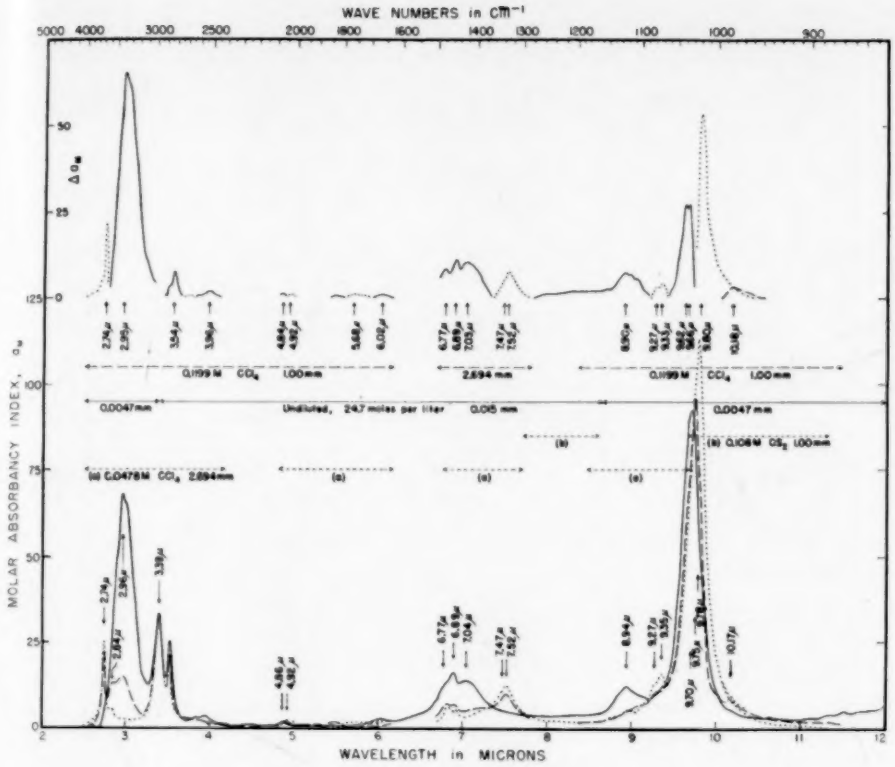

FIGURE 9. *Spectrum of methanol, showing bands that change in intensity as a result of dilution in* CCl_4 *or* CS_2.

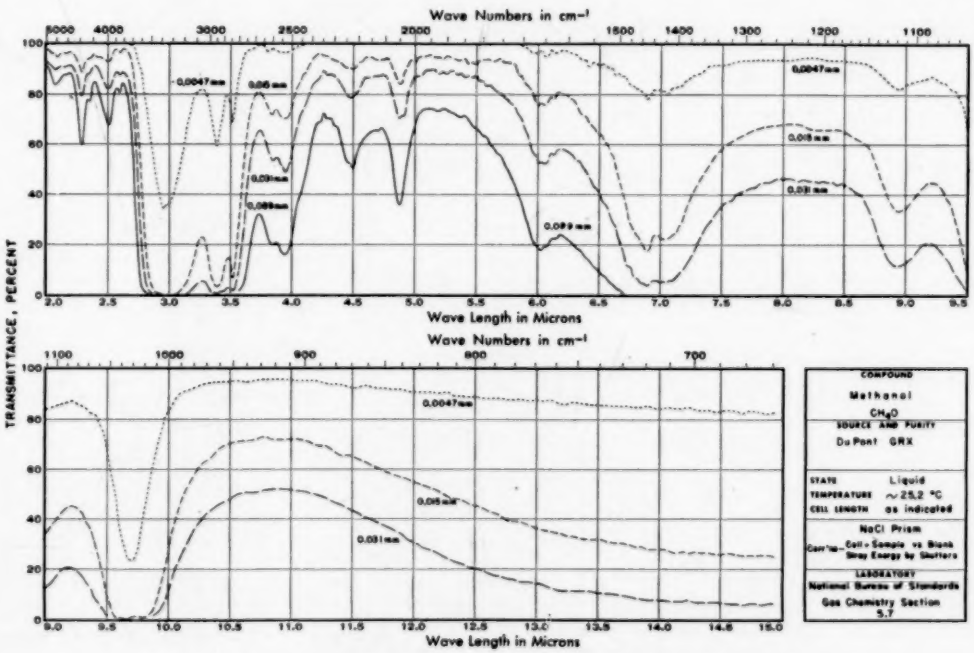

FIGURE 10. *Spectrum of liquid methanol from 2 to 15 microns;* NaCl *prism.*

UNIVERSITY OF MICHIGAN LIBRARIES

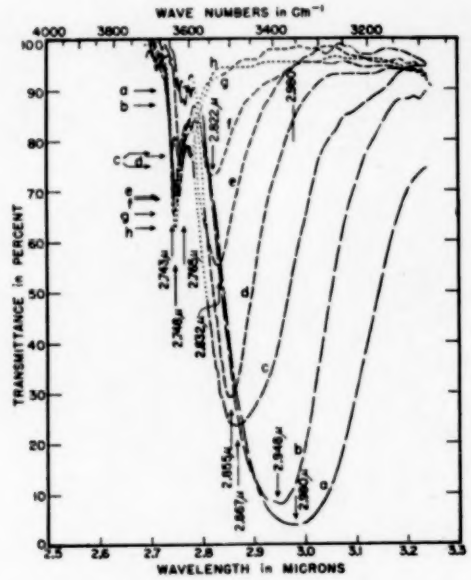

FIGURE 11. O—H *stretching fundamental showing progressively decreased association resulting from increased branching of alkyl derivatives of 3-pentanol.*

Curve (a) 3-pentanol; (b) 3-methyl-3-pentanol; (c) 2,2,4-trimethyl-3-pentanol; (d) 2,4-dimethyl-3-ethyl-3-pentanol, (e) 2,2,4-trimethyl-3-ethyl-3-pentanol; (f) 2,2,4-trimethyl-3-isopropyl-3-pentanol; (g) 2,2,4,4-tetramethyl-3-n-propyl-3-pentanol; (h) 2,2,4,4-tetramethyl-3-isopropyl-3-pentanol.

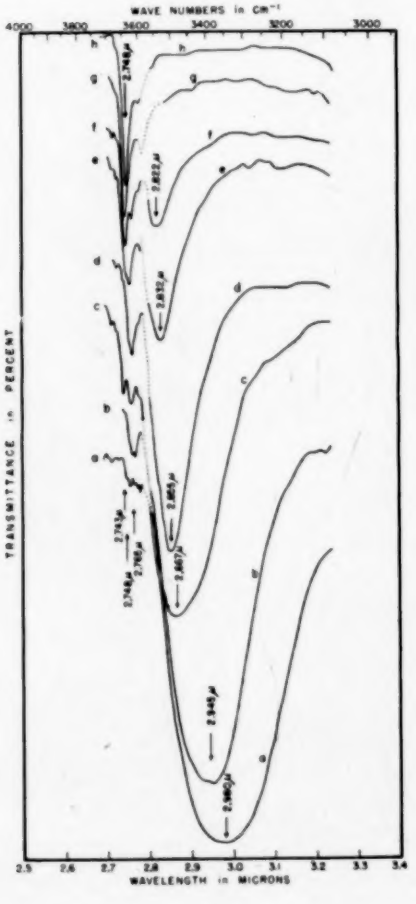

FIGURE 12. *Curves of figure 11 offset to show details of the free hydroxyl peaks.*

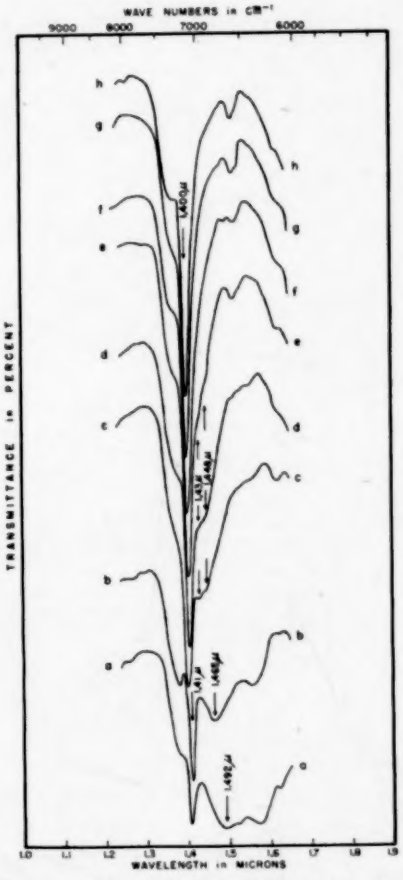

FIGURE 13. O—H *stretching first harmonic showing progressively decreased association resulting from increased branching of alkyl derivatives of 3-pentanol.*

The ordinate scale is offset to avoid overlapping. Curve (a) 3-pentanol; (b) 3-methyl-3-pentanol; (c) 2,2,4-trimethyl-3-pentanol; (d) 2,4-dimethyl-3-ethyl-3-pentanol; (e) 2,2,4-trimethyl-3-ethyl-3-pentanol; (f) 2,2,4-trimethyl-3-isopropyl-3-pentanol; (g) 2,2,4,4-tetramethyl-3-n-propyl-3-pentanol; (h) 2,2,4,4-tetramethyl-3-isopropyl-3-pentanol.

be somewhat uncertain. Bands in the vicinity of 6.2 and 9.4 μ have been assigned by others to O—H vibrations. It was hoped that changes in any bands of these alcohols in this range that accompanied dilution would serve to identify them as O—H bands.

Figure 8 presents the spectrum of 3-pentanol from 6.65 to 9.70 μ, where preliminary trials indicated such changes. The band at 6.84 μ (1,462 cm^{-1}) was used as the internal standard. The solid line represents the undiluted, or associated, alcohol and the dotted curve the most dilute solution (0.1408 moles/liter). Dashes of intermediate lengths indicate intermediate concentrations listed in the caption. One good isosbestic point appears at 8.82 μ (1,134 cm^{-1}) with a molar absorbancy index of 28.6. There are several other indications of possible isosbestic points. The location of such points in the spectra of compounds that dissociate on dilution may be of assistance in such analytical situations as those discussed by Coggeshall [16]. The differences in molar absorbancy index between the undiluted alcohol and the most dilute solution have been plotted in the upper part of figure 8. The solid curves indicate bands resulting from the associated molecules, and the dotted curves indicate those resulting from molecules most of which are monomeric as indicated by the small residual absorptions at 2.95 and 2.85 μ of curve d of figure 5. The large number of bands in this region affected by dilution may be the result of perturbations of the O—H bending by the terminal methyl groups of 3-pentanol, which can, and possibly do, come very close to the hydroxyl when the whole molecule is flexed.

It was expected that this situation could be prevented and the result simplified by the use of a simpler molecule. Figure 9 presents the spectrum of methanol from 2.5 to 12 μ obtained with a rock-salt prism. The band at 3.39 μ was used as the internal standard. The solid curve represents the undiluted alcohol, almost completely associated, as indicated by the small absorption at 2.74 μ. The dotted curve represents a dilute solution (0.0478 moles/liter) in which the molecules are essentially monomeric, as indicated by the small absorptions at 2.96 and 2.84 μ. The dashed curve represents an intermediate concentration. Carbon tetrachloride and carbon disulfide were used as solvents. The gaps between 4.16 and 4.80 μ and between 6.16 and 6.68 μ in the curves for the solutions result from the opacity of both solvents in this region. Differences in molar absorbancy index between the undiluted alcohol and the dilute solution are shown in the upper part of the figure. The solid difference curves represent peaks resulting from associated molecules, and the dotted curves indicate those resulting from molecules most of which are monomeric.

The strong band at 9.70μ (1,031 cm^{-1}), ascribed by Borden and Barker [17] and by Davies [6] to the C—O stretching vibration between the methyl and hydroxyl groups, moves from 9.70μ in the undiluted alcohol to 9.78μ and greater intensity at 0.108 molar in carbon disulfide. At an intermediate concentration the band appears at an intermediate wavelength and intensity. The change in wavelength from undiluted alcohol to 0.108 molar is the same (0.08μ) as that reported by Davies for his solutions in chloroform.

A slight shoulder appears on the short-wavelength side of the peaks of both solid and dotted curves, which may be caused by the inplane deformation vibration that Borden and Barker predicted, but did not find, for monometer at 9.71μ. The shoulder appears here in the dotted curve at 9.74μ, and in the undiluted alcohol at 9.67μ.

Instead of the weak absorption reported by Davies at 9.31μ, (1,074) cm^{-1}) an unequal doublet appears with components at 9.27 (1,079 cm^{-1}) and 9.35μ (1,070 cm^{-1}). The latter, which is stronger, corresponds exactly in wavelength with the "difference tone" between the two fundamentals (1,340 cm^{-1}—270 cm^{-1}=1,070 cm^{-1}, or 9.35μ) mentioned by Davies in this connection. Both appear to be connected with free hydroxyl.

Instead of the weak band at 9.01μ, ascribed by Davies to the in-plane deformation vibration of O—H in associated molecules, we find an absorption connected with polymer at 8.94μ. Davies states, however, that this absorption moves to 8.96μ at 7.90 molar in chloroform.

One of the fundamental vibrations (ν_6 of Borden and Barker, at 7.47μ (1,339 cm^{-1}) was found by Davies as a single sharp peak at 7.52μ. Borden and Barker attributed this to the C—O bending vibration, resolvable into two mutually perpendicular components one in and one out of the C O H plane and predicted a close doublet. The doublet, however, was unresolved by them in vapor or by Davies in dilute chloroform solution. This absorption appears in figure 9 as a close unresolved doublet with the stronger component at 7.52μ, (1,330 cm^{-1}) where Davies found a single peak, and the weaker at the 7.47μ, (1,339 cm^{-1}) predicted by Borden and Barker for the other component of the doublet.

Although Davies makes a good case for the assignment of this band to C—O bending, its wavelength falls in the general range of free O—H bending vibrations. This is too short a wavelength to be compatible with a C—OH bending vibration unless the hydroxyl is associated. Figure 9 shows that the band increases in intensity on dilution, which connects it with a free vibration rather than an associated one, as did its presence in the vapor of Borden and Barker and the dilute solution of Davies. Its assignment by them to a fundamental C—O bending vibration therefore seems highly questionable, especially since they have assigned the strong band at 9.70μ to C—O stretching.

The band reported by Davies at 7.14μ (1,401 cm^{-1}), and attributed by him to the counterpart for polymer of the 7.52μ (1,330 cm^{-1}) monomer band, appears in figure 9 at 7.04μ (1,420 cm^{-1}).

Two C—H bending fundamentals (ν_4 and ν_3 of Borden and Barker at 6.77 and 6.87μ in vapor) appear in figure 9 at 6.77 and 6.89μ, but seem to be affected by dilution, which should not be the case unless they represent additional contributions to a

UNIVERSITY OF MICHIGAN LIBRARIES

broad polymer absorption that overlaps their wavelengths.

The validity of the small difference peaks between 3.6 and 6.3μ is in some doubt, because of the extremely small absorptions from which they are derived and because the dashed curve for the intermediate concentration does not in general fall between the other two. However, the monomer peak at 4.92μ (2,033 cm^{-1}) and the polymer peak at 4.86μ (2,058 cm^{-1}) are the first harmonics of the intense bands at 9.7μ, and they bear the same relation to the intense bands in both wavelengths and intensity. Furthermore, the curve representing the intermediate concentration appears between the other two in both cases.

The peak at 10.17μ in figure 9 was observed in the carbon tetrachloride solution but not in carbon disulfide. It has not so far been accounted for, but it appears to be connected with monomer.

The spectrum of liquid methanol from 2 to 15μ obtained with a rock-salt prism and several cells is presented in figure 10. The solid curve of figure 9 was plotted on its linear ordinate scale (molar absorbance index) from the same data from which two of the curves of figure 10 were plotted. In the latter, the ordinate scale (transmittance in percentage) is logarithimic in absorbance. Each type of plot emphasises and facilitates the presentation of spectral information that the other cannot.

3. Effect of Steric Hindrance on Association

Several workers, notably Coggeshall [15] and Sears and Kitchen [18] have shown that steric hindrance affects the intra- and intermolecular formation of hydrogen bridges in phenols. The effect of progressive branching on the association of a series of alkyl derivatives of 3-pentanol is shown in figures 11, 12, and 13. Figures 11 and 12 present the effect on the O – H stretching fundamental, and figure 13 shows the effect on its first harmonic. Figure 12 presents the curves of figure 11 with the intensity scale offset to avoid obscuring details of the bands of free hydroxyl. The curves are lettered from (a) to (h) in the order of increasing branching. It is seen that the progressive effect on association is in the same order.

In the light of the information developed in the dilution experiments with individual alcohols, the following interpretation of figure 11 is offered. In the alcohols represented by curves a, b, c, and d, monomer, dimer, and polymer coexist in differing relative proportions. Considering them in turn from a to d, the polymer absorption at 2.98 progressively decreases, with a corresponding increase in dimer absorption at 2.855, which reaches a maximum in c and decreases again in d. This gives rise to the apparent progressive shift of the center of the band to successively shorter wavelengths. Curve a is symmetrical. Curve b indicates a predominance of polymer with a slight bulge on the short wavelength side, indicating an increasing contribution of dimer to the absorption. Curve c indicates a predominance of dimer with a bulge on the long wavelength side, indicating the residual contribution of polymer to the absorption. Curve d, which is again approximately symmetrical, indicates that although the dimer population is less than in c, the polymer population has almost disappeared, as shown by the small absorption at 2.98μ. Simultaneously with these changes the population of free hydroxyl has progressively increased, as may be seen more readily in figure 12.

Considering curves d, e, f, g, and h, as more and more methyl groups are substituted for the hydrogen atoms on the chain, the mutual repulsion of the mass of hydrogen atoms of one molecule for those of another prevents as close an approach of the hydroxyl groups as had been possible before. Not only does the formation of polymer become impossible, but the hydrogen bridge to form dimer is progressively stretched out. The progressively weakened bridge in dimer exerts less and less effect upon the O—H valence bond, with the result that the force constant of the latter is greater and the wavelength of its vibration is progressively shorter until in f it appears at 2.822μ. In curve g the dimer population has decreased until the absorption is a mere vestige, which has disappeared in h. Simultaneously the population of free hydroxyl has continued to increase, as may be seen from both figures 11 and 12.

The free hydroxyl band of curve c in figure 11 is a doublet with the stronger peak at 2.765μ and the weaker at 2.743μ. It will be noted that as branching increases from curve a to curve h the more intense absorption in the free hydroxyl band tends in general to shift from 2.765 to 2.748μ.

In figure 12 it will be seen more readily that the free hydroxyl peaks of curves a and b occur in the vicinity of 2.76μ. The doublet of curve c occurs at about 2.76 and 2.74μ, and those of curves d and e occur at about 2.76μ with shoulders on the short-wavelength sides. In curves f, g, and h the free hydroxyl peak occurs at 2.748μ, in curve f with a spur, and in curve g with a shoulder, on the long-wavelength side. These data support those presented above in connection with the dilution study of 2,4-dimethyl-3-ethyl-3-pentanol, illustrated in figure 6, and are strongly indicative of the existence of a single-bridge type of dimer. Of course the single-bridge type of linkage between molecules lends itself to the formation of polymeric aggregates by the addition of more molecules to dimer, as in figure 1. Unless these aggregates form closed rings, there would always be one free O—H per aggregate of polymer, which would contribute its absorption at so nearly the same wavelength as the free hydroxyl of dimer as to be indistinguishable from it. The relative contribution of such terminal hydroxyl groups would of course decrease as the size of the aggregate increased. In the less branched molecules polymer would predominate, and the free hydroxyl absorption of curves a and b of figure 12 would be accounted for by relatively few dimeric pairs linked by a single bridge. Then as branching increases, dimer would predominate, with some monomer as indicated by the shoulders on the short wavelength sides of the

peaks of curves d and e. On further branching the remaining dimer would dissociate until finally almost all the free hydroxyl absorption would be from monomer, as indicated by curves g and h at 2.748μ.

Several of the curves show minor peaks from 2.78 to 2.79μ that vary with the different alcohols. These may be artifacts or contributions of other vibrations in the molecule than those of O–H.

The free hydroxyl absorption, as shown by the first harmonic in figure 13, follows the same general pattern as that just described, occurring at wavelengths as long as 1.41μ in curves a and b and appearing consistently at 1.400μ in curves f, g, and h. Small absorptions at 1.43μ in curves c, d, and e may be those of dimer. Those at 1.492μ in a and at 1.465μ in b probably represent polymer. The small shoulders at 1.448μ in curves c, d, and e have not been identified.

The absorptions from 1.37 to 1.38 μ and those above 1.50 appear not to be connected with hydroxyl.

The spectra of the alkyl derivatives of 3-pentanol, successively branched by the substitution of methyl groups for hydrogen, as observed using the rock-salt prism, are shown in figures 14 to 21, and as observed by using the lithium fluoride prism in figures 22 to 29. It will be seen in the latter group of figures that the first harmonic of the free hydroxyl vibration at about 1.4μ is always stronger, relative to the bands resulting from associated hydroxyl, than is the case with the fundamentals, as noted by Stanford and Gordy [19].

In connection with steric effects, it may be of interest to note the use of the difference in wavelength between monomer and polymer bands as a measure of the electronegativity of the group or atom to which the bridge-forming hydrogen is attached, such as in the studies by Gordy and others, of which the paper by Gordy and Stanford [20] is an example. Also to be noted is the use of the difference as a measure of steric hindrance in studies like those of Coggeshall [16] and Sears and Kitchen [18] with phenols. It would appear that such studies may be expected to yield valid results only where the effect of each factor is considered in the study of the other. The variations in size, and the effects on the distance of approach; of molecules produced by branching in the present study have negligible effect upon the electronegativity of the carbon atom to which the hydroxyl is attached. It is believed that observed differences in wavelength result predominantly from steric effects.

4. Confirmation of the Assignment of the 2.86-Micron Band to Dimer

It will have been noted that in the case of the O—H stretching fundamental, the spectra of all the alcohols studied at concentrations intermediate between the undiluted alcohol and very dilute solutions show a band in the vicinity of 2.86μ. This band also appears in carbohydrates such as sugars and cellulose. It has been ascribed to the dimer state of aggregation by several workers [3, 4], but attempts at proof have been indirect and not entirely conclusive. Direct methods have been unsuccessful because, invariably in solutions over a range of concentrations, monomer, dimer, and polymer states of aggregation coexist. The presence of polymeric aggregates, varying in the number of alcohol molecules per aggregate, and none of them known, made impossible for previous workers a direct solution for an equilibrium constant between monomer and dimer.

An examination of curve d of figure 11 in comparison with the other curves shows that 2,4-dimenthyl-3-ethyl-3-pentanol, undiluted, has a strong relatively sharp band at 2.855μ and only a relatively small absorption at 2.98μ, indicating that this alcohol exists essentially as monomer and dimer. Any polymer present appears to be small relative to dimer and decreases on dilution, as shown in figure 6.

2,4-Dimethyl-3-ethyl-3-pentanol (referred to hereinafter as the alcohol) was measured in successively more dilute solutions in carbon tetrachloride until the only significant absorption was that of free hydroxyl.

By plotting molar absorbancy index at 2.76μ versus the log of the concentration in formula weights per liter as in figure 30 and extrapolating to a constant value of the index, the working value of 44 was established for the molar absorbancy index of monomer.

Two assumptions were then made: (1) That the formula weight absorbancy index for the free hydroxyl of single-bridge dimer would be substantially the same as that for monomer; (2) that the absorptions of monomer at 2.76μ and dimer at 2.85μ separately would obey Beer's law. Then, using the value 44, (the molar absorbancy index of monomer), as a measure of free hydroxyl, the molar concentrations of total free hydroxyl in five solutions with total concentrations from 0.201 molar to the undiluted alcohol (5.92 molar) were determined.

On the basis of the evidence developed above for the existence of single-bridge dimer, values for the percentage of monomer in the mixture of monomer and single-bridge dimer contributing to the absorption of free hydroxyl were assumed in each of the six cases. This gave six values for the concentration of monomer, which, with the known total concentration, gave by difference six corresponding values for the concentration of the associated alcohol in formula weights per liter. From these and the measured absorptions at 2.86μ, six values of the absorbancy index were obtained. Having assumed that this absorption obeys Beer's law, which implies that all six values of the formula weight absorbancy index should be the same, the values assumed above for the percentage of monomer in the mixture of monomer and single-bridge dimer were adjusted until the resulting six values of formula weight absorbancy index at 2.86μ were the same to $\pm$0.5 percent. The assumed values of the percentage of monomer required to accomplish this result were plotted versus total concentration in figure 31. They were found to fall on a smooth curve and to be entirely reasonable.

The average value (61.42) for the formula weight

UNIVERSITY OF MICHIGAN LIBRARIES

absorbancy index for the remaining (associated) alcohol was then used with the cell thicknesses and measured absorptions at 2.86μ to compute six values for the concentrations of the remainder that did not differ significantly from those obtained by difference, but which had been smoothed slightly by adjusting and averaging the indices.

These formula weight concentrations of monomer and of the remainder as derived above were then used to compute the equilibrium constants K_1=[remainder]/[monomer], K_2=[remainder as dimer]/[monomer]^2, and K_3=[remainder as trimer]/[monomer]^3.

The result is presented in the following table.

Solution	Total concentration (Formula weight per liter)	Equilibrium constants		
		K_1	K_2	K_3
o	5.92	34.1	198.5	1,150
a	2.85	2.15	2.39	2.65
x	1.345	0.623	0.751	0.906
b	0.898	.437	.698	1.12
e	.468	.245	.652	1.74
d	.201	.114	.679	4.13

It will be noted that K_1 and K_3 show no indication of an approach to a constant value, whereas values of K_2 for total concentrations below about 1 molar are much more nearly constant than those of K_3. The fact that the values derived on the assumption of dimer are relatively constant for the lower concentrations tends to support the assignment of the absorption at 2.86μ to dimer. The increase in K_2 for solutions above about 1 molar indicates that monomer is decreasing faster than dimer is increasing. This probably means that above about 1 molar some polymer begins to form.

As an independent means of determining the state of aggregation, a method of isotonic vapor pressures similar in principle to that described by Lassettre and Dickinson [21] was chosen. Experiments of a preliminary nature were performed to determine the suitability of the method and to delineate the technique and control of variables that would be required for an accurate determination of the state of aggregation.

Solutions of orthoterphenyl and of alcohol of different concentrations in carbon tetrachloride were prepared by weight, placed in platinum cans with a large glass ball in each to insure mixing, the cans enclosed in a gold-plated brass bomb that was then evacuated and the assembly agitated during the approach toward equality of the vapor pressures of the two solutions. The formula weight absorbancy index of each solution at 2.76 and 2.86μ was determined before and after the experiment.

This, with the weights of the cans and contents before and after the experiment, permitted the computation of the final concentration of monomer and of the associated alcohol remaining as dimer or trimer, with one-half or one-third as many aggregates, respectively, as for monomer.

Had the uncertainties in the values of the several variables involved been sufficiently small, and had equilibrium been certainly attained, the final molar concentration of aggregates in the final alcohol solution should equal that in the final reference monomer solution. Compared with the molar concentration found by weighing for the reference monomer, the result favored dimer only slightly more than trimer, with monomer being definitely eliminated. Nevertheless, the results from this preliminary and inadequately controlled experiment tend to support those obtained by the other method. The information developed indicates that much more precise results may be expected under more accurately controlled experimental conditions.

The results of both methods lend support to the assignment of the O—H stretching vibration at 2.86μ to dimer.

VI. Conclusions

On the basis of information developed by others, as well as in the present study of progressively diluted alcohols, it is concluded that the use of the expression "wavelength shift" in connection with the difference in wavelength of absorption bands characteristic of monomer, dimer, and polymer states of aggregation may be misleading. It is suggested that this term be reserved for those cases in which the wavelength of a band changes progressively with changing conditions.

The effects of steric hindrance and of dilution upon the association of alcohols appear to be roughly parallel.

The location of suitable isosbestic points in the spectra of associated materials may facilitate the use of their spectra in quantitative analytical procedures.

The evidence for the existence of a single-bridge dimer appears to be as good as previous evidence against it, with the possibility that both single-bridge and double-bridge types may coexist.

The assignment to the dimeric state of aggregation of the band at 2.86 μ has been given strong support by more direct methods, made possible by the use of 2,4-dimethyl-3-ethyl-3-pentanol. This assignment will facilitate the interpretation of the structure of carbohydrates by means of their spectra.

The consistent and reasonable results obtained by two independent methods used to confirm the dimer assignment lend confirmation to the assumptions upon which the computations were based: (a) That monomer and dimer separately obey Beer's law, (b) that a single-bridge type of dimer exists, and (c) that monomer and single-bridge dimer contribute to the free hydroxyl absorption in approximately the proportions assumed.

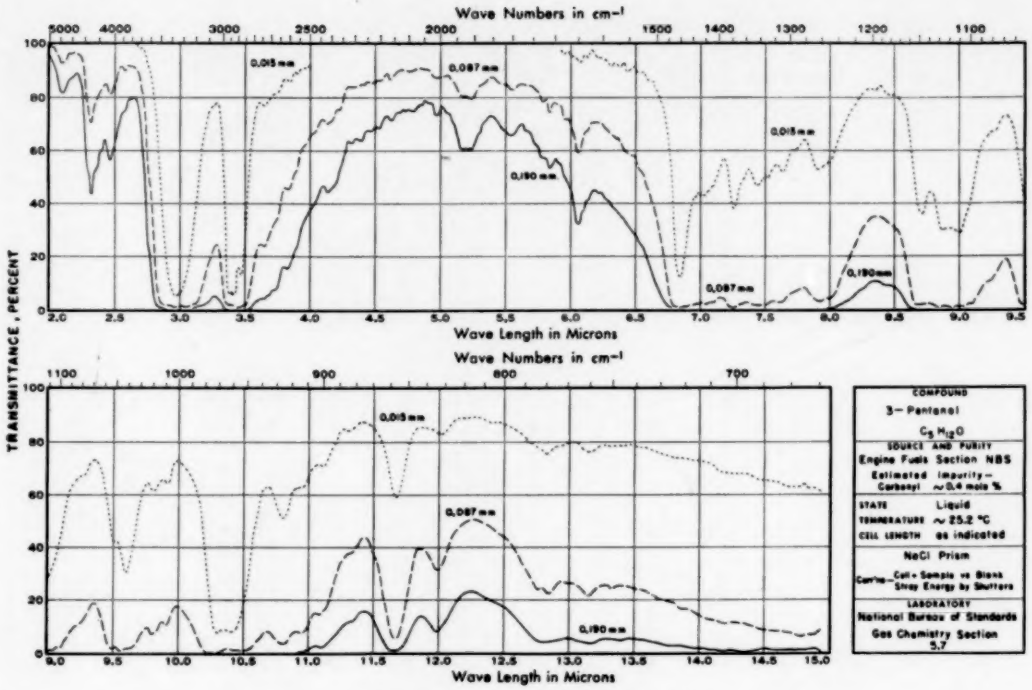

FIGURE 14. *3-Pentanol;* NaCl *prism.*

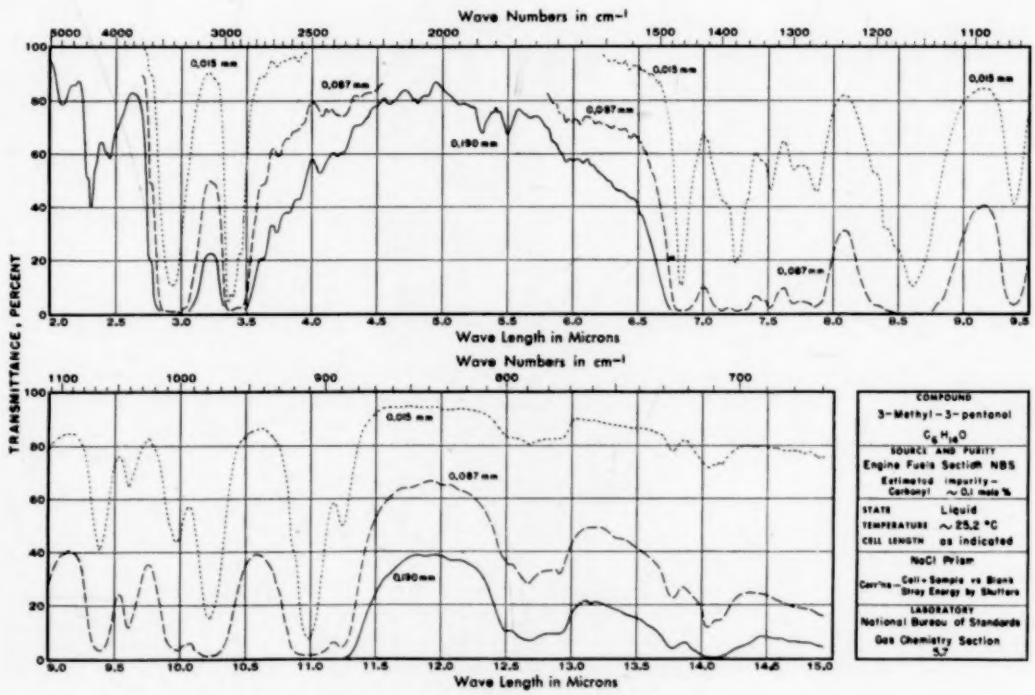

FIGURE 15. *3-Methyl-3-pentanol;* NaCl *prism.*

UNIVERSITY OF MICHIGAN LIBRARIES

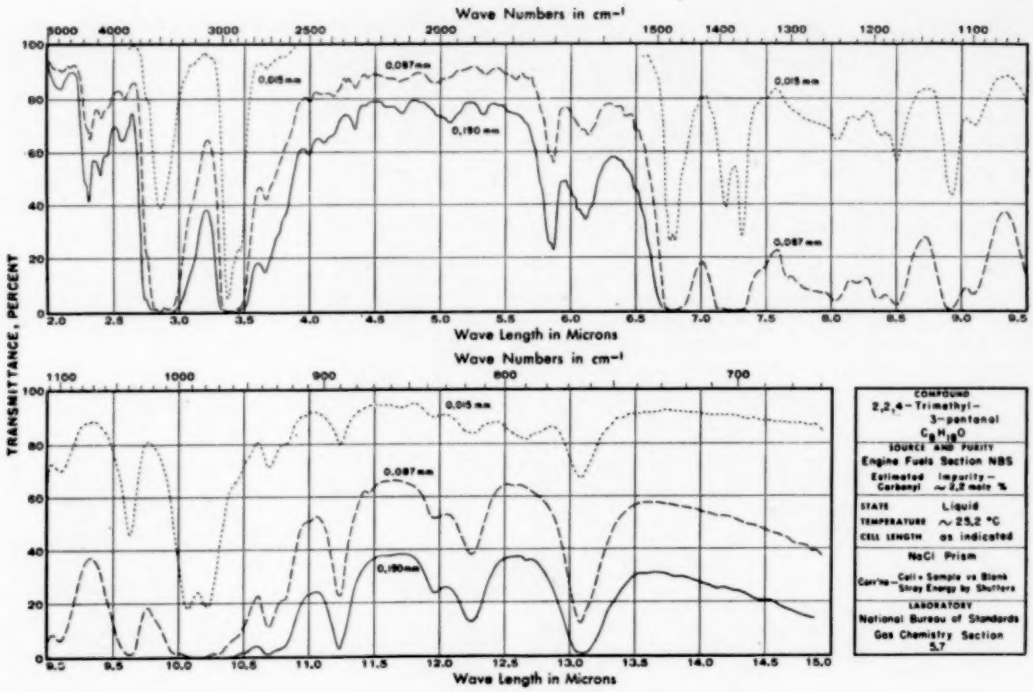

FIGURE 16. *2,2,4-Trimethyl-3-pentanol;* NaCl *prism.*

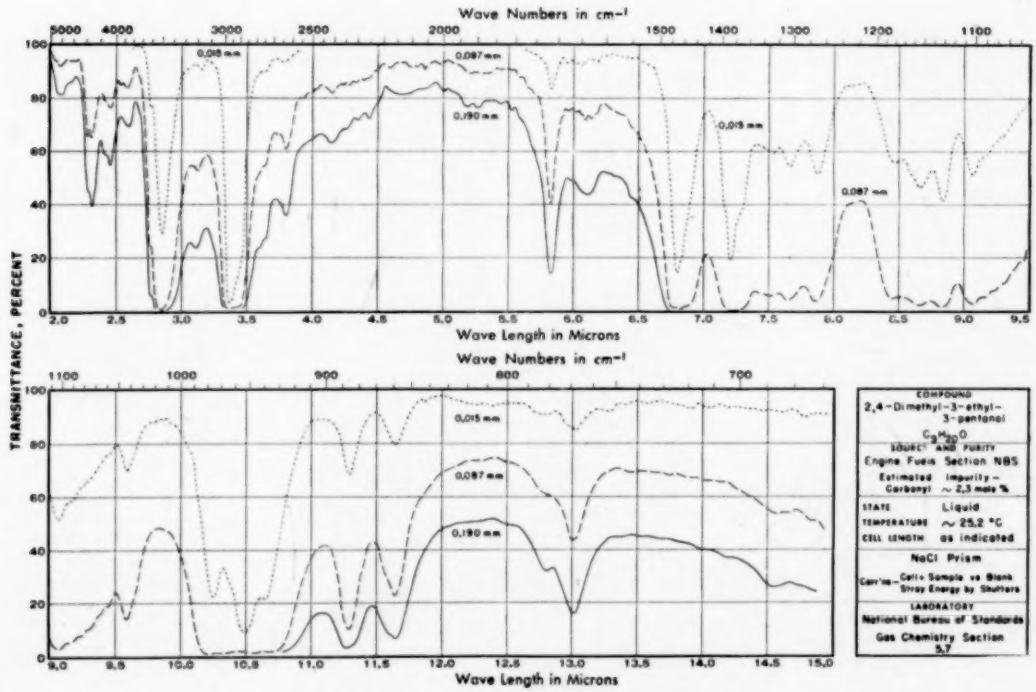

FIGURE 17. *2,4-Dimethyl-3-ethyl-3-pentanol;* NaCl *prism.*

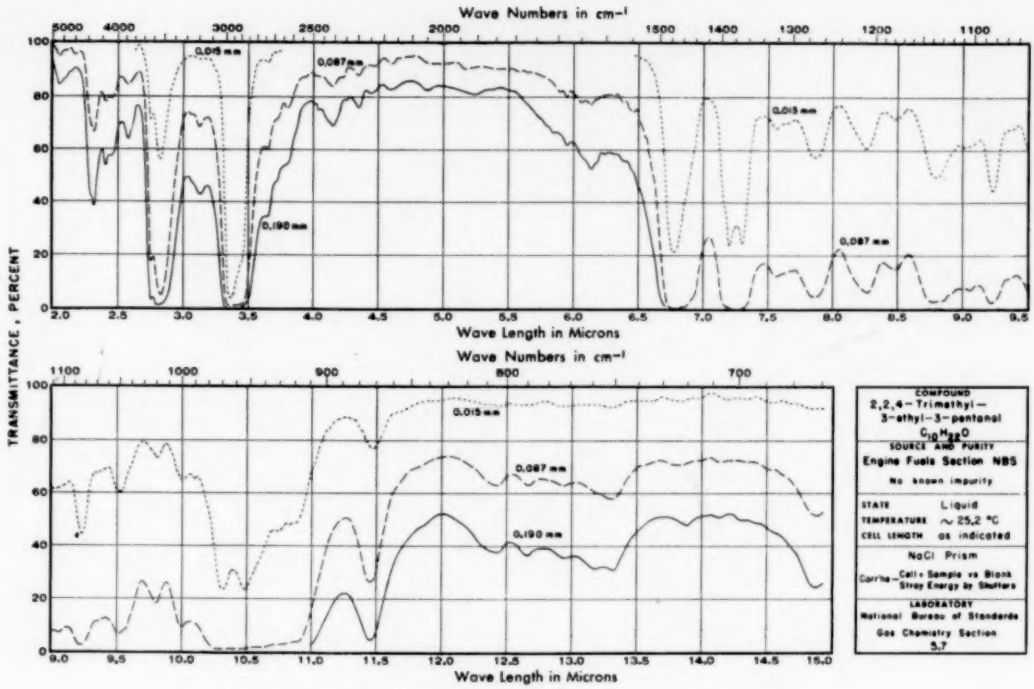

FIGURE 18. *2,2,4-Trimethyl-3-ethyl-3-pentanol;* NaCl *prism.*

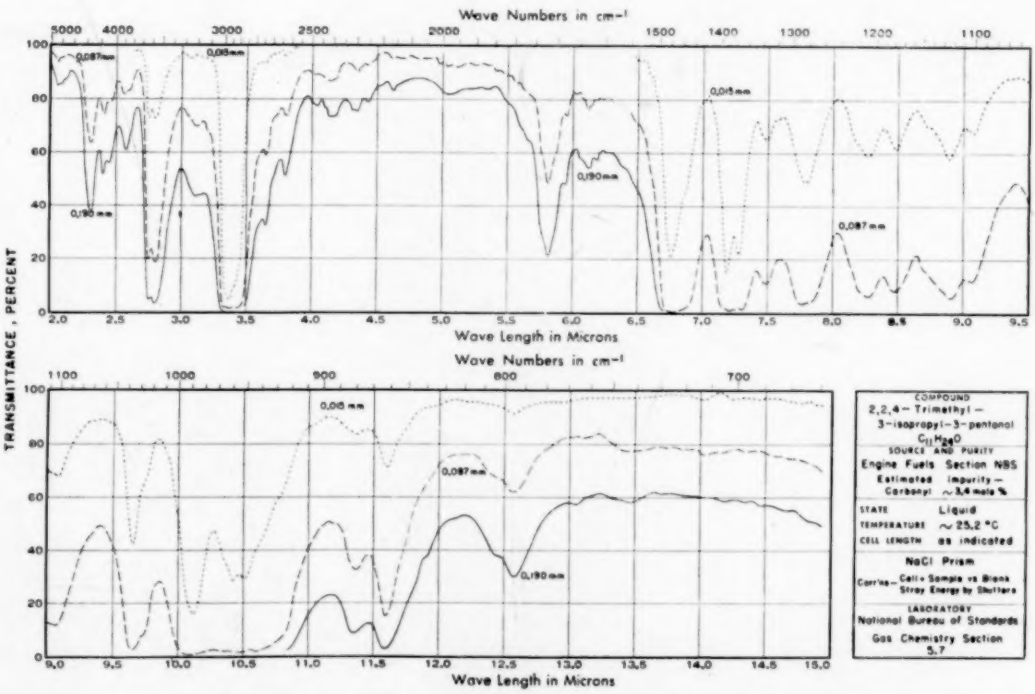

FIGURE 19. *2,2,4-Trimethyl-3-isopropyl-3-pentanol;* NaCl *prism.*

916783—51—6

UNIVERSITY OF MICHIGAN LIBRARIES

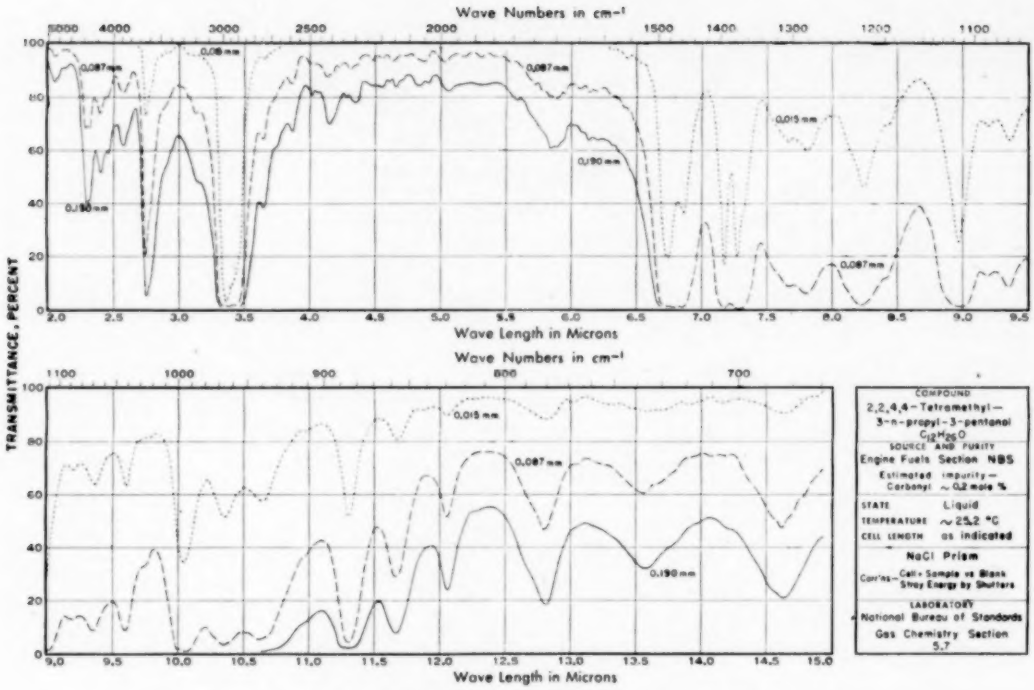

FIGURE 20. *2,2,4,4-Tetramethyl-3-n-propyl-3-pentanol;* NaCl *prism.*

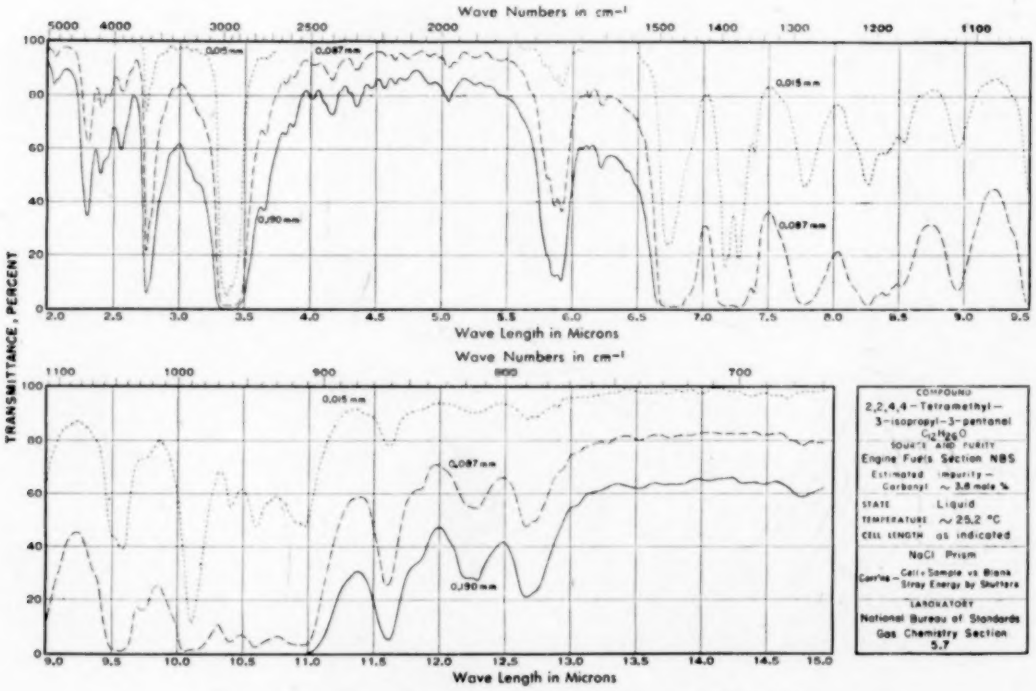

FIGURE 21. *2,2,4,4-Tetramethyl-3-isopropyl-3-pentanol;* NaCl *prism.*

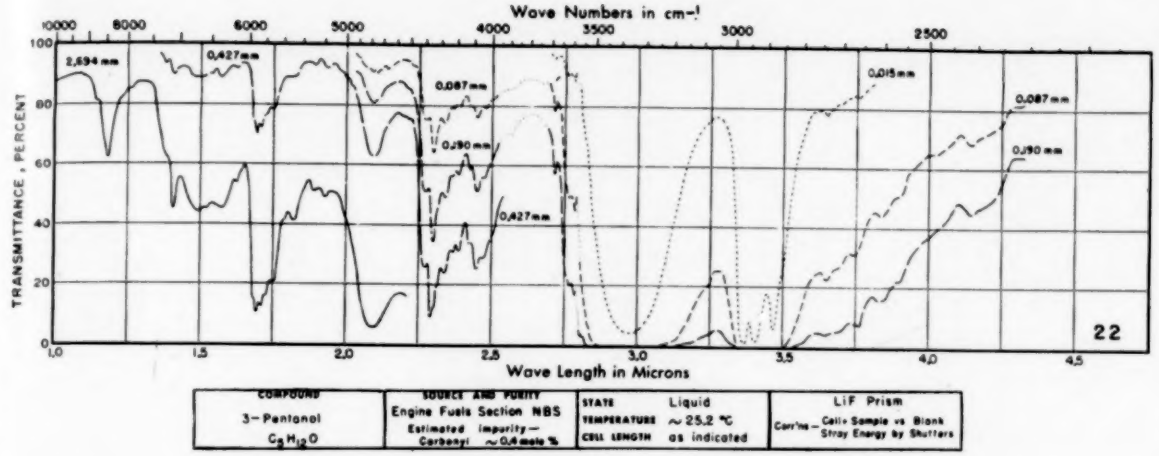

COMPOUND	SOURCE AND PURITY	STATE	LiF Prism
3-Pentanol $C_5H_{12}O$	Engine Fuels Section NBS Estimated impurity— Carbonyl ~0.4 mole %	Liquid TEMPERATURE ~25.2 °C CELL LENGTH as indicated	Corr'ns—Cell+Sample vs Blank Stray Energy by Shutters

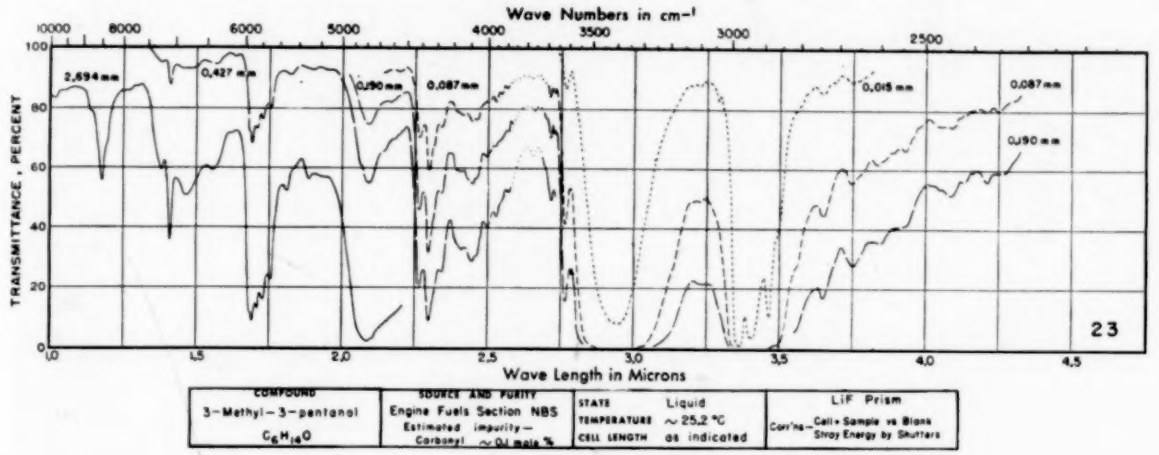

COMPOUND	SOURCE AND PURITY	STATE	LiF Prism
3-Methyl-3-pentanol $C_6H_{14}O$	Engine Fuels Section NBS Estimated impurity— Carbonyl ~0.1 mole %	Liquid TEMPERATURE ~25.2 °C CELL LENGTH as indicated	Corr'ns—Cell+Sample vs Blank Stray Energy by Shutters

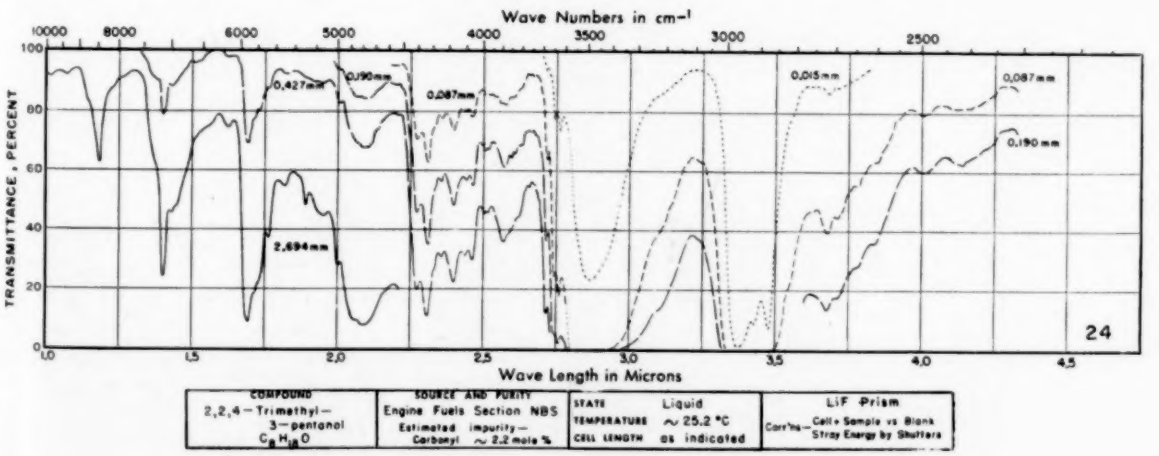

COMPOUND	SOURCE AND PURITY	STATE	LiF Prism
2,2,4-Trimethyl-3-pentanol $C_8H_{18}O$	Engine Fuels Section NBS Estimated impurity— Carbonyl ~2.2 mole %	Liquid TEMPERATURE ~25.2 °C CELL LENGTH as indicated	Corr'ns—Cell+Sample vs Blank Stray Energy by Shutters

FIGURE 22. *3-Pentanol;* LiF *prism.* FIGURE 23. *3-Methyl-3-pentanol;* LiF *prism.*
FIGURE 24. *2,2,4-Trimethyl-3-pentanol;* LiF *prism.*

UNIVERSITY OF MICHIGAN LIBRARIES

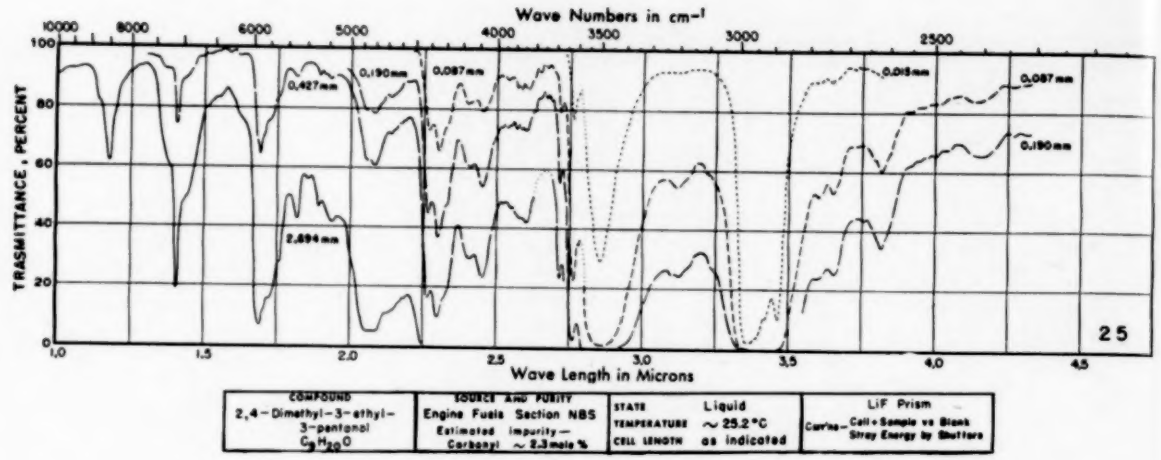

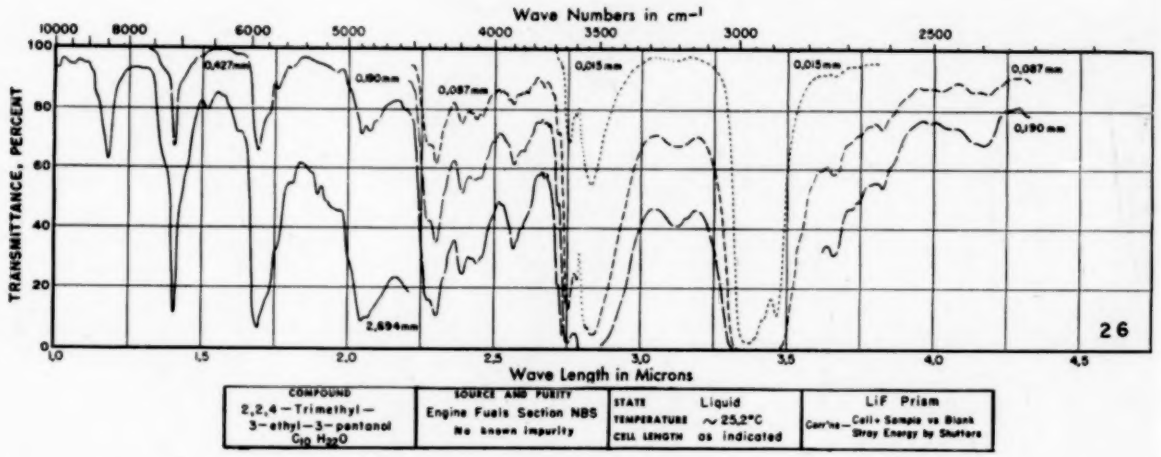

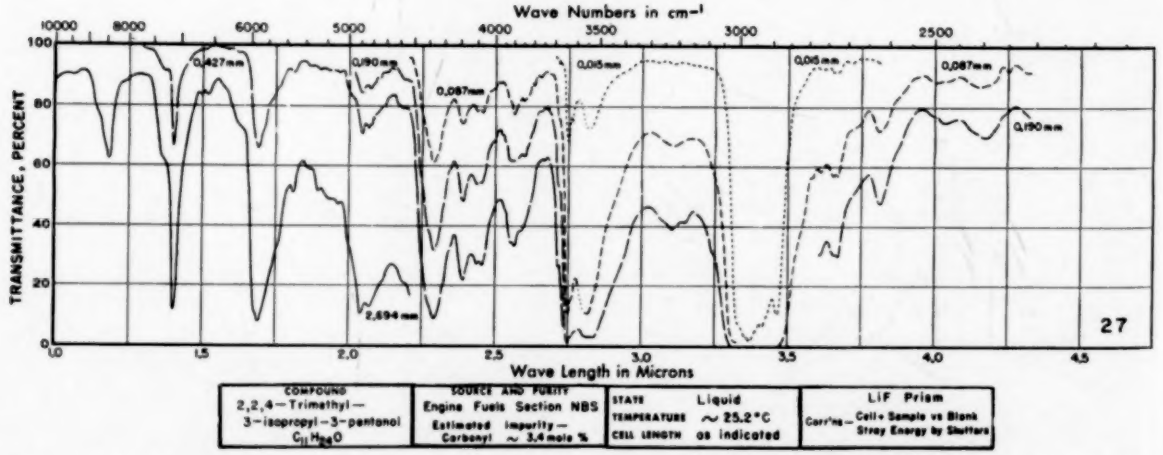

FIGURE 25. *2,4-Dimethyl-3-ethyl-3-pentanol;* LiF *prism.* FIGURE 26. *2,2,4-Trimethyl-3-ethyl-3-pentanol;* LiF *prism.*
FIGURE 27. *2,2,4-Trimethyl-3-isopropyl-3-pentanol;* LiF *prism.*

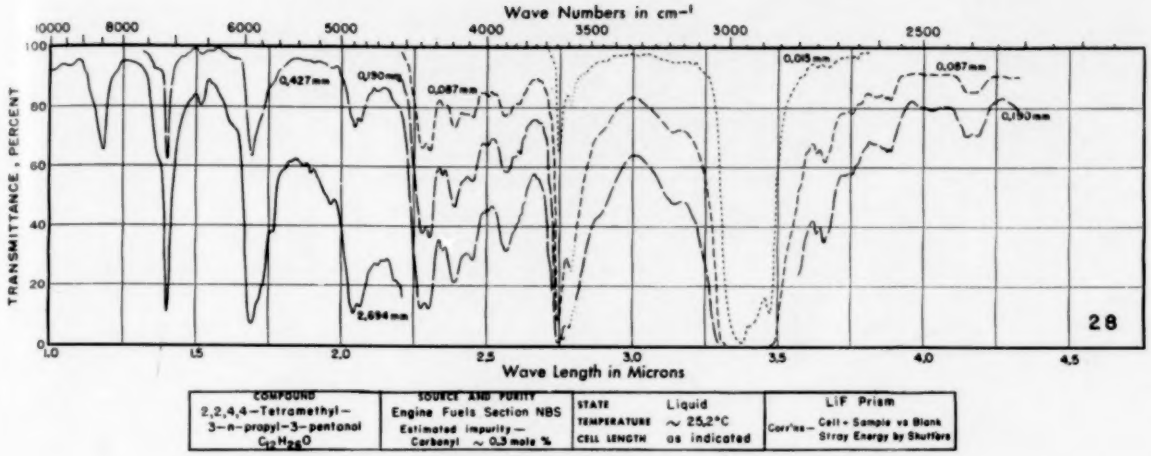

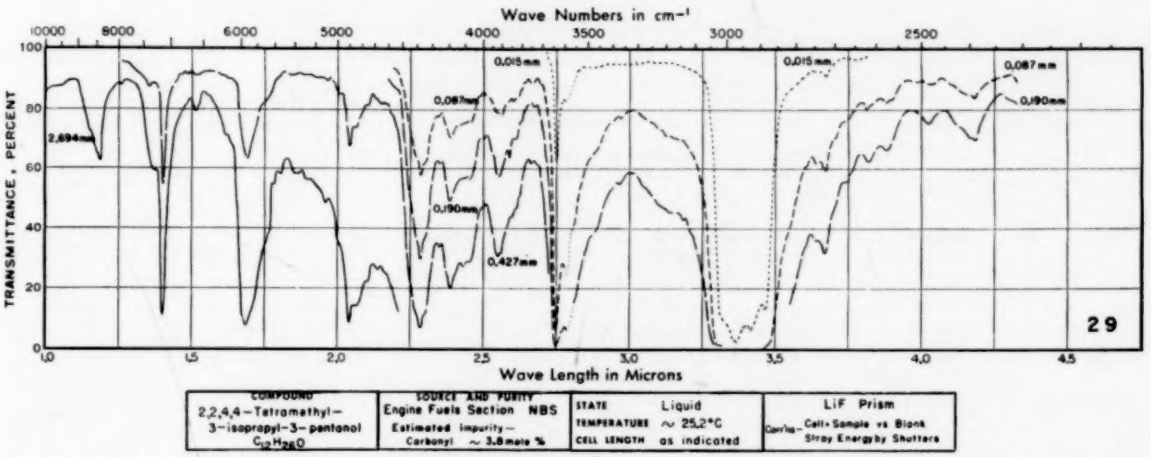

FIGURE 28. *2,2,4,4-Tetramethyl-3-n-propyl-3-pentanol;* LiF *prism.*

FIGURE 29. *2,2,4,4-Tetramethyl-3-isopropyl-3-pentanol;* LiF *prism.*

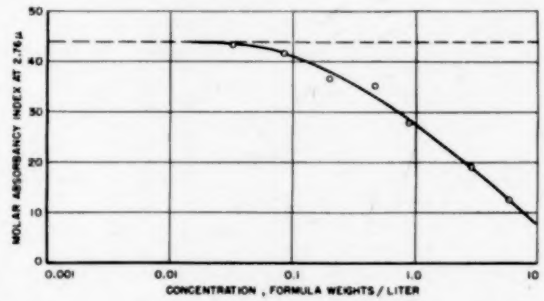

FIGURE 30. *Molar absorbancy index for free hydroxyl (2.76 microns) versus concentration of 2,4-dimethyl-3-ethyl-3-pentanol.*

UNIVERSITY OF MICHIGAN LIBRARIES

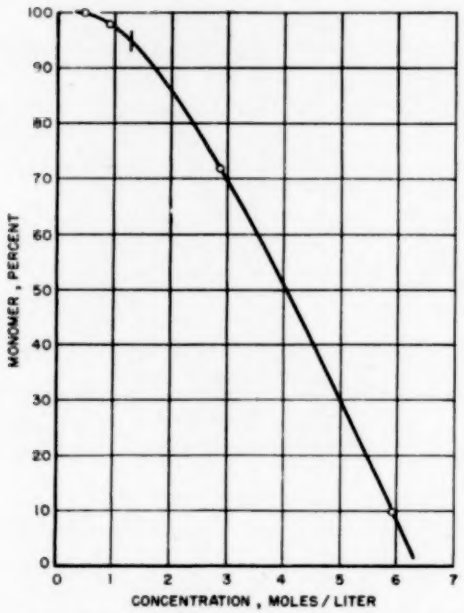

FIGURE 31. *Percentage of monomer contributing to the free hydroxyl absorption versus total molar concentration of 2,4-dimethyl-3-ethyl-3-pentanol.*

The authors express their appreciation to Frank L. Howard and Thomas W. Mears of the Engine Fuels Section of this Bureau for their cooperation in supplying the series of branched alkyl derivatives of 3-pentanol and data concerning their preparation and physical properties; to the Physical Chemistry Section for the use of the isotonic vapor pressure equipment; to Alan W. Smith, who assisted in the work with 2,4-dimethyl-3-ethyl-3-pentanol to prove the dimer assignment; and to John D. Hoffman, who supplied the 1-dodecanol.

VII. References

[1] Maurice L. Huggins, J. Org. Chem. **1,** 407 (1936).
[2] Linus Pauling, The nature of the chemical bond Chapter IX (Cornell Univ. Press, Ithaca, N. Y., 1939).
[3] J. J. Fox and A. E. Martin, Proc. Roy. Soc. (London) **A162,** 419 (1937).
[4] J. Errera, R. Gaspart, and H. S. Sack, J. Chem. Phys. **8,** 63 (1940).
[5] E. G. Hoffman, Z. physik. Chem. **B53,** 179 (1943).
[6] Mansel Davies, J. Chem. Phys. **16,** 267 (1948).
[7] Norman D. Coggeshall, J. Chem. Phys. **18,** 978 (1950).
[8] John D. Hoffman and Charles P. Smyth, J. Am. Chem. Soc. **71,** 431 (1949).
[9] Edward A. Cadwallader, Abraham Fookson, Thomas W. Mears, and Frank L. Howard, J. Research NBS **41,** 111 (1948) RP1909.
[10] E. Carroll Creitz and Francis A. Smith, J. Research NBS **43,** 365 (1949) RP2031.
[11] Francis A. Smith and E. Carroll Creitz, Anal. Chem. **21,** 1474 (1949).
[12] Don C. Smith and Elmer C. Miller, J. Optical Soc. Am. **34,** 130 (1944).
[13] Eleanor L. Saier and Norman D. Coggeshall, Anal. Chem. **20,** 812 (1948).
[14] J. J. Fox and A. E. Martin, Trans. Faraday Soc. **36,** 897 (1940).
[15] Norman D. Coggeshall, J. Am. Chem. Soc. **69,** 1620 (1947).
[16] Norman D. Coggeshall, Anal. Chem. **22,** 381 (1950).
[17] A. Borden and E. F. Barker, J. Chem. Phys. **6,** 553 (1938).
[18] William C. Sears and Leland J. Kitchen, J. Am. Chem. Soc. **71,** 4110 (1949).
[19] S. C. Stanford and Walter Gordy, J. Am. Chem. Soc. **62,** 1247 (1940).
[20] Walter Gordy and S. C. Stanford, J. Am. Chem. Soc. **62,** 497 (1940).
[21] Edwin N. Lassettre and Roscoe G. Dickinson, J. Am. Chem. Soc. **61,** 54 (1939).

WASHINGTON, October 13, 1950.

UNIVERSITY OF MICHIGAN LIBRARIES